bulletin

RHI MAGNESITA

Bulletin

The Journal of Refractory Innovations

Cover picture: The image depicts the lower section of a RH degasser, a secondary metallurgical unit used in steel plants. In the RH degassing process, snorkels are submerged into liquid steel contained in the casting ladle. Argon gas is purged through the inlet snorkel, creating a suction effect that draws liquid steel into the lower vessel of the RH degasser, where a vacuum is applied. The steel treated in the lower vessel flows back to the ladle through the outlet snorkel, creating a continuous steel circulation between the ladle and the RH degasser. The strong negative pressure (vacuum) within the RH degasser facilitates various metallurgical processes that enhance steel quality, with the key process steps including degassing, decarburisation, deoxidation, and alloying under vacuum. Rail steel, flat steel for the automotive industry, and steel plates for shipbuilding are just a few examples of products that benefit from the RH degasser. Prefabricated snorkels, which RHI MAGNESITA manufactures ready for use and delivers to our globally operating customers, are essential components of the RH degasser.

RHI Magnesita Worldwide news

Successful Implementation and Expansion of FAST TO CAST Tundish Lining Mixes

Beginning in mid-2023 and continuing through most of 2024, RHI Magnesita successfully trialled and implemented the FAST TO CAST (ANKERTUN FTC) tundish lining mixes at several steel casters. This proprietary technology delivers performance comparable to traditional spray mixes. The FAST TO CAST mixes have reduced material consumption by approximately 15% per tundish and decrease the heat required to eliminate moisture by ≥50%. The benefits of this mix have been successfully demonstrated at several of North America's largest integrated slab casters. Additional benefits include reducing the required dry-out time by as much as 4 hours and effectively eliminating the dry-out step, enabling the tundish to go straight to preheating. This technology reduces the time a tundish needs to be under a heat source, thereby contributing to CO_2 emission reductions. It also aligns with RHI Magnesita's unwavering commitment to decarbonisation by lowering natural gas consumption as well as containing a minimum of 10% circular raw materials. The FAST TO CAST mixes are part of RHI Magnesita's contribution to reducing the carbon footprint of steelmaking.

Green Taphole Clay for Blast Furnace Applications

RHI Magnesita continues to strengthen its market position for blast furnace taphole clay. The well-established, resin-bonded, and environmentally friendly SEVEN TAP taphole clay product range contains the lowest polyaromatic hydrocarbon levels in industry. SEVEN TAP provides customers with clear benefits in terms of operator health and reductions in emissions from casting operations, compared to conventional tar-bonded taphole clay. Across all European regions, several integrated steel plants are either in the trial phase or already established with SEVEN TAP. During field trials, close collaboration with customer engineering and production teams enables the product performance characteristics to be optimised.

RHI Magnesita Invests in a New Rotary Kiln

RHI Magnesita's new rotary kiln, the largest in the company's operations around the globe, has been in operation in Brumado (Brazil) since the first half of 2024. The commissioning began in May, when the ignition tests were initiated. Throughout the year, crucial adjustments have been made to the plant's exhaust and feeder systems. The team continues working to optimise operation of the new production line, although the new sinter, an even more optimised and eco-friendly raw material, is already being produced. Additionally, new sinters are under evaluation, with tests scheduled to take place in the coming months.

The investment will strengthen RHI Magnesita's position as one of the world's largest producers of refractory raw materials. Furthermore, it enhances vertical integration, ensures final product quality and supply security for customers, while reinforcing a local-for-local approach and, at the same time, supports supply of RHI Magnesita's operations on a global scale. The new kiln technology will extend the Pedra Preta mine's lifespan from 27 to 60 years, ensuring the long-term viability of the Brumado plant. The kiln has an annual production capacity of 140000 tonnes, increasing productivity by 25%. The start-up is being phased to ensure the system's operational safety and well-being of those involved. Over 2 million man-hours have been worked on the project without any lost-time accidents, including both direct employees and contractors.

Europe

4PRO Installation Service at Wöllner

In October, RHI Magnesita carried out the repair of a sodium silicate furnace with a melting surface of 22 m^2 at our long-term customer Wöllner (Germany). The order comprised renewal of the entire furnace, namely the basin side walls, superstructure (excluding burner wall), doghouse (including doghouse corners and doghouse cover) as well as the complete insulation. The side walls were designed as a monolithic cast-in-place (CIP). All the required refractory materials, except the fused cast products, were supplied by RHI Magnesita. This included magnesia bricks for the superstructure as well as fireclay, sillimanite and mullite grades for the tuckstone and doghouse. The order was executed as a full-service package (4PRO) for the customer, which meant that, in addition to the refractory materials, RHI Magnesita also provided refractory installation with supervision, heat-up support with joint sealing, and the addition of tank and chamber insulation.

The work was carried out very professionally and quickly, so that after only 9 days the construction was completed, one day earlier than planned. The customer was highly satisfied with the quality of the work and the entire team's professionalism. We would like to congratulate our customer and joint team for the good collaboration, including the excellent result, and are looking forward to future projects as we further develop the 4PRO activities.

Europe

Successful Implementation of BOF Gas Purging Solution Supports CO$_2$ Emission Reductions

RHI Magnesita's green and smart solution for a more sustainable BOF operation was successfully commissioned at a customer using a two-BOF vessel parallel operation in Western Europe. In the first campaign, not only were metallurgical results and process safety improved compared to the standard system, but significant cost savings and CO$_2$ reductions across the individual greenhouse gas emission scopes were also achieved. Due to the very impressive results obtained during the initial campaigns, the customer has already equipped the second converter with this system as well.

Europe

Successful Training for the Nonferrous Metals Industry

RHI Magnesita is pleased to announce the successful completion of the first organised Training Center for the Nonferrous Metals Industry, held from October 21–24, 2024. Customers from key nonferrous metal industries attended the training to learn the latest strategies and enhance their knowledge of refractory products and best installation practices. The training also focused on design solutions for various nonferrous metal furnaces, common installation challenges, and other critical aspects of the refractory world. The programme, conducted at the Technology Center Leoben (Austria), included both theoretical and practical sessions as well as a visit to the Radenthein plant on the first day. The course was divided into four modules: Refractory Fundamentals, Advanced Refractory Applications, Troubleshooting and Design Optimisation, and Operational Excellence.

The course provided participants with a unique opportunity to gain hands-on experience through practical sessions designed to enhance understanding and skill development. Additionally, attendees had the chance to interact with RHI Magnesita's experts from various departments, including Supervision, Technical Marketing, Engineering, Projects and Design, Process Technology, R&D, and Mineralogy. The programme also facilitated networking with industry partners, enabling participants to engage with professionals from various nonferrous metal fields and countries, fostering knowledge sharing and collaboration. Twenty participants from companies including Rio Tinto Kennecott, Boliden, KCM, and Ecobat attended this long-awaited training course. The positive and enthusiastic feedback from participants was highly encouraging and two additional training sessions are planned for 2025, scheduled for May 12–15 and October 27–30. Please contact installationservices@rhimagnesita.com for more information about these upcoming events.

Europe

Record–Breaking Recycling Rates in Europe

We are thrilled to announce that our recycling efforts in the European region have reached unprecedented levels. For the first time, we achieved a remarkable recycling rate of over 20% in September and 18% year-to-date, thanks to the joint venture MIRECO and operational initiatives across all product groups within RHI Magnesita. For example, the recycling rate in basic mixes has been increased by 2% compared to 2023. Major contributors to this success include the implementation of tundish mixes with more than 10% circular raw materials and a portfolio of high-recycling gunning mixes containing between 20% and 100% circular raw materials. Furthermore, the launch of new ANKERHARTH brands, featuring 10% recycled content, has also enhanced sustainability efforts.

These achievements are not only about meeting RHI Magnesita's goals—they reflect the broader commitment to responsible waste management and environmental stewardship. Together, RHI Magnesita and MIRECO are making a positive impact on the environment, by leading the green change in refractories.

A letter from our editor

The steel industry is undergoing a profound transformation as it embraces more sustainable practices, moving towards what many call "green steel". Today's refractory industry is at a critical juncture: It must respond to the demands of greener steel, cement, glass, and nonferrous metals production while managing the environmental impact of its own materials and processes. The manufacture and disposal of refractories has traditionally involved energy-intensive processes and nonrenewable materials, but new developments are pointing the way to sustainable, high-performance refractory solutions. One area where refractory development is gaining traction is in the sourcing of sustainable raw materials. For decades, refractories have been primarily produced from nonrenewable resources such as bauxite and magnesite. However, an increasing focus on circularity has led manufacturers to explore more sustainable, often locally sourced, and recycled alternatives. Spent refractories, which were previously discarded as waste, can now be reprocessed and reintroduced into production cycles, reducing dependency on virgin raw materials and mitigating the environmental impact of mining. For example, new technologies, like automated sensor-based sorting, enable the efficient separation and repurposing of used refractory materials, which can then be reintegrated into new products without significant performance loss. This closed-loop approach not only conserves natural resources but also reduces waste generation, aligning the industry with circular economy principles.

High-tech coating technologies, improved bonding agents, and hybrid composites have emerged as promising solutions, providing enhanced durability and chemical resistance. Longer-lasting refractories mean fewer resources are consumed and metallurgical production processes face less downtime, both of which contribute to improved efficiency and reduced environmental impact.

A key pillar of the green steel revolution is the shift toward hydrogen-based direct reduction. Refractories that can withstand the unique demands of hydrogen reducing environments—such as increased resistance to hydrogen and compatibility with hydrogen atmospheres—are essential for this transition. Our researchers are developing refractories tailored specifically for hydrogen-based processes, ensuring that these materials will continue to play a supportive role in the green steel ecosystem. The path towards green steel is challenging, but by investing in sustainable raw materials, energy-efficient production, product durability, and hydrogen-compatible refractories, RHI Magnesita can not only keep pace but also lead the way.

This shared journey towards sustainability is not just about reducing emissions; it is about reimagining the industry, securing a healthier planet, and preparing for the future. By fostering a spirit of innovation and collaboration, the refractories industry will continue to be an indispensable partner in the transformation of steel, building a more sustainable tomorrow.

Thank you for joining us on this journey into the world of refractories.

Yours sincerely

Thomas Prietl
Head of Global R&D and Innovation
RHI Magnesita

66 One area where refractory development is gaining traction is in the sourcing of sustainable raw materials. For decades, refractories have been primarily produced from nonrenewable resources such as bauxite and magnesite. However, an increasing focus on circularity has led manufacturers to explore more sustainable, often locally sourced, and recycled alternatives. 99

Contents

Subscriptions Service and Contributions

We encourage you, our customers and interested readers, to relay your comments, feedback, and suggestions to improve the publication quality.

Email
bulletin@rhimagnesita.com

Phone
+43 50213 5300

Erick J. Estrada Ospino, Daniela Gavagnin, Uxia Dieguez, Miriam Schnalzger and Stefan Postrach

Decarbonisation and the Impact of Hydrogen on Refractory Linings in the Iron and Steel Industry

Global efforts towards decarbonisation have recently gained support from various industries. One of the most feasible paths to reduce carbon emissions is by implementing hydrogen as a fuel and/or a process gas. The refractory industry plays an important role in this initiative, being integral in many different applications and production processes. The most significant impact is likely to be seen in the steel industry, where anticipated changes in current production technologies could affect both operations and the performance of refractory linings. Different wear mechanisms are expected in direct reduced iron units due to the increased hydrogen content and additionally the electric arc furnace will also experience changes due to the increased use of sponge iron over scrap.

Introduction

Decarbonisation presents challenges to most of the high-temperature industries. Multiple companies have planned different initiatives, and hydrogen is undoubtedly a key pillar towards limiting carbon emissions. This is especially crucial in steelmaking, as this industry alone contributes up to 9% of global greenhouse gas emissions [1]. Therefore, efforts are currently underway to bring these figures down, including efficiency optimisation and adapting current production processes. For example, alternatives include investing in new direct reduced iron (DRI) units to target emission reductions when compared to the blast furnace (BF) route. Electric arc furnaces (EAFs) are well-established technologies that nowadays are predominantly charged with only scrap. However, the increased hydrogen atmospheres in DRI units may not only impact the lining performance, but in addition the higher use of DRI in the EAF can lead to changes related to the electrical and chemical energy demands, hot heel, and slag operation, which will directly affect the refractory lining selection.

Hydrogen Production and its Use in Iron and Steelmaking

In recent years, the world has seen diverse initiatives promoting emission and energy consumption reductions. Many countries and companies worldwide are striving to achieve shared energy and climate goals within the next decade, with the main industry sectors considering various alternatives, such as continuous improvement, process enhancements, and carbon capture, among other possibilities. The use of hydrogen as a fuel and a process gas is one of the most important trends for reducing CO_2 emissions in a relatively short time.

Hydrogen can be produced in various ways, resulting in a colour-based classification system, typically divided into main colours and others (Table I). The main colours of hydrogen production are: (1) Green, (2) Grey/brown/black, and (3) Blue. The first group highlights hydrogen sources such as biomass, biomethane, and all alternative routes of water electrolysis using renewable energy (e.g., solar, wind,

Table I.

The hydrogen colour spectrum [2]. Abbreviations include carbon footprint (CFP) and carbon dioxide equivalent per kg of hydrogen ($CO_2e/kg(H_2)$).

Hydrogen source	Colour code	Production technology	Primary energy	CFP in [$CO_2e/kg(H_2)$]	H_2 terminology
Biomass	Green	Thermolysis	Biomass	<3	Renewable
Biomethane	Green	Steam reforming	Biomethane	<3	Renewable
Water	Green	Electrolysis	Electricity from renewable energy	<2	Renewable
Water	Yellow	Electrolysis	Electricity from network or solar	Source dependent	Low carbon
Water	Pink	Electrolysis	Electricity from nuclear power	<2	Low carbon
Coal, lignite, or natural gas	Blue	High carbon H_2 + carbon capture	Energy from fossil fuels	<3	Low carbon, considered transition technology
Natural gas	Turquoise	Pyrolysis	Energy from fossil fuels	<3 + solid carbon	Considered transition technology
Natural gas	Grey	Steam reforming	Energy from fossil fuels	~11	High carbon
Lignite	Brown	Gasification	Energy from fossil fuels	>20	High carbon
Bituminous coal	Black	Gasification	Energy from fossil fuels	>20	High carbon
Natural occurrence	White	-	-	-	-

and hydroelectric) that avoid using or generating any greenhouse gases. The second group includes all processes based on hydrocarbons, which generate CO_2 that is afterwards released into the atmosphere. The third group encompasses the same processes as the second but includes carbon capture and storage at the end of the production chain. From these main groups, additional colours such as pink, turquoise, and brown are derived, representing other possible routes to produce hydrogen. Each of these methods impacts emissions and energy consumption in different ways [3].

Recent global statistics show that hydrogen production has been increasing in the last years. For example, in 2022, total hydrogen production was about 95 million tonnes, 3% higher than the previous year. Currently, most production is performed using fossil fuels, as the majority of low-emission hydrogen production processes are still projects under development or at the feasibility study stage. In total, these low-emission plants accounted for only 0.7% of overall worldwide production in 2022. Nevertheless, a significant increase of up to 30% is already planned by 2030 [4]. In most industries, once hydrogen has been produced, it can be used either as fuel or a process gas. Different impacts on the refractory lining are expected, as there is a main difference between both cases, which relates to the direct contact of refractory materials with hydrogen gas.

One of the main planned developments in the iron and steelmaking industry is the increased use of hydrogen in DRI units, upstream of the EAF or electric smelting furnace/ BOF routes (Figure 1). Although current DRI technologies already use a gas mixture based on H_2 and CO, efforts are underway to develop an even cleaner process where the use of carbon can be reduced and substituted by up to 100% hydrogen. Wear mechanisms in the refractory linings may change in these DRI units, as well as in the subsequent EAF, where part of the scrap may be substituted by DRI.

Hydrogen as a Process Gas in DRI Units

For over 70 years, various DRI technologies have been developed around the globe as an alternative to the BF route. With these technologies, the reduction of oxidised iron ore occurs in a gaseous environment using a mixture of reducing gases, usually based on H_2 and/or CO. These processes achieve a very high level of metallisation of the iron ore, which is then used in steelmaking shops.

Global DRI production was 127.36 million tonnes in 2022 [6]. This represents about 7% of the steel production during that year, which totalled 1885 million tonnes worldwide [7]. Although the impact of DRI on the industry is currently still low, it is expected that the installed capacity will increase significantly in the coming years due to recent net-zero emission initiatives.

The state-of-the-art DRI process typically uses a H_2/CO gas ratio of about 1.6 on average, operating at temperatures around 900 °C. The partial pressures can vary depending on the technology, and in some cases this ratio may even rise to nearly 3.9 [8]. This is due to the use of natural gas as the main feedstock for the reformation stage, to prepare the gas mixture used as a reductant. Although current DRI technologies still produce some CO_2 in their off-gases, these processes potentially reduce CO_2 emissions by 38–61% compared to the standard BF route [9].

Decarbonising the steel industry may require several different actions from most of the important players in this market segment. For example, in the ironmaking stage carbon capture, BF enhancements, and/or the implementation of DRI units are feasible solutions to reduce emissions effectively.

Figure 1.

Two options for green steelmaking using direct reduction: EAF plant based on hot and/or cold DRI (HDRI/CDRI) and a DRI unit combined with a continuous electric smelting furnace, followed by the BOF process [5].
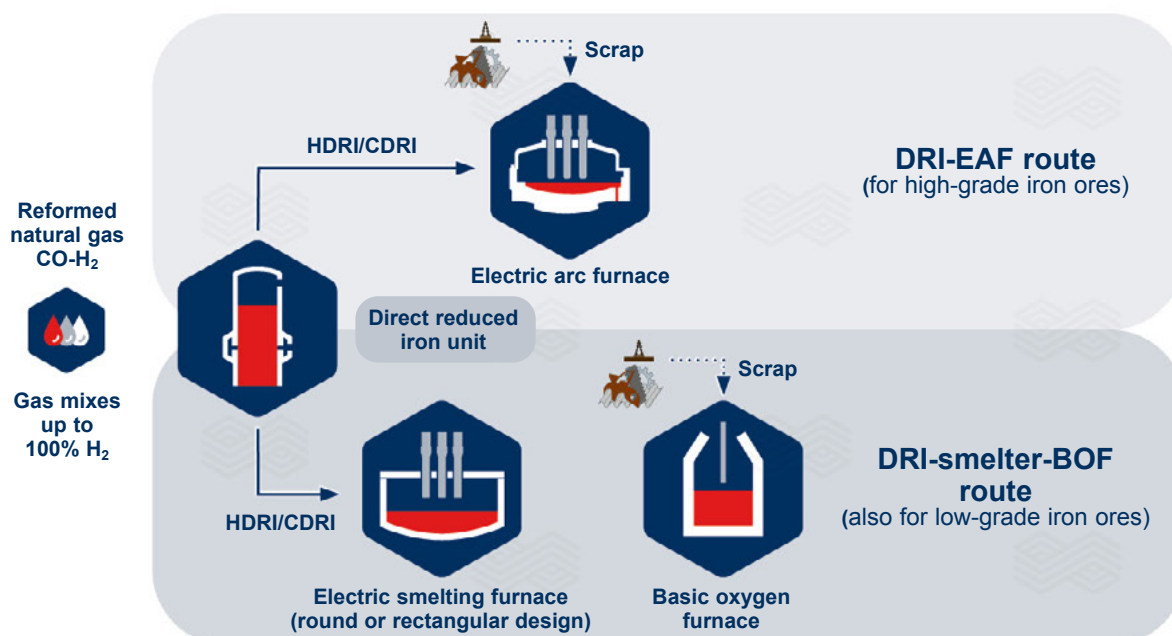
The main DRI original equipment manufacturers (OEMs) are also developing new processes that are targeting 100% hydrogen-based units. These emerging technologies may require updated refractory concepts, as changes to the process parameters, which in most cases affect the gas composition, could lead to more aggressive wear mechanisms in the refractory lining, primarily caused by the enriched hydrogen atmosphere.

Only a few investigations have been conducted to analyse the behaviour of different refractory materials in pure hydrogen atmospheres [10] and the different methods and types of furnaces used led to various results that in some cases were contradictory. However, overall it has been confirmed that one of the oxides contained in refractory materials, namely SiO_2, reacts very easily with H_2. The resulting silica loss is a phenomenon where hydrogen reacts with the refractory material, reducing the brick or castable, causing a detrimental effect on the properties of the refractory lining. This reaction is primarily driven by temperature and pressure, occurring more rapidly at higher temperatures. In contrast, the opposite behaviour is observed for pressure, where higher pressures somehow slow down the same reaction [10,11].

Thermodynamic modelling can be used to calculate the weight loss of SiO_2 and SiO_2-containing refractory raw materials (e.g., mullite) due to the reduction of SiO_2 by pure hydrogen at increasing temperatures (Table II). This reaction accelerates in cases where either the SiO_2 content is higher, the temperature is higher, or the partial pressure is lower. These observations also align with studies of SiO_2-containing refractory brick samples exposed to the same atmospheres and temperature conditions [12].

One of the main challenges that refractory producers and OEMs are now facing is understanding the possible impacts of changes in operating conditions that increase the hydrogen content. However, recent laboratory studies provided an insight into the reduction mechanism of silica-containing refractories [11]: First, the glassy phase, prone to react with hydrogen, forms SiO gas; second, SiO_2 is reduced in the mullite phase; and third, secondary alumina forms over time when an Al_2O_3/SiO_2 ratio higher than 2.6 is reached (Figure 2).

The conclusions from these studies were substantiated by postmortem analyses performed on refractory bricks taken from state-of-the-art DRI units after years in operation. A representative microstructure of a sample recovered from the reduction zone showed that the glassy phase had been

Table II.

Results of thermodynamic calculations to determine weight loss of SiO_2 and mullite samples (100 g) in a hydrogen atmosphere (8064 g H_2 at 1 bar) at various temperatures, after reaching equilibrium conditions.

Temperature [°C]	Silica weight loss [%]	Mullite weight loss [%]
800	0.00	0.00
900	0.02	0.01
1000	0.19	0.14
1100	1.22	0.86
1200	6.13	4.04
1300	24.86	15.88
1400	84.88	28.21

Figure 2.

Reduction mechanism of a silica-containing refractory matrix in a hydrogen atmosphere. (a) typical silica-containing refractory matrix, (b) preferential reduction of glassy phase due to the formation of SiO gas, (c) SiO_2 loss from the mullite phase resulting in the formation of secondary alumina, and (d) complete replacement of the mullite phase by secondary alumina.
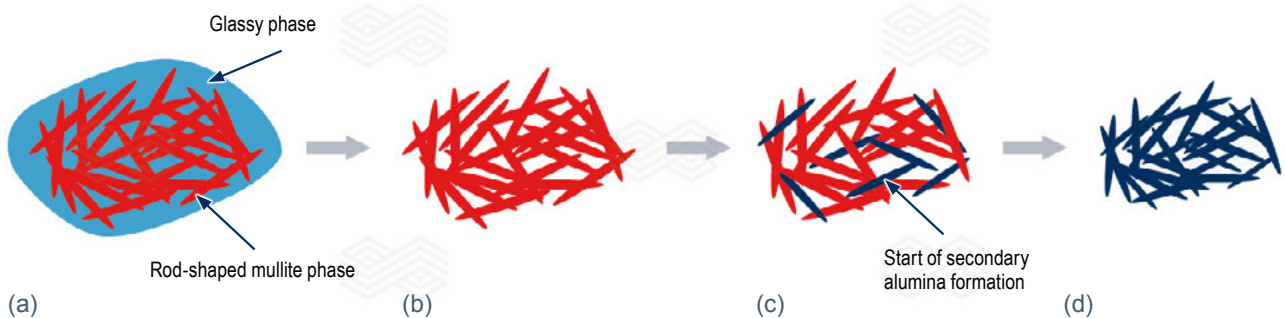
attacked by the reducing gas mix on the outer most part of the hot face (Figure 3 delineated by red dots), while the mullite network remained intact and was not affected by reduction (Figure 3 highlighted by red arrows).

In general, refractory linings in DRI shaft furnaces withstand current process conditions for several years. However, the anticipated increase in hydrogen content will necessitate refractory lining enhancements, such as increased Al_2O_3 contents, which reduces SiO_2 weight loss but also impacts other important factors, such as the heat transfer coefficient, overall refractory lining weight, and its costs. Many investigations are currently underway to test various types of refractory materials against different hydrogen-reducing atmospheres at different temperatures and partial pressures [11]. These activities can be performed at RHI Magnesita's Technology Center Leoben (Austria), supporting decision-makers by providing specific insights in this regard. So far,

preliminary results have shown that the reduction wear mechanism is expected to change slightly compared to current technologies and may impact widely used refractory products. Furthermore, these investigations will continue, as refractory producers are committed to supporting major OEMs understand the potential effects on refractory products and their properties due to long-term operation with new process parameters, while maintaining cost competitiveness in any future greenfield projects.

RHI Magnesita offers worldwide production capacity, including customisable refractory linings tailored to each customer's specific needs. For DRI applications, a wide variety of refractory bricks and castables are available for the different equipment within these units. A combination of well-known brands, such as MAXIAL, RESISTAL, DURITAL, COMPRIT, DIDURIT, and LEGRIT, positions RHI Magnesita as a reliable partner for this growing application.

Figure 3.

Scanning electron micrograph of a postmortem refractory brick taken from the reduction zone of a DRI shaft furnace. The glassy phase was lost on the outer most part of the hot face (above red dotted line) leaving the residual mullite network (red arrows) [13].
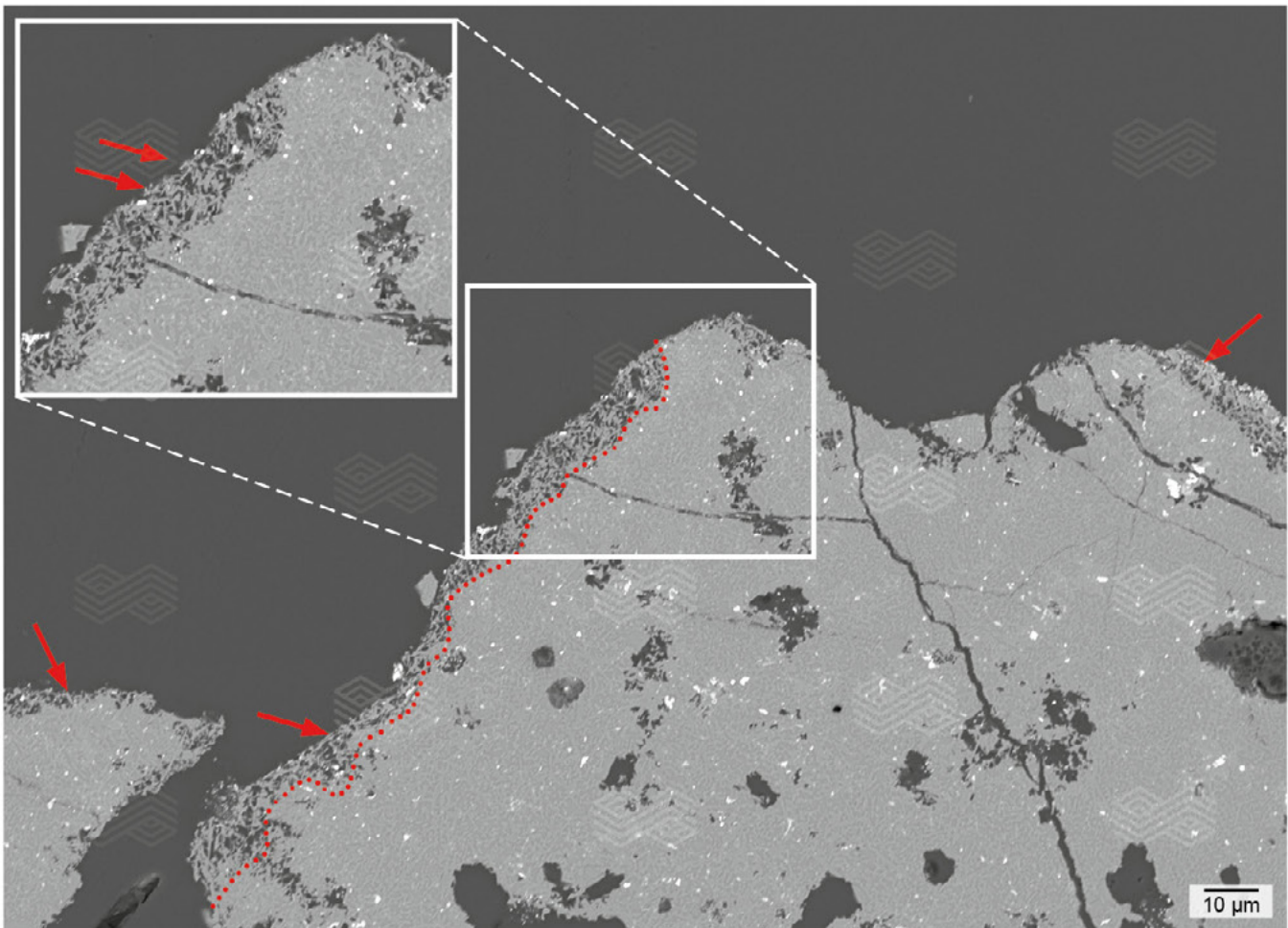
Refractories for DRI Charged EAFs

Once the high-grade DRI has been produced, it is delivered to the steel shop in either pellet or briquette form, cold or hot, and charged into the EAF through its roof. In general, use of DRI in the EAF offers advantages, such as controlling residual elements like Cu or Mo, and tends to reduce nitrogen levels in crude steel. This enables the production of high-quality steel grades, which are currently produced mainly through the BF-BOF route. However, its use presents many challenges for the furnace operation, including higher electrical energy consumption, higher slag volumes, and longer tap-to-tap times compared to a standard EAF charged with 100% scrap. The main reason for these changes is related to the DRI chemical and physical properties. Two of the most important parameters affecting the furnace operation are the degree of metallisation, defined as the level of metallic iron in the pellet, and the gangue content, which is mainly formed from acidic oxides such as SiO_2 and Al_2O_3 (Table III).

The expected variances in EAF process conditions may directly affect the refractory consumption in the steel shop. For example, an increased SiO_2 content in the DRI would require more lime to reach the optimal basicity, while also necessitating more electrical energy to melt the additional slag formers. Additional studies have shown that if the EAF charging mix contains more than 20% DRI, there may be a negative impact on productivity, refractory lifetime, power-on time, consumables, and energy consumption [14]. Furthermore, the need for high-performance refractory lining grades and maintenance mixes may also increase [15].

Usually, for cases of increased DRI charge ratios in the EAF, some basic requirements must be fulfilled:

- Focus on health and safety in the work environment for refractory personnel.
- Stable, balanced lining wear behaviour during the campaign, targeting an optimum refractory consumption.
- Minimum downtimes due to maintenance.
- Sustainable refractory lining concepts, with a reduced product carbon footprint.
- Circular economy concepts that avoid landfilling.

To support customers in these and other areas, RHI Magnesita offers a range of refractory solutions for the EAF (Table IV).

Table III.

EAF refractory wear caused by DRI input [14,15].

Considerations when charging DRI	Main wear mechanism	Main EAF impacted area
Metallisation degree: Increased FeO in the slag	Corrosion/chemical wear	Sidewall and bottom
Gangue: Acidic gangue must be compensated for with slag formers to reach optimal basicity	Chemical wear	Sidewall
Bulk density: Arching in open bath	Thermal and mechanical	Sidewall
Charging rate: Formation of icebergs, skulls, and cold spots	Spalling	Sidewall

Table IV.

RHI Magnesita's refractory solutions for the EAF. Abbreviations include computational fluid dynamics (CFD).

Technology	Functionality	Benefits	Ref.
RADEX BLOCK (Wall wear indicator)	Change of surface wear patterns on the hot face during the campaign	• Identification of prewear areas • Enhanced process control and operational safety • Gunning indicator	[14]
ANKERDOOR Prefabricated slag door	Improve mechanical stability	• Simple and quick slag door installation • Reduced specific refractory consumption (maintenance effort) • Reduced downtime of the EAF	[16]
RADEX DPP Direct purging plug	Ar or N_2 purging to improve furnace mixing behaviour	• Decreased DRI melting time • Decreased specific electrical energy demand • Increased metal yield and oxygen efficiency • Avoid delayed CO boiling and slopping • Higher reliability of temperature and metal composition probes • Metallurgical benefits, such as decrease of N_2 levels	[5,17]
ANKERTAP Eccentric bottom taphole (EBT)	Preassembled CFD-optimised channel bricks	• Less operator effort for installation • More stable tapping duration during the campaign • Faster start tap time with the same diameter • Less carryover slag into ladle • Increased lifetime	[18]
Hot Taphole Jacker (HTJ)	Breakout and removal of the worn EAF taphole	• Less physical strain on operators • Rapid breakout in a hot furnace • Higher availability of the furnace • Low maintenance costs • Pneumatically powered	[18]
TERMINATOR XL Hot repair maintenance	Application of gunning and fettling with an easy changeover at high flow rates	• Increased EAF availability • Highest safety for operating personnel • Reduced rebound and repair time • Remote maintenance • Storage of data for reports and further analysis of trends	-
ANKERJET X/Y High circular raw material (CRM) gunning mixes	By implementing CRM products, the carbon footprint of the mix is reduced	• Engineering more sustainable lining concepts by implementing CRMs through refractory recycling	[19]
Customer Portal	Digital service	• Transparency and constant improvement • Monitoring the consumption and carbon footprint of refractories in each furnace	[20]

Conclusion

Currently, the future of the steel industry is very dynamic, with activities focused on diverse decarbonisation initiatives to tackle carbon emission reductions from various perspectives. From the ironmaking stages all the way down to the cast houses, key stakeholders are working on developing cleaner processes to achieve global environmental goals. The use of hydrogen offers potential solutions to this issue, whether as a fuel or a process gas. It is very likely that refractory linings will need to be reviewed, especially when hydrogen is used as a process gas, since this significant change in the operational parameters may impact refractory performance. Therefore, RHI Magnesita is conducting multiple analyses to simulate the possible effects of various hydrogen-reducing atmospheres at different temperatures, with the target of designing tailored refractory solutions for hydrogen-enriched DRI units. Furthermore, an increased use of DRI in EAFs is also expected, and while variations in operation are anticipated, there is significant potential for improvement by selecting the right refractory lining concept. As a global leader in this field, RHI Magnesita is committed to supporting customers with state-of-the-art refractory solutions, specialised process know-how, and a network of worldwide production sites and technology centres.

References

[1] Kim, J., Sovacool, B.K., Bazilian, M., Griffiths, S., Lee, J., Yang, M. and Lee, J. Decarbonizing the Iron and Steel Industry: A Systematic Review of Sociotechnical Systems, Technological Innovations, and Policy Options. *Energy Research & Social Science*. 2022, 89, 102565.

[2] Pollet, B.G. Les enjeux des minéraux critiques et stratégiques dans la filière hydrogène. Presented at Journée bretonne Hydrogène R&D – Industries – formations, Saint Malo, France, 29 May, 2024.

[3] Broadleaf Capital International Pty Ltd., Australia. The Colour of Hydrogen. August 2021. https://www.broadleaf.com.au/resource-material/the-colour-of-hydrogen/

[4] International Energy Agency. *Global Hydrogen Review 2023*. December 2023. France. https://iea.blob.core.windows.net/assets/ecdfc3bb-d212-4a4c-9ff7-6ce5b1e19cef/GlobalHydrogenReview2023.pdf

[5] Kirschen, M., Dieguez, U., Gruber, M., Schmidt, V. and Trummer, B. Energy Savings and Additional Benefits of Inert Gas Stirring in Electric Arc Furnaces with a Focus on Green Steelmaking. *Bulletin*. 2023, 18–25.

[6] Midrex Technologies, Inc., Charlotte, USA. 2022 World Direct Reduction Statistics. September 2023.

[7] World Steel Association, Brussels, Belgium. 2023 World Steel in Figures. 2023.

[8] Millner, R., Rothberger, J., Rammer, B., Boehm, C., Sterrer, W., Ofner, H. and Chevrier, V. MIDREX H_2 – The Road to CO_2-Free Direct Reduction. Proceedings of AISTech 2021, Nashville, USA, June 29–July 1, 2021.

[9] Ling, J., Yang, H., Tian, G., Cheng, J., Wang, X. and Yu, X. Direct Reduction of Iron to Facilitate Net Zero Emissions in the Steel Industry: A Review of Research Progress at Different Scales. *Journal of Cleaner Production*. 2024, 441, February.

[10] Ribeiro Gomes, M., Leber, T., Tillmann, T., Kenn, D., Gavagnin, D., Tonnesen, T. and Gonzalez-Julian, J. Towards H_2 Implementation in the Iron- and Steelmaking Industry: State of the Art, Requirements, and Challenges for Refractory Materials. *Journal of the European Ceramic Society*. 2024, 44(3), 1307–1334.

[11] Ribeiro Gomes, M., Ducastel, A., Konrad, L., Janssen, T. and Ospino, E.E. Hydrogen-Resistant Refractories for Direct Reduced Iron Production. Proceedings of METEC and 6th ESTAD, Düsseldorf, Germany, June 12–16, 2023.

[12] Ospino, E.E., Hebenstreit, G., Postrach, S., Gavagnin, D. and Janssen, T. Challenges for the Refractory Industry to Support the Foreseen Large-Scale Transition to DRI Shaft Kilns. Proceedings of AISTech 2023, Detroit, USA, May 8–11, 2023.

[13] Gavagnin, D., Kyrilis, E., Estrada Ospino, E.J., Spreij, M. and Postrach, S. Refractory Lining Challenges in Transitioning from Established to Hydrogen-Ready Operations in DRI Shaft Furnace Technologies. *La Metallurgia Italiana - International Journal of the Italian Association for Metallurgy*. 2024, November/December (in press).

[14] Hanna, A. and Zettl, K. Modern Electric Arc Furnace Processes and Their Requirements for Improved Lining Concepts. *RHI Bulletin*. 2015, 1, 17–24.

[15] Kirowitz, J., Schnalzger, M., Janssen, T., Kirschen, M., Spanring, A., Moulin-Silva, W., Ratz, A., Kollmann, T. and Wucher, J. Electric Melting Furnaces for Green Steel Transformation of Integrated Steel Plants – Requirements, Challenges, and Solutions from a Refractory Perspective. Procedures of the 9th European Oxygen Steelmaking Conference. Aachen, Germany, Oct. 17–22, 2022.

[16] Servos, K., Madey, M., Hanna, A., Hochegger, M. and Debisarran, R. Installation and Practical Experience with Preassembled EAF Slag Door Blocks at Arcelor Mittal Point Lisas. *RHI Bulletin*. 2015, 1, 25–28.

[17] Kirschen, M., Dieguez, U., Gruber, M., Schmidt, V. and Trummer, B. Energy Savings and Additional Benefits of Inert Gas Stirring in Electric Arc Furnaces with a Focus on Green Steelmaking. *Bulletin*. 2023, 18–25.

[18] Zettl, K., Zottler, P., Bachmayer, J. and Kirschen, M. State of the Art Tapping Solutions for Bottom Tapping EAFs. *Berg- und Hüttenmännische Monatshefte*. 2013, 158, 13–16.

[19] Kirowitz, J., Lanzenberger, R., Petritz, B., Rechberger, L. and Dieguez, U. Sustainable Refractory Solutions—New Gunning Mixes Containing Circular Material. *Bulletin*. 2023, 26–32.

[20] Souza, P., Freitas, C., Arth, G., Penido, G., Zettl, K., Bolognani, J., Lamare, C., Lammer, G., Moser, G. and Hoffert, A. Next Level of Digital Refractory Contracts. *Bulletin*. 2022, 52–59.

Authors

Erick J. Estrada Ospino, RHI Magnesita, Ontario, Canada.
Daniela Gavagnin, RHI Magnesita, Leoben, Austria.
Uxia Dieguez, RHI Magnesita, Vienna, Austria.
Miriam Schnalzger, RHI Magnesita, Vienna, Austria.
Stefan Postrach, RHI Magnesita, Wiesbaden, Germany.
Corresponding author: Erick J. Estrada Ospino, Erick.Ospino@rhimagnesita.com

Return to Content

Kevin Christmann, Bernd Neubauer, Hartwig Kunanz, Xiang Yong Li, Lin Zhang, Weizhen Xiong, Walter De Queiroz Cassete, Leandro Rocha Martins and Gabriela Ladeira Fajardo

Case Studies of High-Recycling Containing Magnesia-Carbon Bricks in High-Performance Steelmaking Applications

In order to drive sustainability and contribute to ongoing global green steel transformation initiatives, RHI Magnesita has developed tempered magnesia-carbon (MgO-C) bricks with a circular (i.e., recycled) raw material content of up to 30%, showing comparable results to standard high-performance wear lining refractories. This study provides detailed practical examples of such material in use in steel ladle and electric arc furnace applications.

Introduction

The steel industry is globally entering the so-called green steel transformation. Steel producers worldwide are seeking to reduce scope 1 emissions basically by transitioning primary steelmaking from the blast furnace route to electrical steelmaking, with the electric arc furnace (EAF) steelmaking route being combined with hydrogen-based direct reduction. New technical possibilities to reduce CO_2 emissions are being explored all over the steelmaking industry worldwide. Hence, scope 3 emissions are also becoming increasingly important and steel producers are examining the carbon footprint associated with refractory materials, for example tempered MgO-C bricks. Additionally, scrap originating from spent refractory material is causing steel producers issues with regards to landfilling, undesired storage, and logistics costs, as well as potential taxes related to governmental regulations for waste disposal [1,2]. Of course, refractory producers like RHI Magnesita are also looking to reduce scope 1 emissions [3,4].

The raw materials in MgO-C bricks are responsible for up to 90% of the total carbon footprint of the final product. That is why, for refractory producers, a major lever to reduce their own scope 1 emissions and contribute to steel producers' efforts in lowering costs and scope 3 emissions is using circular raw materials in tempered MgO-C bricks at significant amounts of 30% or more. The literature contains many investigations about this type of material, showing positive results [2,5–7]. In addition to the already existing circular raw material containing products for low-wear area applications, RHI Magnesita has developed a new type of product with comparable results to standard high-performance wear lining MgO-C refractories. This study provides detailed practical examples of this material's use in steel ladle and EAF applications.

High-Performance, Tempered MgO-C Refractories Containing Circular Raw Material

Since 2020, RHI Magnesita has globally developed more than 50 tempered MgO-C products containing ≥20% circular raw material for use in steelmaking applications. These products are successfully used in basic oxygen furnaces (BOFs), EAFs, and steel refining ladles in both high- and low-wear areas. The design of these tempered MgO-C products with high amounts of circular raw material requires tight quality control of incoming spent refractory materials and expertise regarding the required processing steps (Figure 1) [5,7].

Figure 1.

Processing steps required to reuse spent refractories in MgO-C products [8].

Dismantling   Sorting and cleaning   Stabilisation   Crushing and sieving   Utilisation
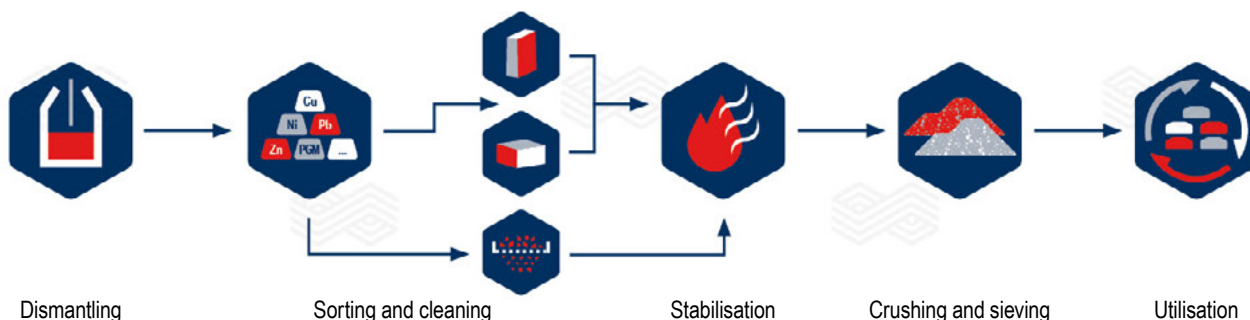
The chemistries of typical circular raw materials used in MgO-C bricks are shown in Table I. These are just examples, demonstrating that there is not one single type, but various types of circular raw material available. This is due to different originating applications (e.g., EAF, BOF, and steel ladle), multiple refractory suppliers, variable presorting in the steel plants, as well as diverse sorting, cleaning, and stabilisation measures in place at different circular raw material suppliers.

The production of MgO-C products with elevated circular raw material content also requires adaptions to the recipe design, as well as the refractory production process itself, to achieve the necessary physical and chemical properties of the final product. Figure 2 shows the typical microstructure of a tempered MgO-C brick with high circular raw material content (Circular-MgO-C) and a standard product without circular material. As can be seen in Figure 2, the matrix of the Circular-MgO-C shows no significant differences to the standard grade at higher magnification. The graphite is homogenously distributed in both cases and the matrix filling degree is mid to high. Furthermore, both materials contain the same fused magnesia quality, namely type 97% MgO. At lower magnification, small agglomerations of alumina-based material surrounded by antioxidants can be detected in the Circular-MgO-C (Figure 3).

Table I.

Typical chemistry examples of circular raw materials used in MgO-C brick grades.

Circular raw material chemistry	MgO [wt.%]	CaO [wt.%]	Fe_2O_3 [wt.%]	Al_2O_3 [wt.%]	SiO_2 [wt.%]	C [wt.%]
Example 1	94	1.5	1.0	1.0	1	10
Example 2	93	1.5	0.7	1.5	1	10

Figure 2.

Microstructure examples of (a) standard MgO-C and (b) typical Circular-MgO-C bricks.
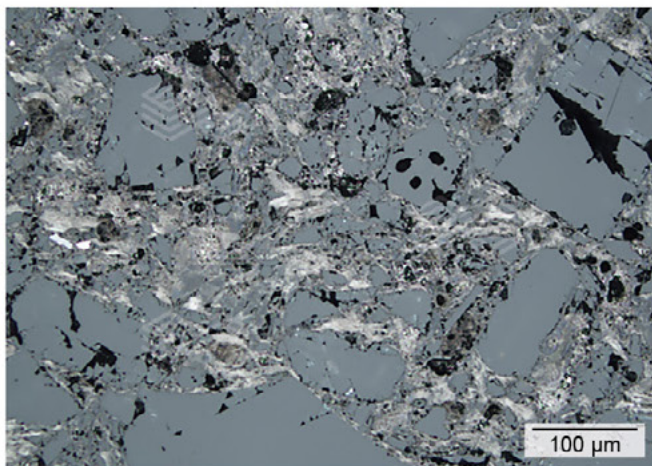
(a)
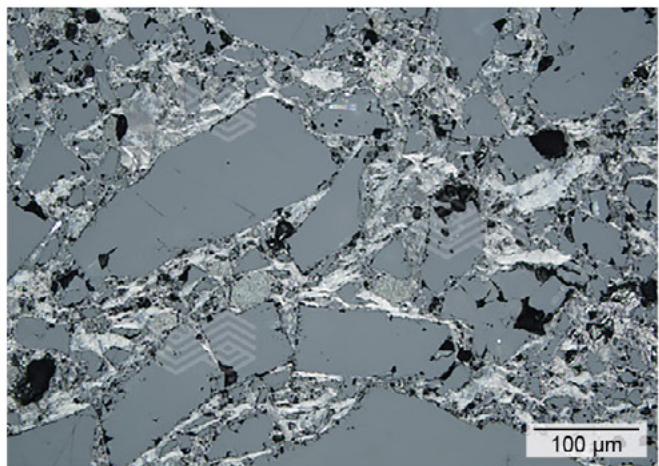
(b)

Figure 3.

Microstructure of a Circular-MgO-C brick with an alumina-based particle (1) and antioxidants (2).
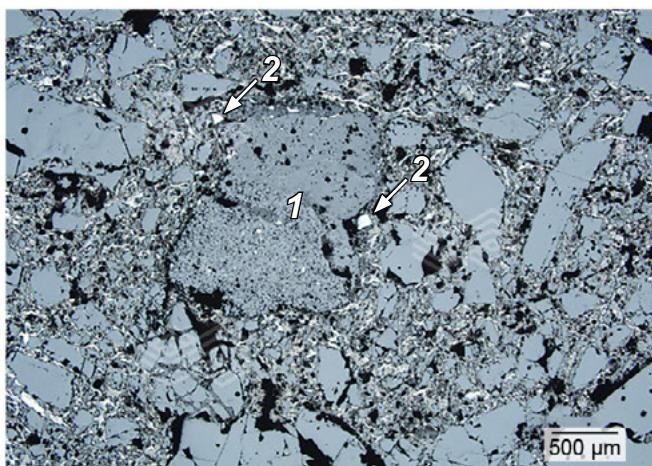
Case Studies

Case 1: 200-tonne steel ladle slag zone lined with Circular-MgO-C bricks containing 30% circular material

Circular-MgO-C was tested against standard MgO-C bricks in the slag zone of a 200-tonne steel ladle. Both materials had a total carbon content of 14% and no additional antioxidants. The raw material basis of both products was the same, namely fused magnesia type 97% MgO with a lime to silica ratio of 1:1. In the Circular-MgO-C bricks, 30% of the fused magnesia component was replaced with circular raw material. Table II provides a comparison of the chemical and physical properties of both brick types. Clearly, the Al_2O_3 content of the Circular-MgO-C was elevated and although the physical properties after tempering showed a slight

Table II.

Chemical and physical properties of the standard MgO-C and Circular-MgO-C bricks, with the same raw material basis, tested in the steel ladle slag zone. Abbreviations include tonne of CO_2 equivalent per tonne of product (t CO_2e/t product).

	Standard MgO-C	Circular-MgO-C
MgO [wt.%]	95.7	93.5
Al_2O_3 [wt.%]	0.5	2.0
Fe_2O_3 [wt.%]	0.8	0.8
CaO [wt.%]	1.5	1.6
SiO_2 [wt.%]	1.5	2.0
C [wt.%]	14.0	14.0
Tempered:		
Bulk density [g/cm^3]	3.02	2.98
Apparent porosity [vol.%]	2.0	2.5
Cold crushing strength [N/mm^2]	45	40
Coked (1000 °C):		
Bulk density [g/cm^3]	2.93	2.94
Apparent porosity [vol.%]	9.5	10
Cold crushing strength [N/mm^2]	30	25
Product carbon footprint [t CO_2e/t product]	2.757	2.094

deterioration compared to the standard material, after coking the values were comparable. The product carbon footprint was calculated according to ISO 14067 [9].

The steel plant operates two 190-tonne BOFs and a ladle furnace, as well as one billet caster. The product portfolio consists mainly of structural steel, with the share between Al-killed and Si-killed steel being approximately 70% and 30%, respectively. Table III shows typical examples of Al-killed and Si-killed steel ladle slags from this plant, which can be highly aggressive against basic refractories.

In Figure 4 the slag zone area (layer 29–41), where the standard MgO-C and Circular-MgO-C bricks were tested, is indicated in orange. The barrel and bottom were lined with alumina-magnesia-carbon (AMC) bricks. The slag zone lining was designed with MK8 and MK9 mini key shapes, with a thickness of 203.2 mm and 228.6 mm, respectively.

In total three sets of the Circular-MgO-C bricks were tested and the results compared to standard MgO-C material. The

Figure 4.

200-tonne steel ladle lined with 14% carbon-containing MgO-C in the slag zone.

Table III.

Examples of typical ladle slag compositions during the trial period for case study 1.

	MgO [wt.%]	Al_2O_3 [wt.%]	SiO_2 [wt.%]	CaO [wt.%]	TiO_2 [wt.%]	Cr_2O_3 [wt.%]	MnO [wt.%]	Fe_2O_3 [wt.%]	B4
Ladle slag (Al-killed)	1.55	21.22	13.64	62.48	0.26	0.11	0.14	0.33	1.84
Ladle slag (Si-killed)	8.45	12.60	31.46	18.38	2.42	0.32	15.37	10.33	0.61
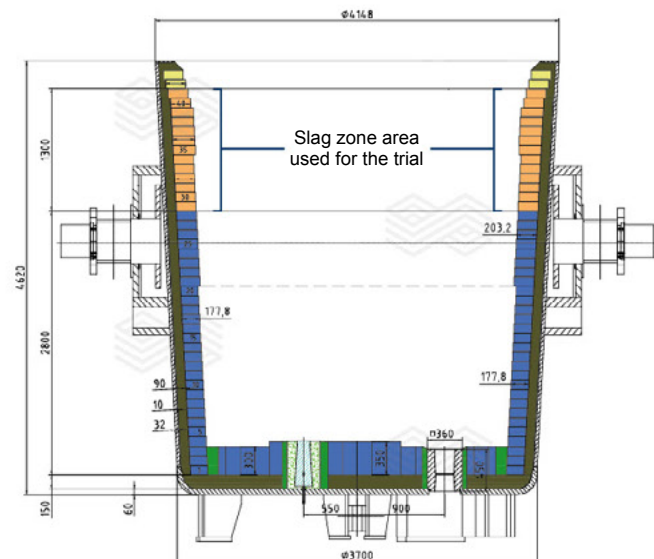
target lifetime of the ladles running in this plant is 75 heats, which was achieved by the ladles equipped with the Circular-MgO-C. Figure 5 shows a comparison between the standard and Circular-MgO-C bricks at 73 and 75 heats, respectively.

There was no difference in maintenance schedules for the standard and Circular-MgO-C lined steel ladles. The average wear rate of the Circular-MgO-C was 2.07 mm/heat, compared to 2.02 mm/heat for the standard bricks. This very minor difference in performance, combined with a 9% cost decrease and 24% CO_2 equivalent reduction, led to the decision to completely replace the standard slag zone material with Circular-MgO-C.

Case 2: 340-tonne steel ladle slag zone (upper and lower part) lined with two types of Circular-MgO-C bricks containing 20% circular material

Two Circular-MgO-C brick grades were tested in 340-tonne steel ladles against standard MgO-C materials. At this steel plant the steel ladle slag zone is separated into high- and low-wear areas. For the high-wear area bricks, a fused magnesia type with 98% MgO was used while for the low-wear area a fused magnesia type with 97% MgO was selected. The corresponding Circular-MgO-C in both areas had the same fused magnesia basis. The total carbon content of all the materials was 12%.

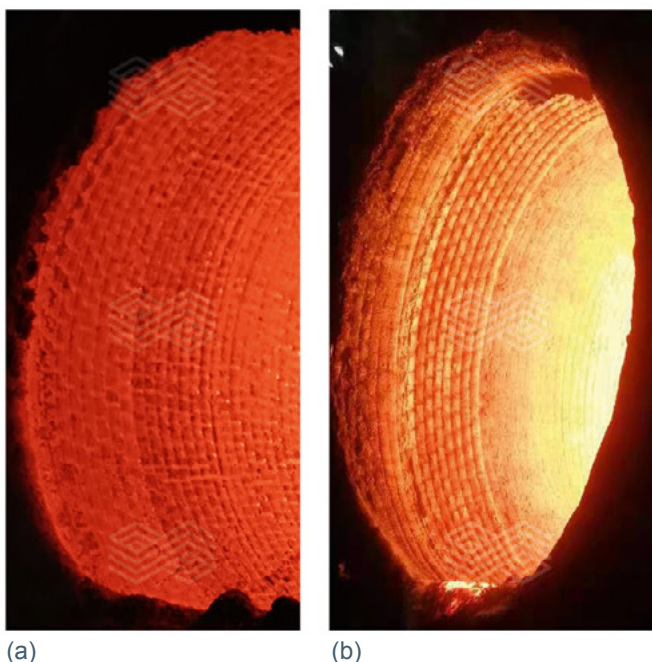Table IV and Table V provide a comparison of the two Circular-MgO-C brick grades with the equivalent standard MgO-C materials for the high- and low-wear areas of the steel ladle slag zone. As in the material comparison described for case 1, differences between the standard and Circular-MgO-C bricks were mainly the Al_2O_3 content and physical properties after tempering. However, the typical coked values for both the high- and low-wear area

Circular-MgO-C materials were similar to the standard materials, and for the low-wear area the density of the Circular-MgO-C material was even higher than the standard MgO-C. The carbon footprint reduction was 37% and 13% for the high- and low-wear area Circular-MgO-C materials, respectively.

Table IV.

Chemical and physical properties of the standard MgO-C and Circular-MgO-C bricks, with the same raw material basis, tested in the high-wear area of the steel ladle slag zone. Abbreviations include tonne of CO_2 equivalent per tonne of product (t CO_2e/t product).

	Standard MgO-C	Circular-MgO-C
MgO [wt.%]	97.4	95.3
Al_2O_3 [wt.%]	0.2	0.9
Fe_2O_3 [wt.%]	0.6	1.5
CaO [wt.%]	1.1	1.2
SiO_2 [wt.%]	0.6	0.8
C [wt.%]	12.0	12.0
Tempered:		
Bulk density [g/cm³]	3.06	3.08
Apparent porosity [vol.%]	3.0	3.0
Cold crushing strength [N/mm²]	50	50
Coked (1000 °C):		
Bulk density [g/cm³]	2.97	2.96
Apparent porosity [vol.%]	10.0	10.8
Product carbon footprint [t CO_2e/t product]	2.977	1.887

Table V.

Chemical and physical properties of the standard MgO-C and Circular-MgO-C bricks, with the same raw material basis, tested in the low-wear area of the steel ladle slag zone. Abbreviations include tonne of CO_2 equivalent per tonne of product (t CO_2e/t product).

	Standard MgO-C	Circular-MgO-C
MgO [wt.%]	97.0	95.9
Al_2O_3 [wt.%]	0.2	0.9
Fe_2O_3 [wt.%]	0.6	0.8
CaO [wt.%]	1.3	1.5
SiO_2 [wt.%]	0.7	0.9
C [wt.%]	12.0	12.0
Tempered:		
Bulk density [g/cm³]	3.06	3.04
Apparent porosity [vol.%]	3	4.5
Cold crushing strength [N/mm²]	50	43
Coked (1000 °C):		
Bulk density [g/cm³]	2.94	2.97
Apparent porosity [vol.%]	10.5	9.0
Product carbon footprint [t CO_2e/t product]	2.832	2.463

Figure 5.

(a) standard bricks at 73 heats and (b) Circular-MgO-C bricks at 75 heats in the slag zone of a 200-tonne steel ladle.

(a)   (b)

This steel plant operates two 340-tonne BOFs, two ladle treatment stations, one aluminothermal heating station (on average 50% of the total heats per ladle), two RH degassers (on average 50% of the total heats per ladle), and two continuous casters. The plant produces construction and automotive steel, as well as steel for domestic appliances, agribusiness, and the energy sector. The steel is 100% Al-killed and Table VI shows the chemistry of a typical steel ladle slag.

During the trials it was possible to directly compare the Circular-MgO-C and standard bricks in the same lining (Figure 6). As can be seen in Figure 6, the standard materials were installed on the right-hand side from layer 12–19 for the low-wear area, indicated in yellow (152 mm lining thickness), and layer 20–27 for the high-wear area, denoted by purple (152 mm and 178 mm lining thickness), in 180° of the ladle lining. On the opposite side of the standard material, a 180° panel of the Circular-MgO-C materials was installed in the high-wear area, marked blue, and the low-wear area, indicated in green. In total 3 trials were conducted with the circular material, and in the 3rd trial the entire slag zone (360°) was lined with Circular-MgO-C.

Figure 7 shows a direct comparison of the Circular-MgO-C and the standard MgO-C materials during a ladle campaign. As can be seen, the Circular-MgO-C behaved in a similar manner to the standard MgO-C. The target lifetime at this

Figure 7.

Steel ladle campaign showing the slag zone (high- and low-wear areas) lined with Circular-MgO-C on the left-hand side and the standard MgO-C on the right-hand side of the blue bar.

Figure 6.

Steel ladle lining setup to directly compare the Circular-MgO-C and standard MgO-C bricks.
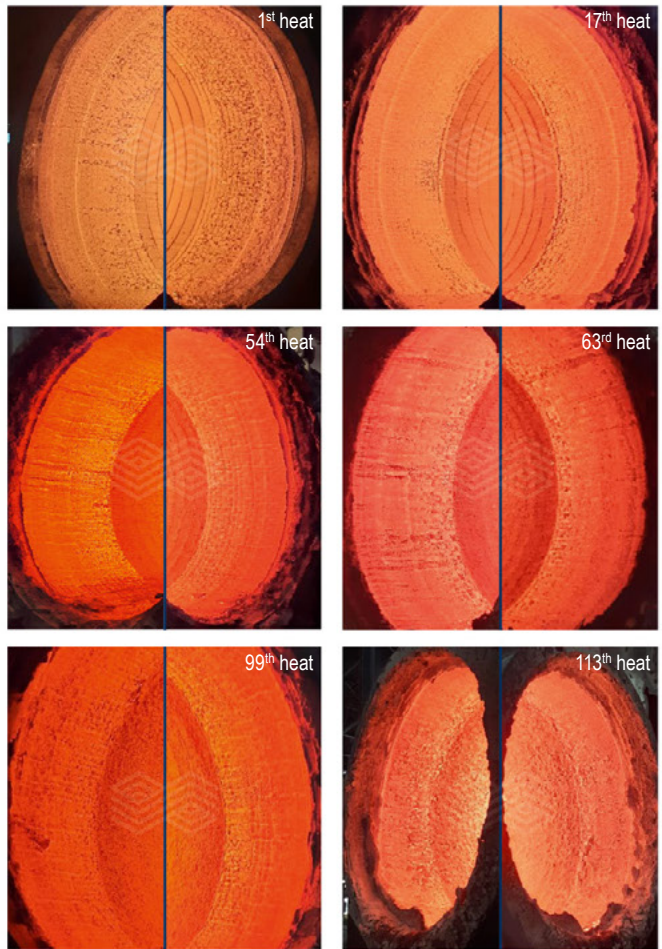
Table VI.

Example of a typical ladle slag composition during the trial period for case study 2.

	MgO [wt.%]	Al$_2$O$_3$ [wt.%]	SiO$_2$ [wt.%]	CaO [wt.%]	P$_2$O$_5$ [wt.%]	MnO [wt.%]	Fe total [wt.%]	S [wt.%]	TiO$_2$ [wt.%]	B4
Ladle slag (Al-killed)	9.61	29.85	5.19	50.45	0.08	1.45	1.18	0.16	0.29	1.71

steel plant is 120 heats for the steel ladles, which was achieved by the Circular-MgO-C bricks. Figure 8 shows a typical tear out profile of the slag zone lined with Circular-MgO-C bricks.

The average wear rates of the standard and Circular-MgO-C materials in the high-wear area were 1.04 and 1.05 mm/heat, respectively. For the low-wear area, the average wear rate for the standard material was 0.55 mm/heat, while the Circular-MgO-C in this area achieved on average 0.64 mm/heat. Since the target was 120 heats and a minimum safety thickness of 40 mm is demanded, the requirements were achieved with the Circular-MgO-C. With regards to gunning maintenance, the ladles lined with circular material in the slag zone had a specific consumption of 0.30 kg/tonne$_{steel}$ while the historical specific consumption was 0.28 kg/tonne$_{steel}$. The combination of both Circular-MgO-C bricks reduced the carbon footprint of the steel ladle slag zone by 26%. The plant has shifted to operating 25% of the steel ladle slag zones with Circular-MgO-C.

Case 3: 35-tonne EAF slag zone lined with Circular-MgO-C bricks containing 30% circular material

In the third case study, Circular-MgO-C based on a fused magnesia type with 97% MgO was tested in the slag zone of a 35-tonne EAF. The standard MgO-C material had the same fused magnesia basis. Both materials had a total carbon content of 10%. Table VII provides a comparison of the Circular-MgO-C and standard MgO-C materials, with regards to their chemistry and physical properties. The comparison in Table VII shows that in this case the differences between the standard MgO-C and Circular-MgO-C bricks were significant, not only regarding the Al_2O_3 content, but especially the bulk density and porosity. Unlike in the other 2 cases presented, the coked values of the Circular-MgO-C and the standard MgO-C material were not on a comparable level.

Figure 8.

Typical tear-out profile of a Circular-MgO-C slag zone.

Table VII.

Chemical and physical properties of the standard MgO-C and Circular-MgO-C bricks, with the same raw material basis, tested in the EAF slag zone. Abbreviations include tonne of CO_2 equivalent per tonne of product (t CO_2e/t product).

	Standard MgO-C	Circular-MgO-C
MgO [wt.%]	97.0	95.6
Al_2O_3 [wt.%]	0.5	1.5
Fe_2O_3 [wt.%]	0.6	0.7
CaO [wt.%]	1.3	1.5
SiO_2 [wt.%]	0.6	0.9
C [wt.%]	10.0	10.0
Tempered:		
Bulk density [g/cm^3]	3.14	3.05
Apparent porosity [vol.%]	3.7	5.5
Cold crushing strength [N/mm^2]	50	45
Coked (1000 °C):		
Bulk density [g/cm^3]	3.08	2.98
Apparent porosity [vol.%]	8.0	9.5
Product carbon footprint [t CO_2e/t product]	2.646	2.139

This steel plant is mainly producing stainless steel. The steel plant has two 35-tonne EAFs, one 90-tonne argon oxygen decarburization (AOD) converter, one 80-tonne oxygen blowing furnace (OBF), one 80-tonne hot metal treatment station, one 90-tonne ladle furnace, two 80-tonne vacuum oxygen decarburization (VOD) units, and two continuous casters. The EAF in this steel plant melts scrap, including ferrochrome, and feeds the AOD and OBF with this so-called premelt. A typical EAF slag composition at this plant is shown in Table VIII.

The Circular-MgO-C bricks were installed in the EAF slag zone (350 mm lining thickness), entirely replacing the standard MgO-C material in this area. Figure 9 shows this EAF slag zone in a light blue colour. In total three trial campaigns were run with the Circular-MgO-C material and after each campaign the remaining brick thickness was measured during the wrecking (Figure 10). The minimum lifetime requirement at this EAF plant is 600 heats and the Circular-MgO-C containing vessels achieved on average 680 heats. The wear rate of the standard MgO-C material was on average 0.17 mm/heat, whereas the Circular-MgO-C material achieved an average of 0.19 mm/heat. Furthermore, the gunning maintenance for the 3 trial campaigns was not increased. By using the Circular-MgO-C material, the carbon footprint of the slag zone was reduced by 19% and the steel plant has already switched one EAF entirely to the Circular-MgO-C bricks in the slag zone.

Figure 10.

(a–b) dismantling the EAF refractory lining and (c–e) wear rate measurements of the slag zone Circular-MgO-C bricks.

Table VIII.

Example of a typical EAF slag composition during the trial period for case study 3.

	MgO [wt.%]	Al$_2$O$_3$ [wt.%]	SiO$_2$ [wt.%]	CaO [wt.%]	Cr$_2$O$_3$ [wt.%]	MnO [wt.%]	FeO [wt.%]	B4
EAF slag	12.08	11.09	29.38	40.78	3.61	1.31	1.75	1.31

Figure 9.

35-tonne EAF refractory lining design with the Circular-MgO-C bricks in the slag zone indicated with a light blue colour.
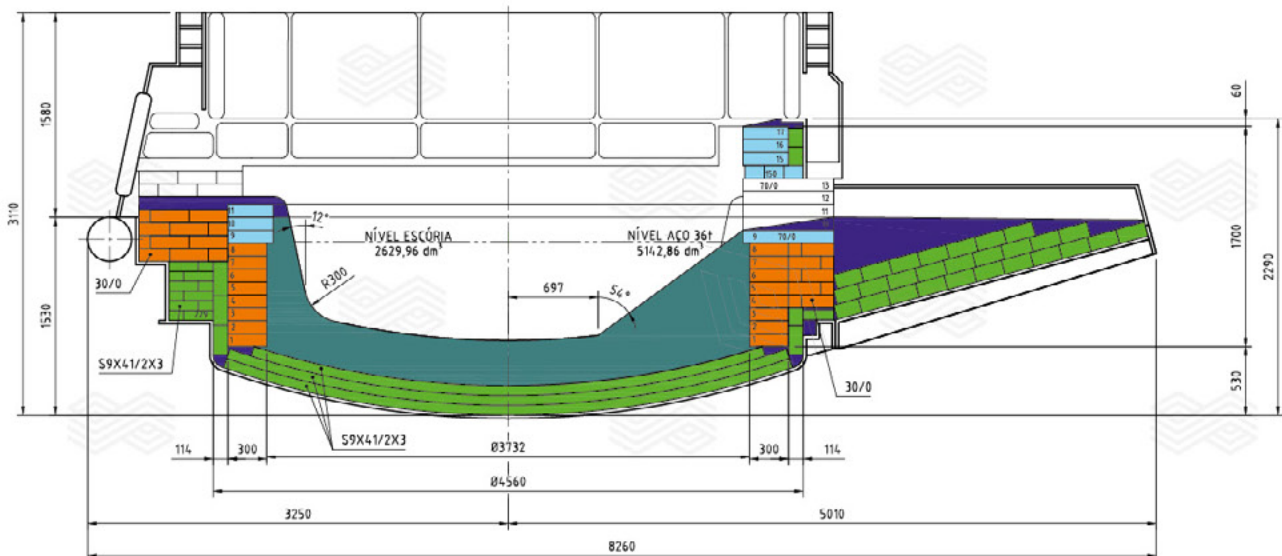
Summary and Conclusion

In this article, three different case studies have been presented where standard MgO-C was replaced by Circular-MgO-C bricks in high-wear areas. The trials covered different steel plants and applications (i.e., EAF and steel ladle), including Al- and Si-killed steels. In all cases, the Circular-MgO-C material significantly reduced the carbon footprint while achieving comparable wear rates to the standard material, even in highly aggressive environments. Furthermore, the Circular-MgO-C has replaced the corresponding standard MgO-C materials for regular production. The global success of these new types of high-performance Circular-MgO-C bricks is mirrored in the development of shipments (Figure 11). From 2020 to the end of 2023, the volumes sold have steadily increased and the share of total global sales for these high-performance Circular-MgO-C will reach 20% in 2024. It is expected that this trend will further accelerate globally, with the increasing need to reduce CO_2 emissions, avoid landfilling, and additional costs for storage and logistics of spent refractory materials.

In conclusion, the trials described in this article demonstrate that MgO-C bricks based on circular raw materials are suitable for high-wear areas and aggressive environments. Furthermore, even with a circular raw 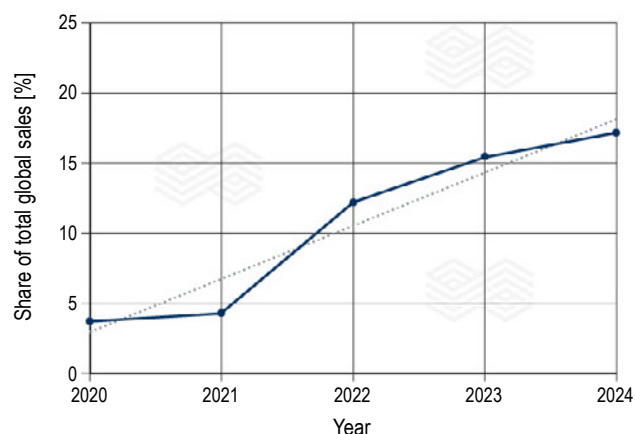material content of up to 30%, the latest generation of Circular-MgO-C bricks developed by RHI Magnesita achieves performance comparable to standard MgO-C material, along with significant CO_2 savings.

Figure 11.

Increased global sales of high-performance Circular-MgO-C bricks since 2020 (solid line) and the average share of total global sales (dotted line).

References

[1] Horckmans, L., Nielsen, P., Dierckx, P. and Ducastel, A. Recycling of Refractory Bricks Used in Basic Steelmaking: A Review. *Resources, Conservation and Recycling*. 2019, 140, 297–304.

[2] Moritz, K., Dudczig, S., Endres, H.G., Herzog, D., Schwarz, M., Schöttler, L., Veres, D. and Aneziris, C.G. Magnesia-Carbon Refractories from Recycled Materials. *International Journal of Ceramic Engineering & Science*. 2022, 4, 53–58.

[3] https://www.rhimagnesita.com/our-sustainability/

[4] RHI Magnesita 2023 Sustainability Report. https://www.rhimagnesita.com/wp-content/uploads/2024/04/rhim-sustainability-report-2023-final-2.pdf

[5] Ludwig, M., Śnieżek, E., Jastrzębska, I., Prorok, R., Sułkowski, M., Goławski, C., Fischer, C., Wojteczko, K. and Szczerba, J. Recycled Magnesia-Carbon Aggregate as the Component of New Type of MgO-C Refractories. *Construction and Building Materials*. 2021, 272, 121912.

[6] Moritz, K., Kerber, F., Dudczig, S., Schmidt, G., Schemmel, T., Schwarz, M., Jansen, H. and Aneziris, C.G. Recyclate-Containing Magnesia-Carbon Refractories – Influence on the Non-Metallic Inclusions in Steel. *Open Ceramics*. 2023, 16, 100450.

[7] Kunanz, H., Nonnen, B., Kirowitz, J. and Schnalzger, M. Successful Implementation of a High Recycling Containing Magnesia-Carbon Brick in Steel Ladles. *Bulletin*. 2022, 17–20.

[8] Moraes, M., Leitner, A., Nogueira, G., Zocratto, B., Heid, S. and Mühlhäußer, J. Technical Challenges for Refractory Recycling and Innovative Processing Solutions. *Bulletin*. 2023, 33–38.

[9] Joos-Bloch, M., Rechberger, L., Haider, C., Moulin-Silva, W., Wucher, J. and Drnek, T. Product Carbon Footprint of Refractory Products. *Bulletin*. 2023, 39–44.

Authors

Kevin Christmann, RHI Magnesita, Wiesbaden, Germany.
Bernd Neubauer, RHI Magnesita, Leoben, Austria.
Hartwig Kunanz, RHI Magnesita, Leoben, Austria.
Xiang Yong Li, RHI Magnesita, Dalian, China.
Lin Zhang, RHI Magnesita, Dalian, China.
Weizhen Xiong, RHI Magnesita, Dalian, China.
Walter De Queiroz Cassete, RHI Magnesita, Contagem, Brazil.
Leandro Rocha Martins, RHI Magnesita, Contagem, Brazil.
Gabriela Ladeira Fajardo, RHI Magnesita, Contagem, Brazil.
Corresponding author: Kevin Christmann, Kevin.Christmann@rhimagnesita.com

Return to Content

Luca Folco and Alan Kranjc

Steel Ladle Lining Management: A Comparison Between Different Maintenance Technologies to Increase Performance, Reduce Refractory Consumption and Waste Disposal of Used Materials

Optimum management of steel ladles plays a crucial role for efficient and sustainable steel production. Regarding ladle wear linings, steelmakers typically have two main approaches. The most common is a fully bricked lining, offering advantages such as slag and high-temperature resistance, along with reliable campaign lifetimes. An alternative, which has demonstrated many benefits in recent years, is monolithic technology based on alumina spinel. However, whichever lining concept is used, performance can be further improved with intermediate repairs of high-wear areas using shotcrete. This article presents results collected over multiple years at different steelworks, all of which benefited from this type of repair method. For example, savings in the quantity of refractories used were observed, as well as reductions in waste and CO_2 emissions.

Introduction

Over many years, ample proof has accumulated that zoning different areas of the steel ladle with specific refractory materials is the most effective and safe approach to optimise service life. Currently, steelmakers generally rely on one of two concepts for the ladle refractory wear lining. While the majority trust bricks, which provide good high-temperature resistance, excellent slag protection, easy heat up, and reliable service life, others have already switched to monolithic solutions based on alumina spinel, with high thermal stability, good hot strength, excellent resistance to thermal spalling, as well as low carbon pickup and decreased thermal conductivity, which are important for the production of ultra low carbon steels and energy saving, respectively. However, since both concepts see uneven refractory wear in different zones, repair of these regions with sprayable materials has emerged as a solution to increase the number of heats before complete relining is required.

Comparison of Two Standard Lining Concepts

Steel ladles play a critical role in steel production, serving as vessels for transporting and refining steel through various stages of secondary metallurgy. The refractory lining of these ladles is subjected to chemical, thermal, and mechanical wear. For these reasons, it is essential to carefully select the type of refractories, installation technique, and maintenance to provide as long a service life as possible. Due to the wide-ranging requirements, there is no one-size-fits-all solution. Steel shop managers need to balance different parameters, such as durability, balanced performance, low consumption, resistance to slag attack, safety, ease of installation, quick heating up, capacity optimisation, insulation properties, flexibility, and cost

effectiveness. Finding the best compromise among these complex requirements is a continuous challenge. While MgO-C bricks have long been favoured for the ladle wear lining, due to their high-temperature resistance and reliable service life, the steel industry is increasingly recognising the potential of alumina spinel monolithic refractories. For example, research conducted over two decades ago revealed that these monolithic products not only compete with traditional lining materials, but also offer additional benefits, such as increased ladle capacity and reduced thermal losses [1].

Recent reports and articles have further supported these findings, highlighting the advantages of alumina spinel monolithic refractories [2–5]. Lower operating costs and improved consistency in the steel carbon content, make these refractories appealing to steelmakers seeking enhanced efficiency and higher quality steel production. Furthermore, transitioning from MgO-C bricks to alumina spinel monolithic refractories can contribute to a reduction in CO_2 emissions, both during refractory production and operation, making them an environmentally sustainable choice. Another advantage of monolithic refractories is their ability to minimise waste generation by enabling targeted repairs instead of complete demolition and relining, thereby optimising resource utilisation in the steelmaking process.

Introduction to Cyclic Shotcrete Repair

A previous article presented at the 63rd International Colloquium on Refractories showcased an innovative cyclic shotcrete repair technique for steel ladle management [6]. The following summary provides an overview of the repair cycle and calculations for long-term analysis after multiple years in use. Cyclic shotcrete repair involves applying protective layers of monolithic castable onto an existing brick

lining in a repetitive manner. By combining the advantages of monolithic and brick linings, this method offers a flexible and reliable solution for ladle lining repair.

The shotcrete technique, known for its flexibility and ability to create refractory linings with similar technical features as traditional casting methods, is utilised in this application. A castable mix is sprayed at high pressure onto the surface, where it rapidly sets, allowing for targeted repairs without complete demolition and relining. A comparison between the typical brick lining cycle and the cycle with shotcrete repair reveals the advantages of shotcrete application (Table I). Without steel zone repair, the slag line can only be replaced once before complete relining becomes necessary. However, with shotcrete repair in the steel zone, the slag line can be changed multiple times before complete relining is required.

The shotcrete application extends the ladle campaign life, reduces specific consumption and costs, while maintaining the use of traditional brick linings. Specifically, wear occurs to the shotcrete layer, while the original bricks remain intact. This technology offers significant benefits, including prolonged ladle campaign life, easy visual wear control, and reduced refractory lining waste. As a result, it leads to substantial reductions in specific refractory consumption and operational costs without compromising the ladle availability, reliability, and safety.

Analysis of Long-Term Cyclic Shotcrete Repair

Shotcrete repair is a standard maintenance solution, applied in numerous steelworks (Figure 1). The increased number of ladles repaired in this way has led to optimised cleaning techniques, installation, and heating curves, resulting in more reliable ladle management. This section presents long-term cyclic shotcrete repair results obtained from two steelworks. On average, the slag line bricks at Steelworks 1 were replaced after approximately 40 heats. The ladle then continued to operate for another 40 heats. However, at around 82 heats, the bricks in the steel zone became too worn to complete another slag zone cycle, resulting in the complete demolition of the ladle. In the new campaign life cycle, the introduction of two shotcrete repairs in the steel zone and two slag zone brick replacements has extended the ladle's campaign life by 50% (Table II).

Table I.

Comparison of a standard steel ladle life cycle and one with shotcrete repair.

	Standard procedure	Shotcrete repair procedure
1	• Complete new brick lining	• Complete new brick lining
2	• 1st part of the campaign • Number of heats = N1	• 1st part of the campaign • Number of heats = N1
3	• Ladle out of service • Replace the slag zone bricks	• Ladle out of service • Replace the slag zone bricks • Clean the application surface • Shotcreting on the steel zone brick lining • Heating up
4	• 2nd part of the campaign • Number of heats = N2	• 2nd part of the campaign • Number of heats = N2
5	• Ladle out of service • Total brick lining demolition • Complete new brick lining installation	• Ladle out of service • Replace the slag zone bricks • Clean the application surface • Shotcreting on the steel zone brick lining • Heating up and continue campaign • Avoid total brick lining demolition and new brick lining installation

Figure 1.

Shotcrete repaired steel ladle during operation.

Table II.

Average steel ladle performance without and with shotcrete repair at Steelworks 1 and 2.

Steel producing plant	Steelworks 1	Steelworks 2
Steel ladle capacity [tonnes]	350	160
No. of ladle campaigns (2020–2023)	350	690
Quantity of bricks for steel zone [tonnes]	26.5	16.0
Quantity of bricks for slag zone [tonnes]	14.3	6.3
Average quantity of shotcrete material per repair [tonnes]	4	3
Lifespan of slag line (heats)	40	60
No. of heats without shotcrete repair	82	100
No. of heats with 2 shotcrete repairs	123	185

Typically, the slag line bricks in Steelworks 2 were replaced after approximately 60 heats and the ladle was operated for a further 40 heats. However, at approximately 100 heats, the steel zone bricks became very worn, resulting in complete wear lining demolition. In the new campaign life cycle, implementing two repairs in the steel zone and two slag zone brick replacements has increased the ladle's campaign to an average of 185 heats, representing a 85% increase (see Table II). Using this data, the specific refractory consumption for the steel ladle walls per tonne of produced steel was calculated (Tables III and IV).

Using the annual steel production figure of 3.5 million tonnes at Steelworks 2, the number of ladle wear linings required per year was calculated. This enabled the annual amount of refractories needed for the steel ladle wall to be estimated for the standard practice and with shotcrete repair, and from this figure the amount of refractory waste, considering the ladle is demolished when the bricks reach 30% of their original thickness. These numbers reflect significant savings in refractory costs, increased steel ladle availability, reduced refractory waste, and lower CO_2 equivalent (CO_2e) emissions coming from refractory production when shotcrete repair is used. The latter was calculated assuming average cradle-to-gate product carbon footprints [7] of 2.472 and 1.344 tonne $CO_2e/tonne_{refractory}$ for the bricks and monolithic, respectively (Table V and VI).

Table III.

Specific refractory consumption ($kg_{refractory}/tonne_{steel}$) for the ladle walls at Steelworks 1 without and with shotcrete repair.

Steelworks 1 ladle capacity	350 tonnes	
Steel zone lining maintenance	Standard practice	Shotcrete repair
Quantity of produced steel [tonnes]	28700	43050
Tonnage of refractories used [tonnes]	55.1	77.4
Specific refractory consumption [$kg_{refractory}/tonne_{steel}$]	1.92	1.80

Table IV.

Specific refractory consumption ($kg_{refractory}/tonne_{steel}$) for the ladle walls at Steelworks 2 without and with shotcrete repair.

Steelworks 2 ladle capacity	160 tonnes	
Steel zone lining maintenance	Standard practice	Shotcrete repair
Quantity of produced steel [tonnes]	16000	29600
Tonnage of refractories used [tonnes]	28.6	40.9
Specific refractory consumption [$kg_{refractory}/tonne_{steel}$]	1.79	1.38

Table V.

Calculated annual figures for the number of ladle wear linings, refractory tonnage for the ladle side wall, refractory waste, and CO_2e emissions in Steelworks 2. The refractory production related CO_2e emissions were calculated assuming average cradle-to-gate product carbon footprints of 2.472 and 1.344 tonne $CO_2e/tonne_{refractory}$ for the bricks and monolithic, respectively.

Annual steel production	3.5 million tonnes	
Steel ladle capacity	160 tonnes	
Steel zone lining maintenance	Standard practice	Shotcrete repair
No. of ladle wear linings per year	219	118
Annual quantity of refractories [tonnes]	6256	4836
Annual refractory waste [tonnes]	1877	1238
Annual refractory production related CO_2e emissions [tonnes]	21450	15720

Table VI.

Yearly savings calculated for Steelworks 2 using shotcrete repair compared to the standard practice.

	Annual saving [%]
No. of ladle wear linings	46.1
Used refractories	22.7
Refractory waste	34.0
CO_2e emissions	26.7

New Installation Method—SHOTGUN

Shotcreting is a versatile monolithic application technique where a castable mix is sprayed onto a surface at high pressure, rapidly setting in place. It offers exceptional flexibility, allowing it to be used in various locations regardless of complex geometries. Crucially, shotcreting achieves refractory linings with comparable technical features to traditional vibrating casting methods, particularly in terms of mechanical parameters. However, shotcrete is typically not used for small repairs due to the higher equipment cost, longer preparation time, and increased cleaning requirements after installation. These limitations are easily overcome by larger steelworks where the number of steel ladles and the quantity of installed material are high, and top-of-the-line performance is expected. On the other hand, for smaller steel mills, these limitations can be a dealbreaker, hindering them from modernising their steel ladle management. To assist them in moving into the greener future, a new installation technique and material that enables utilisation of gunning machines to apply similarly performing material as shotcrete have been developed. A schematic of this SHOTGUN system, which includes a modified gunning machine, high-pressure water pump, compressed air source, accelerator pump, and a special SHOTGUN nozzle (Figure 2), is depicted in Figure 3 [8].
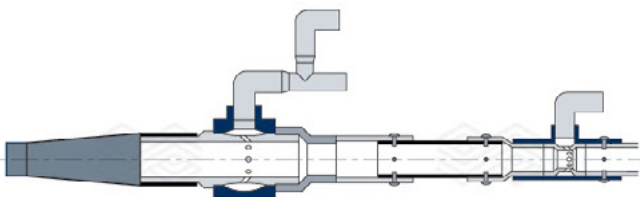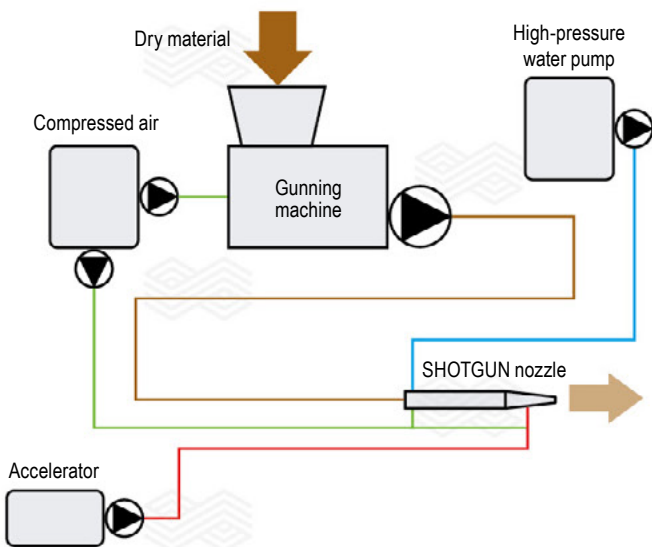
This system eliminates the need for a planetary mixer and shotcrete pump, which take up a lot of space and are costly, while also significantly reducing setup time and manpower. Since water is added at the nozzle, there is no need to clean the pipes, and no material is wasted that would normally remain in the mixer, pump, and pipes. As the existing shotcrete material (e.g., SEVEN SHOT 92 NR 08 Z) was not fully compatible with the new installation system, which requires a material that is dry pumpable without separation and can be wetted out in a short amount of time, the particle size distribution and additives were modified, giving rise to a new family of SEVEN SHOTGUN products.

A comparison of the SEVEN SHOT 92 NR 08 Z and SEVEN SHOTGUN 92 NR 08 Z physical properties shows that both have high cold crushing strength (CCS) values, especially at operating temperatures (Figure 4). Furthermore, the permanent linear change (PLC) is relatively constant for both products and far from the critical value of -1.5% (Figure 5). Although SEVEN SHOTGUN 92 NR 08 Z has slightly lower CCSs, the values are still sufficiently high, and the less negative PLC reduces the stress experienced by the material.

Figure 2.
New SHOTGUN nozzle.

Figure 3.
Schematic of SHOTGUN system.

Figure 4.

Comparison of the CCS for SEVEN SHOT 92 NR 08 Z and SEVEN SHOTGUN 92 NR 08 Z.
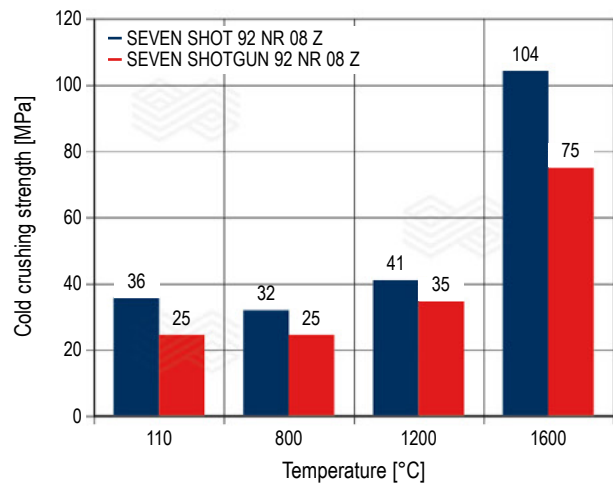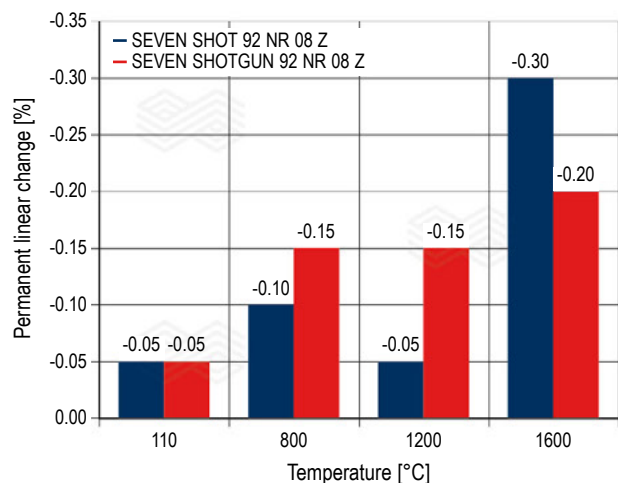

Figure 5.

Comparison of the PLC for SEVEN SHOT 92 NR 08 Z and SEVEN SHOTGUN 92 NR 08 Z.

Industrial Trials of SHOTGUN at Steelworks 3

At Steelworks 3, a bottleneck during the standard campaign was wear in the ladle steel zone lining. The application of SEVEN SHOTGUN 92 NR 08 Z during replacement of the slag zone bricks extended the campaign until the bottom and slag zones became limiting factors for the steel ladle's life cycle. This has been confirmed in several steel ladle campaigns. With this solution, all zones reach their end of life at the same time, which is a crucial parameter in economical calculations for all refractory linings and significantly reduces the amount of wasted material.

Conclusion

Shotcrete repair has proven to be an effective solution to improve steel ladle performance. These repairs extend the ladle service life, reduce waste, and decrease refractory consumption per tonne of steel. As a result, operating costs are lowered, and the environmental impact is reduced. Furthermore, the repair process helps equalise the life cycles of different zones within the ladles, resulting in further refractory waste reductions.

The introduction of the new SHOTGUN solution has made these benefits more accessible and easier to implement. Laboratory tests have shown only minimal reductions in physical values of the SEVEN SHOTGUN 92 NR 08 Z compared to the standard shotcrete material, ensuring high-quality repairs and the feedback from initial field trials has been positive. It is expected that this solution will be particularly useful for smaller steel mills seeking to optimise their steel ladle performance. RHI Magnesita is confident that further industrial trials will establish SHOTGUN as a reliable installation technique, enabling steel producers to transition towards a greener and more efficient future.

References

[1] Buhr, A. Refractories for Steel Secondary Metallurgy. *CN-Refractories*. 1999, 6(3), 19–30.

[2] Vatanen, J. Monolithic Ladle Lining in a 3-Converter-Shop. Presented at Steel Academy's 12th International Seminar on Refractory Technology: Steel Ladle Lining, Concepts for a Complex Reactor. Bonn, Germany, September 14–16, 2022.

[3] Siebring, R. Economics in Refractory Usage. Presented at Steel Academy's 12th International Seminar on Refractory Technology: Steel Ladle Lining, Concepts for a Complex Reactor. Bonn, Germany, September 14–16, 2022.

[4] Buhr, A. Trends in Clean Steel Technology and Steel Ladle Lining. Presented at Steel Academy's 12th International Seminar on Refractory Technology: Steel Ladle Lining, Concepts for a Complex Reactor. Bonn, Germany, September 14–16, 2022.

[5] Akselrod, L.M. and Garten, V. An Alternative Lining of Steel Ladles: Technical and Economic Aspects. *Ferrous Metallurgy Bulletin of Scientific Technical and Economic Information*. 2018, 12, 72–80.

[6] Copetti, G. and Folco, L. Steel Ladle Management: An Integrated View of the Challenges in Resistance, Environmental Impact, and Economic Issues. Presented at 63rd International Colloquium on Refractories (ICR 2020). Aachen, Germany, September 16–17, 2020.

[7] Joos-Bloch, M., Rechberger, L., Haider, C., Moulin-Silva, W., Wucher, J. and Drnek, T. Product Carbon Footprint of Refractory Products. *Bulletin*. 2023, 39–44.

[8] European patent EP 3 858 491 A1. International publication number WO 2020/040665.

Authors

Luca Folco, RHI Magnesita, Divaca, Slovenia.
Alan Kranjc, RHI Magnesita, Divaca, Slovenia.
Corresponding author: Luca Folco, Luca.Folco@rhimagnesita.com

Return to Content

Florian Kek, Andreas Horn, Paulo Souza, Francisco Lopez, Nikolaus Lechner and Patrick Stahl

Green Steel Initiatives Supported by Enhanced Slag Engineering Using High-Alumina Circular Metallurgical Additives

Desulphurisation in the steel ladle requires a reactive slag with high CaO dissolution. Conventional slag fluxing agents applied during this secondary metallurgical refining step include calcium aluminate additives and fluorspar to maximise the dissolved CaO. However, calcium aluminate additives can have a high carbon footprint due to their energy-intensive production process and the use of fluorspar is associated with both environmental concerns and refractory wear. Stahlwerk Thüringen (Germany) is committed to sustainability, with a green steel strategy that includes reducing resource use and implementing stepwise improvements in process efficiency. To support these initiatives, RHI Magnesita and MIRECO conducted an industrial feasibility study to determine if typical fluxes used during steel desulphurisation in the ladle could be replaced by a high-alumina circular metallurgical additive derived from recycled refractory material. This article describes the metallurgical consulting provided by RHI Magnesita during the trial series, as well as the e-tech slag engineering tools that were used for efficiency optimisation calculations and enabled an appropriate balance between desulphurisation rate, additive application, slag volume, and purging gas consumption to be determined. Furthermore, extensive steel and slag sampling was performed, and the chemical and mineralogical results enabled an in-depth evaluation of the metallurgical process during the sequential replacement of calcium aluminate and fluorspar with a cost-effective, low carbon footprint slag fluxing agent.

Introduction

Stahlwerk Thüringen (SWT) is a steel plant in Germany with an annual capacity of approximately 1 million tonnes of high-quality steel. As part of CSN (Brazil), the steel plant comprises an electric arc furnace (EAF), ladle furnace (LF), four-strand beam-blank caster, and a rolling mill. It operates at 120 tonnes of steel per heat and an average of 24 heats a day. 100% scrap is charged in two buckets during each heat and the quality varies considerably, depending on availability and price. Slag forming agents such as lime and dololime are added during the meltdown phase via a hole in the EAF roof. The average tap-to-tap time is up to 50 minutes and the EAF is relined 4 times a year. During EAF tapping, deoxidisers and slag forming additives such as CaO, Al_2O_3-containing materials, and CaF_2 are added to form calcium aluminate and calcium aluminosilicate-based slags. The LF treatment lasts up to 40 minutes, during which time the metallurgical specifications of the steel are adjusted accordingly. Typically, SWT produces steel grades with a sulphur content not exceeding 300 ppm as well as low-sulphur grades with <50 ppm of sulphur.

Sustainability is key to SWT and their Green Steel Strategy includes three pillars: Energy, logistics, and efficiency [1]. For example, 100% of the plant's electrical energy comes from renewable sources, rail transport is prioritised, and energy efficiency is continually improved. As a result, SWT Green Steel had a global warming potential of 335 kg CO_2 equivalent per tonne of steel (CO_2e/tonne_{steel}) in 2024, according to their Environmental Product Declaration [2], making SWT one of the most sustainable steel plants in Europe [3].

In line with the steel plant's strong commitment to reduce the carbon footprint of its products, improve efficiency, and mitigate environmental impact, several trials were conducted with the full support of RHI Magnesita and MIRECO. In the EAF, this resulted in replacing the standard slag former with a circular metallurgical additive to achieve financial savings and CO_2 cradle-to-gate reductions per tonne of steel (i.e., ~10 kg CO_2e/tonne_{steel}), as well as determining areas for improvement that will increase the yield. Additionally, the secondary metallurgical process in the LF was evaluated and the following opportunities were identified:

- Replace the standard calcium aluminate additive with a low carbon footprint, high-alumina circular metallurgical additive.
- Eliminate the use of CaF_2 because it can cause environmental issues related to slag leaching and is detrimental for the refractory lining.
- Improve desulphurisation efficiency.
- Reduce alloy addition.

This article provides an overview of secondary metallurgy in the LF, comparison of a high-alumina circular metallurgical additive and calcium aluminate flux, in addition to describing the trial program that resulted in a more sustainable LF process and cost savings for the plant.

Secondary Metallurgy and Slag Forming Additives

Secondary metallurgy is the steel production stage that starts with tapping the furnace into the ladle and continues until the ladle reaches the continuous casting platform. Within this period, the steel is refined and alloyed to achieve the targeted chemical composition and required casting temperature [4,5]. During the tapping phase, most steel grades are deoxidised with metallic aluminium, silicon, or both, forming Al_2O_3 and SiO_2, depending on the chosen deoxidiser. However, these oxides must be counterbalanced with metallurgical additives to achieve the required

steelmaking slag properties (e.g., basicity and viscosity) and to avoid refractory wear. Typically, using the mixing force of the tapping stream, this process starts with the addition of CaO, and dololime if MgO is required, followed by various fluxing agents (e.g., $CaAl_2O_4$, Al_2O_3, FeSi, and CaF_2), according to the targeted steel grade.

Sulphur is undesirable in almost every steel grade because it makes steel extremely brittle and can cause transverse cracking during casting [6]. Low sulphur contents can be achieved by steel desulphurisation in the ladle when the steel is fully killed (i.e., deoxidised), according to [7]:

$$3(CaO) + 3[S] + 2[Al] = 3(CaS) + (Al_2O_3) \qquad (1)$$

Where CaO is dissolved in the slag and Al and S are present in the liquid steel.

In addition to high CaO dissolution in the slag being critical, other conditions that favour sulphur removal include [7]:

- Low FeO and MnO levels in the slag.
- Low initial sulphur content in the slag.
- Moderate temperature.
- Intense mixing of the slag and steel by argon purging.

The two common criteria used to characterise the efficiency of sulphur removal are the sulphur distribution ratio between the slag and steel at equilibrium (L_S) and the slag's sulphide capacity (C_S) [7]. The latter shows a good correlation with optical basicity over a wide range of slag compositions [8].

As CaO is the means by which sulphur is removed from steel in the ladle, liquid slags that are saturated with CaO are favourable for desulphurisation [7]. Depending on the specific slag chemistry, there are various approaches to increase CaO dissolution, including the addition of CaF_2, B_2O_3, and Al_2O_3 [9]. However, due to considerable environmental concerns associated with CaF2, the limited use of B_2O_3 to boron-containing steel grades, and the detrimental impact of both these fluxes on basic refractory wear, the addition of Al_2O_3 in sufficient amounts (i.e., 20–30%) is an established approach to dissolve CaO in the liquid portion of the slag [9].

High-Alumina Circular Metallurgical Additives

The use of MIRECO's circular metallurgical additives contributes to green steel production, as the carbon footprint of these materials, derived from recycled refractories, is significantly lower (i.e., 0.05 tonne $CO_2e/tonne_{metallurgical\ additive}$) than that of standard slag formers [10]. Furthermore, these sustainable products are distinguished by their cost competitiveness, offering a price advantage of approximately 10%. Within MIRECO's portfolio of high-quality circular raw materials, there are several different high-alumina metallurgical additives that are an environmentally friendly alternatives to standard calcium aluminate and CaF_2 flux materials (Table I). Furthermore, the chemistry of these products can be tailored to the customers' specific metallurgical requirements, and they are available in various grain size distributions. TE 80 was selected as the most appropriate material for the SWT trials and therefore analytical investigations were performed on this material and the standard calcium aluminate additive used in the plant, providing a detailed comparison.

Comparison of TE 80 and a Calcium Aluminate Additive

X-ray fluorescence (XRF), X-ray diffraction (XRD), mineralogical, and physical investigations of TE 80 and the standard calcium aluminate additive used at SWT were conducted at RHI Magnesita's Technology Center Leoben (Austria), on different grain size fractions. As detailed in Table II, the chemical composition of TE 80 was ~79% Al_2O_3 with the predominant Al-containing mineral phase comprising corundum. In addition, minor amounts of other Al-containing phases such as mullite, magnesia-alumina spinel, diaoyudaoite, anorthite, and andalusite were detected. The calcium aluminate additive had an Al_2O_3 content of ~64% and a higher CaO content compared to TE 80, with 4 mineral phases identified in the samples (i.e., calcium aluminate, grossite, magnesia-alumina spinel, and mayenite). Although corundum has a higher melting point than calcium aluminate, the good dissolution behaviour of TE 80 observed during the trials could be attributed in part due to its high specific surface area (3.59 m²/g), which was ten times greater than the standard additive (0.3 m²/g), as well as the SiO_2 content that results in lower melting point phases.

Table I.

Examples of MIRECO's high-alumina circular metallurgical additives, which can be adjusted to each customer's specifications. Abbreviations include tonnes of CO_2 equivalent per tonne of metallurgical additive (t CO_2e/t).

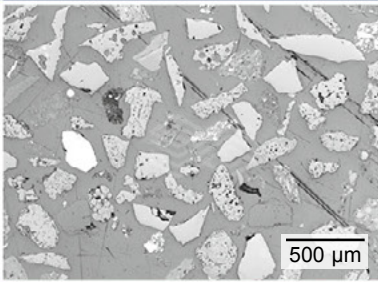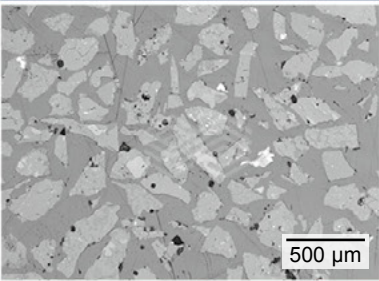| Product name	Al_2O_3 [%]	CaO [%]	MgO [%]	SiO_2 [%]	Fe_2O_3 [%]	TiO_2 [%]	C [%]	t CO_2e/t
TE 80	78.0	2.0	3.0	11.0	2.5	2.0	2.0	0.05
TE 85	85.0		2.5	7.5	0.7	0.4	6.0	0.05
TE 90	90.0	2.5	2.5	1.8	0.8	0.1		0.05

Trial Setup

The first step of RHI Magnesita's slag engineering consulting to optimise the application of circular metallurgical additives is fact-finding. At this stage, the customer's standard operating procedure (SOP) is examined, improvement potentials are identified, and proposed operating procedures (POPs) are defined to achieve benefits within short-term trials [11]. As the literature and experiences in other steel plants had shown that it is feasible to use Al_2O_3 from various sources as a flux, the first POP at SWT completely replaced the calcium aluminate additive with TE 80 but retained the standard CaF_2 addition, and slightly increased the CaO content to target the same $CaO:Al_2O_3$ in the final slag as the SOP.

During this and subsequent trials, the additives were applied during the final third of the EAF tapping procedure. Immediately after tapping, the ladle was moved to the LF where electrodes were used to increase the temperature and inert gas purging (i.e., argon stirring) was started. This further melted the slag formers and alloys as well as increased the interaction between steel and slag. After approximately 5 minutes at the LF, a Celox measurement was conducted to track oxygen activity. Subsequently, steel and slag samples were taken to check the steel chemistry and examine the initial slag composition (e.g., Al_2O_3 content and TE 80 dissolution). During the trials certain LF treatment parameters were kept stable, such as the purging rate. 10 minutes before sending the ladle to the caster another steel and slag sample were taken, enabling the steel sulphur

Table II.

Comparison of MIRECO's TE 80 circular metallurgical additive and the standard calcium aluminate used at SWT. Abbreviations include magnesia alumina (MA). The mineral phase estimates are based on Rietveld refinement.

Additive		TE 80	Calcium aluminate
Light microscopy		500 µm	500 µm
Chemical composition			
Al_2O_3 [%]		79.7	63.9
CaO [%]		2.2	30.5
MgO [%]		3.8	3.9
SiO_2 [%]		10.4	1.1
Fe_2O_3 [%]		2.1	0.3
TiO_2 [%]		1.0	0.1
Cr_2O_3 [%]		0.5	0.1
MnO [%]		0.1	0.1
ZrO_2 [%]		0.3	
Mineral phase analysis			
Calcium aluminate	$CaAl_2O_4$ [%]		56
Grossite	$CaAl_4O_7$ [%]		26
Mayenite	$Ca_{12}Al_{14}O_{33}$ [%]		5
MA-spinel	$MgAl_2O_4$ [%]	4	14
Corundum	Al_2O_3 [%]	69	
Mullite	$Al_6Si_2O_{13}$ [%]	11	
Diaoyudaoite	$NaAl_{11}O_{17}$ [%]	3	
Anorthite	$CaAl_2Si_2O_8$ [%]	3	
Periclase	MgO [%]	3	
Cristobalite	SiO_2 [%]	1	
Andalusite	Al_2SiO_5 [%]	2	
Quartz	SiO_2 [%]	1	
Silicon carbide	SiC [%]	1	
Physical properties			
Bulk weight [g/l]		1364	1243
Specific surface area [m²/g]		3.59	0.30

content to be determined and the slag evolution to be tracked. After sampling, CaSi wire injection was started and the ladle was sent to the caster. Since CaSi treatment serves as the last desulphurisation step, a steel sample was also taken at the tundish and the results were incorporated into the trial evaluation. Figure 1 provides a schematic overview of the secondary metallurgical process and the slag and steel sampling points during the trials.

Trial Results

Results of the first trial showed that an equivalent desulphurisation efficiency could be achieved when TE 80 replaced the standard calcium aluminate additive. Therefore, further trials were conducted in which TE 80 completely replaced the calcium aluminate and the CaF_2 was decreased to zero in a stepwise manner. Additional TE 80 and CaO were added to maintain a similar slag $CaO:Al_2O_3$ as the SOP.

XRF and XRD investigations were performed on all the slag samples at the Technology Center Leoben. These analyses were evaluated in combination with heat report figures, steel chemistry results, and the Celox analysis to provide an in-depth picture of the desulphurisation efficiency, average treatment time, inert gas purging and power-on times, as well as the temperature at the beginning and end of the LF treatment.

By observing the final slag composition and steel sulphur content, it was concluded that TE 80 dissolved appropriately in the slag and provided the necessary fluxing effect to achieve the same desulphurisation efficiency in the ladle as the calcium aluminate additive. Furthermore, the

step-by-step elimination of CaF_2 caused no significant change in the slag's desulphurisation capacity. These outcomes demonstrated that it is technically feasible to replace the standard calcium aluminate with a circular metallurgical additive and that CaF_2 can be completely avoided by using TE 80, even for low sulphur steel grade production. A total cost of ownership (TCO) calculation revealed that a six-digit annual saving in euros could be achieved by introducing TE 80 in the plant, as well as CO_2 cradle-to-gate reductions per tonne of steel (i.e., ~1 kg CO_2e/tonne$_{steel}$), potential lining wear decrease, and the avoidance of ground water pollution from slag containing fluorine.

Having established the parameters to achieve cost savings at SWT using a low carbon footprint slag fluxing agent, the possibility for additional process improvements, including increasing the desulphurisation rate, became apparent after onsite fact-finding and slag modelling. As a result, SWT requested efficiency optimisation calculations to be performed, based on the eco-friendly process parameters, to determine the most appropriate balance between the desulphurisation rate, amount of additive application (e.g., CaO), slag disposal costs, and purging gas consumption. This was performed with the support of RHI Magnesita's e-tech slag modelling tools described in the following sections. The resulting parameters significantly decreased the final sulphur content within the same treatment time, optimised the slag towards CaO saturation, and increased the inert gas purging rate. Although these conditions lead to increased costs regarding CaO use, slag disposal, and argon consumption, the TCO calculation indicated that an additional six-digit annual saving in euros could be achieved due to the decreased alloy requirement, bringing the combined potential savings to over €1 million per year.

Figure 1.

Schematic overview of the secondary metallurgical process and the slag and steel sampling points during the trials.
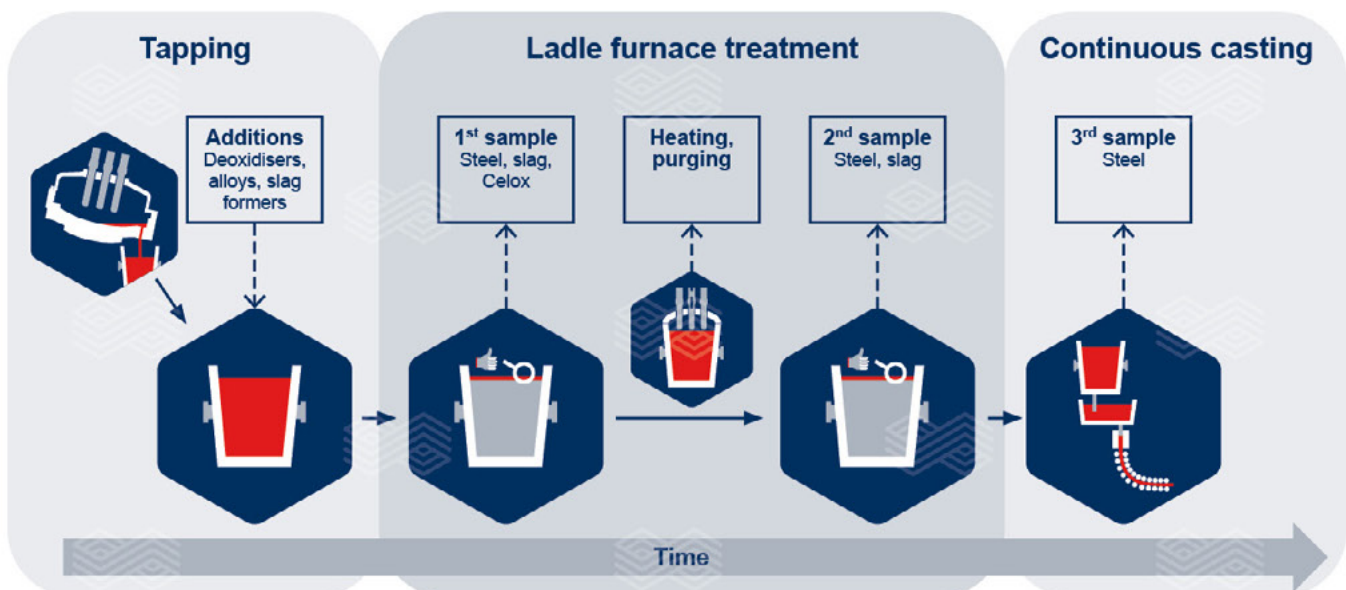
Desulphurisation Slag Modelling Tools

The e-tech platform is a collection of online slag modelling tools available in RHI Magnesita's Customer Portal [12], the secure online environment enabling access to data including order tracking, refractory performance reports, scope 3 CO_2 emissions from consumed refractory products, and gunning consumption figures [13]. The e-tech tools used to determine potential process improvements in the LF at SWT were "Slag Optimisation" and "Kinetic Desulphurisation".

Slag Optimisation Tool

The Slag Optimisation tool (Figure 2) calculates refractory compatible, fluid slags for optimised desulphurisation at specific temperatures and is applicable to magnesia-carbon and doloma refractories. It is possible to select whether the calculated slag should be CaO saturated, MgO saturated, or dual saturated. The tool is based on published phase diagrams and utilises statistical and mathematical approaches to describe the liquidus phase relationships as a function of temperature and composition for basic slags compatible with basic refractories. The Slag Optimisation tool has been designed to work with most EAF, BOF, and ladle reducing slags and utilises the concept of optical basicity and its correlation with sulphide capacity to calculate the final sulphur content in the steel. The calculated final sulphur content represents a "best case" scenario since thermodynamic equilibrium conditions are assumed and no kinetics are included. Therefore, the calculated final steel sulphur content will be achieved with the defined slag chemistry when there is sufficient time for the reactions to reach equilibrium. One output of this tool—the sulphur distribution ratio at equilibrium—is an input parameter for the Kinetic Desulfurisation tool that considers aspects such as time, kinetics, and inert gas purging during the desulphurisation process. Figure 2 shows the input mask for the Slag Optimisation tool, which can be used for both single heats and multiple heats simultaneously.

To demonstrate how the Slag Optimisation tool functions, the chemical analysis of a slag sample from the trials was

input to generate a Slag Optimisation Report (Figure 3). The output showed that the slag would require an additional 306 kg of CaO to have an optimum desulphurisation capacity. The data fields include:

- Initial slag: The chemical composition of the slag sample obtained from XRF analysis.
- Adjusted slag: Predicted slag composition if the recommended 306 kg of CaO are added.
- Desulphurisation results: The calculated slag basicity (CaO:SiO$_2$), optical basicity, sulphide capacity, sulphur distribution ratio, and the final steel sulphur content (predicted for equilibrium conditions) of the initial and adjusted slag.

Figure 3.

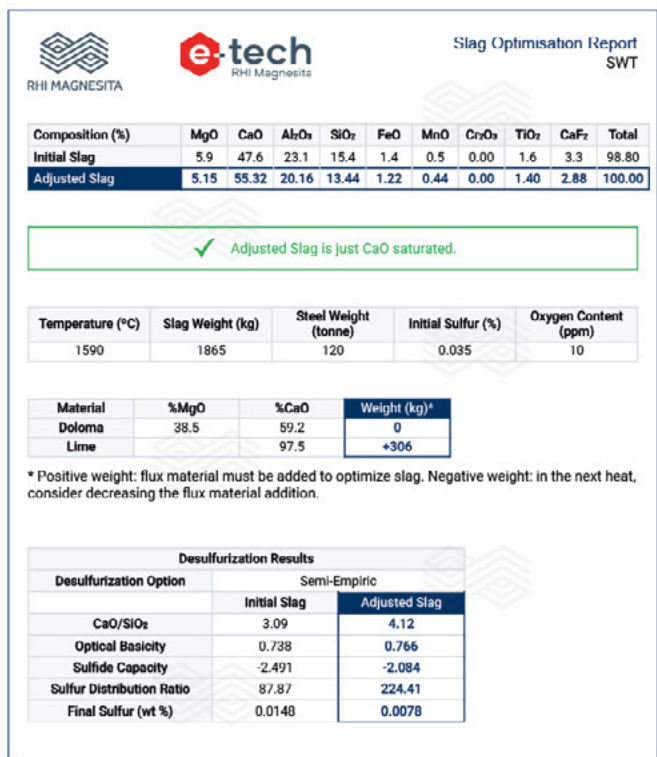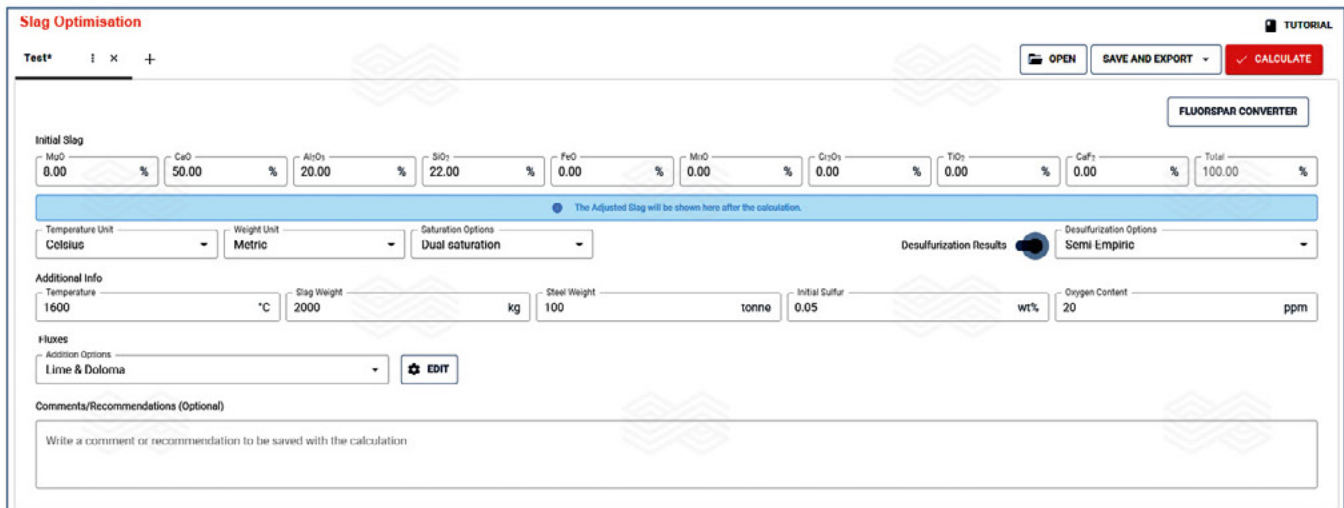**Slag Optimisation Report generated using the chemical analysis obtained for a slag sample from the trials.**

Figure 2.

e-Tech Slag Optimisation tool input mask [12].

Kinetic Desulphurisation Tool

The Kinetic Desulphurisation tool calculates the steel sulphur content at equilibrium and predicts the desulphurisation rate for specific operational parameters. The model also enables comparison of two different cases (A and B) at three time points (I, II, and III), where the time and rate of inert gas purging, slag mass, sulphur distribution ratio, and initial steel sulphur content can be varied to evaluate the effect. The kinetic calculations are based on empirical correlations published in the literature [8] and although these correlations were derived from specific conditions and are not universally applicable, they still provide a useful estimate of the sulphur removal rate and its sensitivity to specific parameters. Figure 4a shows a comparison of the steel desulphurisation rates for the initial and adjusted slags generated by the Kinetic Desulphurisation tool and Figure 4b illustrates the impact of increasing the inert gas purging rate.

In summary, this tool can be used to decrease the LF treatment time, increase the desulphurisation rate, and evaluate the impact of CaO supersaturation. Furthermore, combining both tools is an excellent approach to achieve very low steel sulphur levels in the most time- and resource-efficient manner.

Conclusion

Currently, steelmaking accounts for over 7% of global greenhouse gas emissions, highlighting the urgent need to decarbonise this industry [14]. SWT is committed to green steel production, with multiple initiatives aimed at reducing the carbon footprint of its grades, including using renewable energy sources and continual efficiency improvements. To support these efforts, RHI Magnesita and MIRECO recently conducted industrial trials to determine if traditional fluxes used for steel desulphurisation in the ladle could be replaced by a high-alumina circular metallurgical additive made from recycled refractory material. Using the comprehensive metallurgical consulting provided by RHI Magnesita, the standard calcium aluminate and CaF_2 were replaced by a circular metallurgical additive, generating both cost savings and a carbon footprint reduction. After the successful introduction of this flux material, efficiency optimisation calculations were conducted based on the newly defined eco-friendly process parameters. These calculations, performed with RHI Magnesita's e-tech slag modelling tools, were focused on determining the optimal balance between the desulphurisation rate, additive use, slag disposal costs, and purging gas consumption. As a result, the final sulphur content could be reduced within the same treatment time and potential savings of over €1 million per year were estimated from introducing the circular metallurgical additive and reduced alloy costs.

MIRECO offers a comprehensive range of sustainable additives for the steel production process, facilitating the reintegration of used refractory products into the supply and value chain. In addition to direct sales, the "CERO Waste" service is also available, enabling customers to benefit from MIRECO's expertise and implement closed-loop recycling to significantly decrease CO_2 emissions [15]. The approach complies with the European Waste Framework Directive and focuses on optimising refractory collection, material sorting, and recycling to minimise landfill (Figure 5).

Figure 4.

Comparison of the steel desulphurisation rates calculated for the initial and adjusted slags using the Kinetic Desulphurisation tool using (a) the standard argon purging rate and (b) an increased argon purging rate.
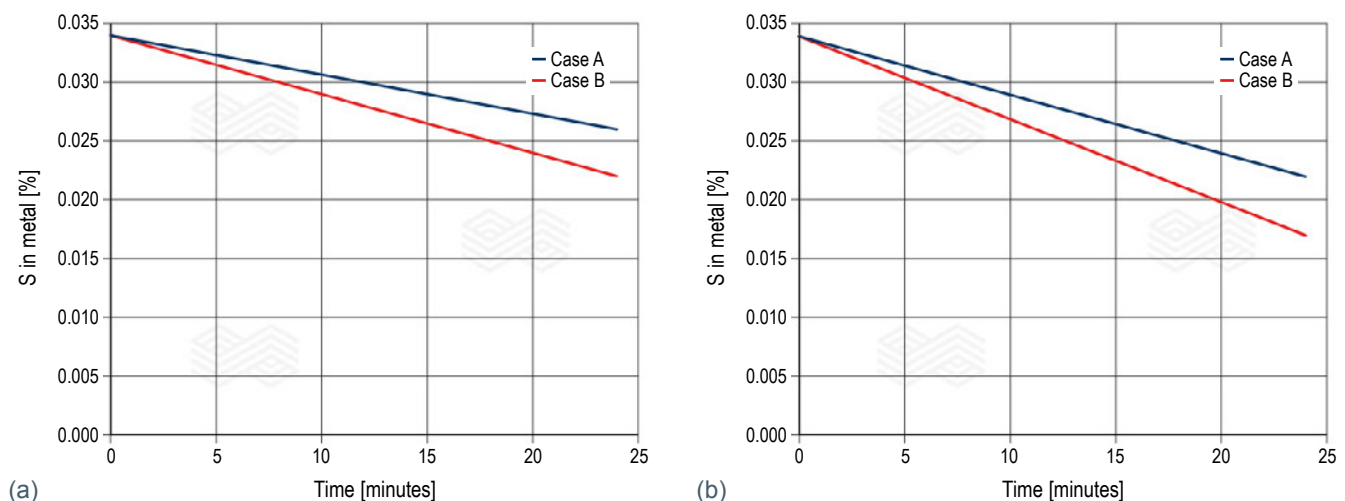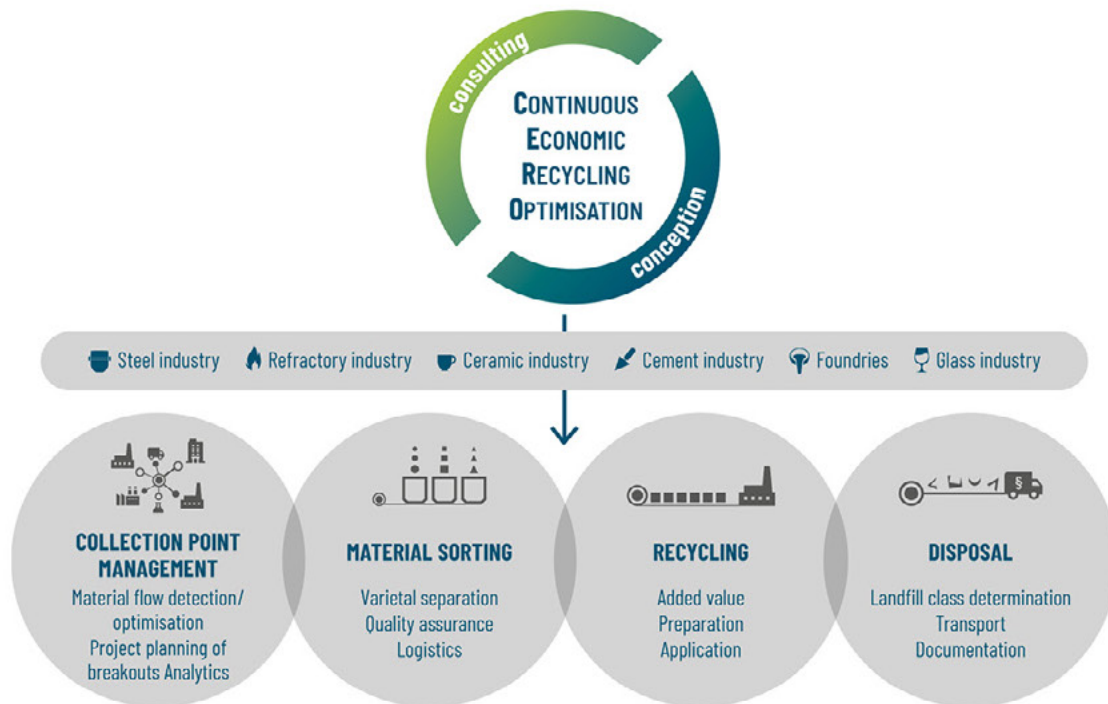

(a)

(b)

Figure 5.

Overview of the "CERO Waste" concept that encompasses the collection, sorting, reuse assessment, disposal, and legal management of reclaimed refractory material.

References

[1] https://www.greensteel-swt.com

[2] https://www.stahlwerk-thueringen.de/files/17EA0F6B493/SWT_Green_Steel_EPD.pdf?randID=1904F40D5C8

[3] https://ibu-epd.com/veroeffentlichte-epds/

[4] Stolte, G. *Secondary Metallurgy: Fundamentals, Processes, Applications*; Stahleisen: Düsseldorf, 2002.

[5] Bergmann, B. and Bannenberg, N. Schlackenführung und Schlackenoptimierung in der Sekundärmetallurgie. *Stahl und Eisen*. 1995, 111(1), 125–131.

[6] Jones, D.W. Ladle Furnace Metallurgy Course. 1997.

[7] Abraham, S.O., Wang, Y., Petty, R., Franks, T., Sprague, T., Brown, G., Woods, W., Nicholson, W., Haberkorn, M. and Bodnar, R. Slag Engineering for Phosphorus Removal in the EAF and Sulfur Removal in the Ladle. *Iron & Steel Technology*. 2020, July, 72–82.

[8] Pretorius, E. and Oltmann, H. Desulfurization. Process Technology Group, LWB Refractories. https://etech.rhimagnesita.com

[9] Pretorius, E. Can Fluorspar be Replaced in Steelmaking? Process Technology Group, LWB Refractories. https://etech.rhimagnesita.com

[10] Kek, F., Lopez, F., Kirschen, M., Souza, P. and Stahl, P. Sustainable Slag Engineering in the Basic Oxygen Furnace Using Circular Additives and Modelling Tools. *Bulletin*. 2023, 45–50.

[11] Kek, F., Griessacher, T., Bauer, C., Zocratto, B., Krump, R. and Koubek, C. Refractory Waste to Slag Engineering Solution—Metallurgical Consulting Supports Steel Plant's Circular Economy Strategy. *Bulletin*. 2022, 21–28.

[12] https://etech.rhimagnesita.com

[13] Souza, P., Freitas, C., Arth, G., Penido, G., Zettl, K., Bolognani, J., Lamare, C., Lammer, G., Moser, G. and Hoffert, A. Next Level of Digital Refractory Contracts. *Bulletin*. 2022, 52–59.

[14] Kim, J., Sovacool, B.K., Bazilian, M., Griffiths, S., Lee, J., Yang, M. and Lee, J. Decarbonizing the Iron and Steel Industry: A Systematic Review of Sociotechnical Systems, Technological Innovations, and Policy Options. *Energy Research & Social Science*. 2022, 89, 102565.

[15] https://www.mireco.com/de/cero-waste.php

Authors

Florian Kek, RHI Magnesita, Vienna, Austria.
Andreas Horn, Stahlwerk Thüringen, Unterwellenborn, Germany.
Paulo Souza, RHI Magnesita, Vienna, Austria.
Francisco Lopez, RHI Magnesita, Contagem, Brazil.
Nikolaus Lechner, RHI Magnesita, Leoben, Austria.
Patrick Stahl, MIRECO, Siegen, Germany.
Corresponding author: Florian Kek, Florian.Kek@rhimagnesita.com

Return to Content

Francesca Capó Tous, Bernd Neubauer, Laura Rechberger, Daniela Mancini Fonseca, Jürgen Schmidl and Dean Gregurek

Flexosphere Technology—Improved Flexibility and Corrosion Resistance of Fired Magnesia–Chromite Bricks

Flexospheres are a recent product development successfully implemented in fired magnesia-chromite bricks at RHI Magnesita. This technology focuses on inhibiting the corrosion mechanism and increasing flexibility of the refractory product. During development, the experimental investigations included chemical and physical analyses as well as standardised corrosion testing at RHI Magnesita's Technology Center Leoben (Austria). The results showed that the Flexosphere technology not only improves corrosion resistance, but also contributes to the formation of a more flexible structure, which results in better thermal shock resistance. Furthermore, a RH degasser field trial validated the laboratory results, revealing a clear performance increase compared to the standard product. Thus, the outstanding properties achieved with the patented Flexospheres make this development suitable for applications under aggressive conditions, such as the tuyere area in copper furnaces or the RH degasser in the steel industry, by guaranteeing a significant quality improvement of the magnesia-chromite product.

Fundamentals of Magnesia-Chromite Bricks

Magnesia-chromite bricks ($MgO-Cr_2O_3$) are employed when resistance to hot erosion and thermal shock is necessary. Moreover, chromite acts as an excellent corrosion barrier against slags of different basicity and has a maximum hot modulus of rupture between 1000–1400 °C. Chromite has the generic formula $(Mg,Fe)(Cr,Al,Fe)_2O_4$ and belongs to the spinel group.

Chromite-containing basic bricks find their application in the iron and steel industry (mostly in RH degassers, AOD converters, and safety lining applications), as well as in the nonferrous metallurgy industry, cement rotary kilns, lime shaft kilns, furnaces for refractory production, and glass furnace regeneration chambers [1].

Thermomechanical degradation and corrosion are the main phenomena involved in refractory wear and directly influence the lining lifetime. Therefore, improving refractory corrosion resistance is of vital importance for the ferrous, nonferrous, cement, and glass industries. The main wear mechanism of magnesia-chromite bricks is crack formation due to thermal shock, followed by infiltration into the refractory structure, which subsequently leads to dissolution and corrosion of the refractory product as well as further crack formation [2].

Optimisation of Magnesia-Chromite Bricks

The Flexosphere technology is based on the Spinosphere technology, which was first introduced by RHI Magnesita in magnesia spinel grades to maintain the flexibility of cement rotary kiln bricks without compromising the hot properties [3]. The principle of this innovation was later transferred to magnesia-chromite bricks and primarily targets enhancement of flexibility and corrosion resistance.

It is well known that MgO has a high thermal expansion and is characterised as a rather brittle material when compared to other refractory oxides. As MgO is one of the two main oxides in magnesia-chromite products, the Flexosphere technology was developed to improve absorption of thermal shock in aggressive environments. There are several methods to evaluate the thermal shock resistance of refractory materials, such as measurement of the dynamic Young's modulus, the wedge splitting test, and the V-modulus. Figure 1 illustrates the Young's modulus (E) for two different materials. Material A demonstrates higher stress than B under the same deformation conditions, which indicates material A has a higher Young's modulus than B.

Figure 1.

Representation of the Young's modulus (E) for different materials [4].
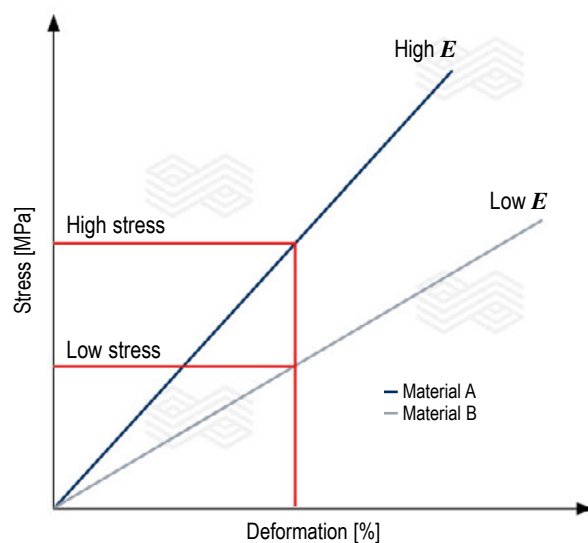
The dynamic Young's modulus is proportional to the compressive stress (σ) divided by a given axial strain or deformation (ε). Moreover, it can be measured with the ultrasonic method and further calculated as the density (ρ) multiplied by the square of the ultrasonic speed (v^2), according to the equation below [4]:

$$E = \frac{Stress}{Deformation} = \frac{\sigma}{\varepsilon} = \rho \cdot v^2 \; [GPa] \tag{1}$$

Lower Young's moduli are characteristic of materials with a better thermal shock behaviour and give an indication of a material's flexibility.
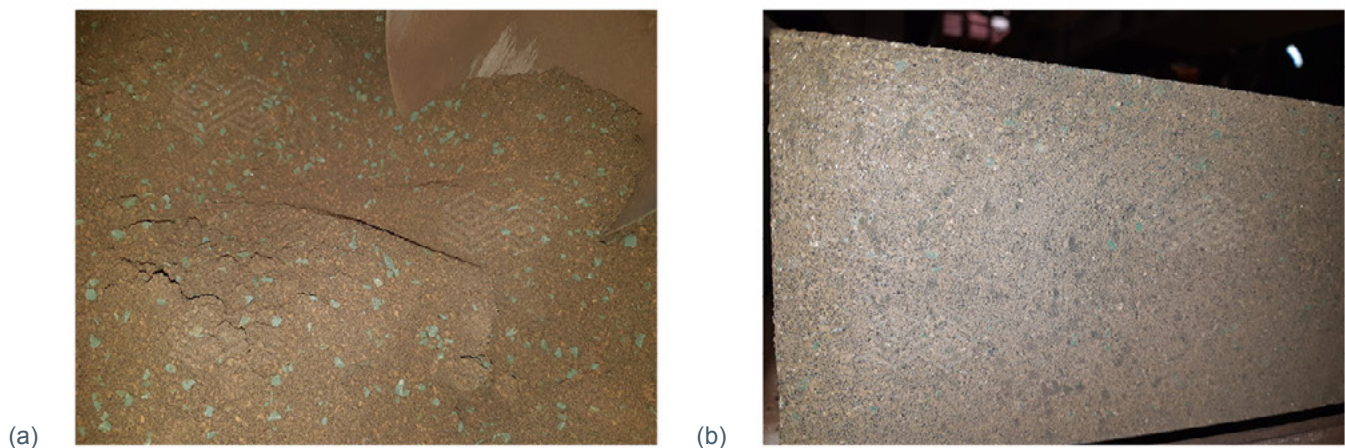
The second competitive advantage of Flexospheres is the deceleration of slag penetration and subsequent corrosion of refractory magnesia-chromite bricks. There are several methods to assess the corrosion mechanisms of refractory samples, such as the crucible test, the rotary finger test, and the rotary slag test [2]. In the present study, dynamic corrosion wear experiments were conducted in a high frequency induction furnace (HF-IF) using the rotary finger test.

Experimental Procedure

The initial investigations performed at RHI Magnesita's Technology Center Leoben (Austria) included preparing and mixing the raw materials, followed by shaping and pressing bricks (Figure 2). The bricks were subsequently fired in one of RHI Magnesita's tunnel kilns to ensure strong ceramic bonding of the raw materials before various chemical and physical properties, including the flexibility and corrosion resistance, were evaluated.

Higher Flexibility and Corrosion Resistance of Magnesia-Chromite Bricks

Based on different investigations, the final refractory product was designed to increase flexibility to a maximum, while at the same time guaranteeing optimum mechanical properties. Figure 3 illustrates the dynamic Young's modulus of three specimens containing different amounts of Flexosphere (V1, V2, and V3) compared to the standard magnesia-chromite product, during a heat up and cool down cycle. The results show that the samples with the Flexosphere technology have a lower dynamic Young's modulus than the standard product and, consequently, a higher flexibility to counteract thermal shock.

Figure 3.

Dynamic Young's modulus of three specimens containing different amounts of Flexosphere compared to the standard magnesia-chromite product, during a heat up and cool down cycle.

Figure 2.

Magnesia-chromite raw materials after (a) mixing and (b) brick pressing.

(a)

(b)
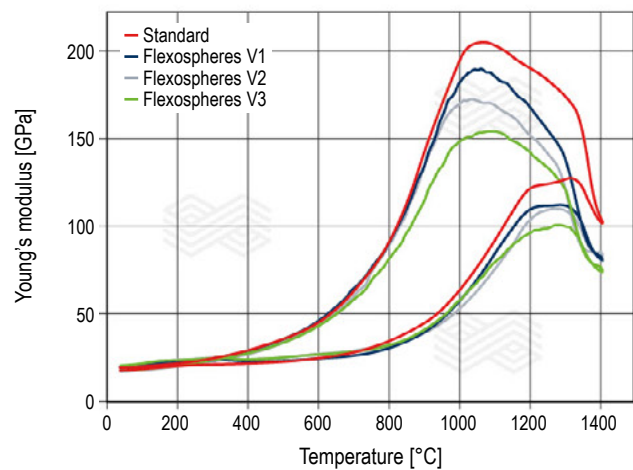
Another parameter to evaluate the flexibility of a product is the V-modulus, where a higher V-modulus indicates a more brittle material that is less stable against thermal shock. The Flexosphere-containing product showed lower V-modulus values indicating a higher capacity to absorb thermal fluctuations in comparison with the standard grade (Table I).

To compare the corrosion resistance of specimens with the Flexosphere technology to standard magnesia-chromite material, rotary finger tests were conducted in a HF-IF. Figure 4 illustrates the experimental setup, where typically one to four refractory fingers are submerged and rotated in the corrosive medium (i.e., metal or slag), which is contained in a crucible surrounded by heating elements [5].

Figure 5 shows macroscopic images of the fingers after a corrosion test to compare the Flexosphere technology with the standard product. Based on the maximum flux line depth, these results confirmed that the Flexosphere-containing refractory had a better performance than the standard sample due to minor slag infiltration into the refractory matrix and therefore a thicker unaltered refractory profile. The maximum flux line depth (d_i) is calculated as follows:

$$d_i = \frac{t_i - t_c}{2} \tag{2}$$

Where t_i is the original finger thickness and t_c is the finger thickness after the corrosion test.

Table I.

V-modulus of Flexosphere and standard magnesia-chromite products.

	V-modulus [N/mm²]
Standard product	8190
Flexosphere product	3437

Figure 4.

Schematic view of a rotary finger test to evaluate the refractory corrosion mechanism.
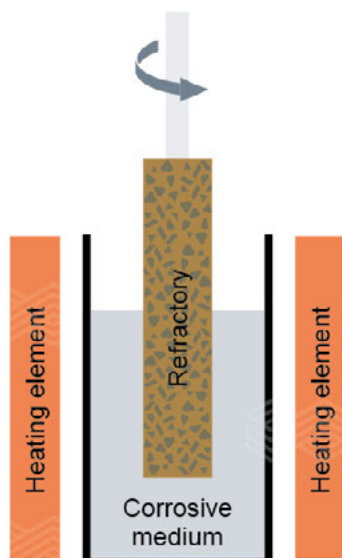
Light microscopy was performed on the corrosion test samples and Figure 6 shows a discontinuous slag precipitation zone on the Flexosphere-containing sample surface (A), the penetration zone (B), and the matrix (C).

Figure 5.

(a) Flexosphere-containing and (b) standard magnesia-chromite fingers after the corrosion resistance test, highlighting the maximum flux line depth (d_i).

Figure 6.

Light micrograph of the Flexosphere-containing material after the corrosion resistance test showing a discontinuous slag precipitation zone on the sample surface (A), the penetration zone (B), and the matrix (C).

Field Trial—Successful Flexosphere Application in the Steel Industry
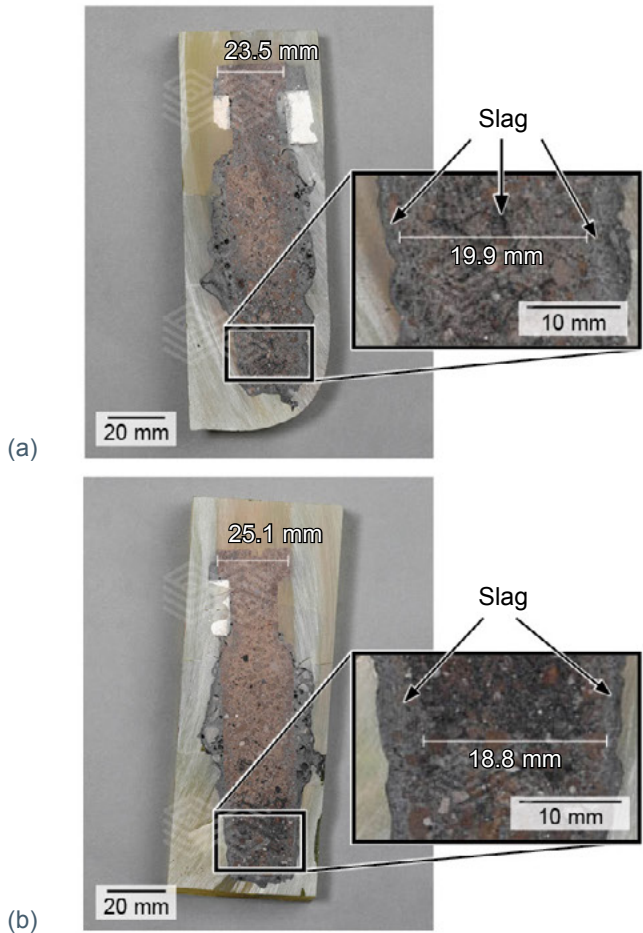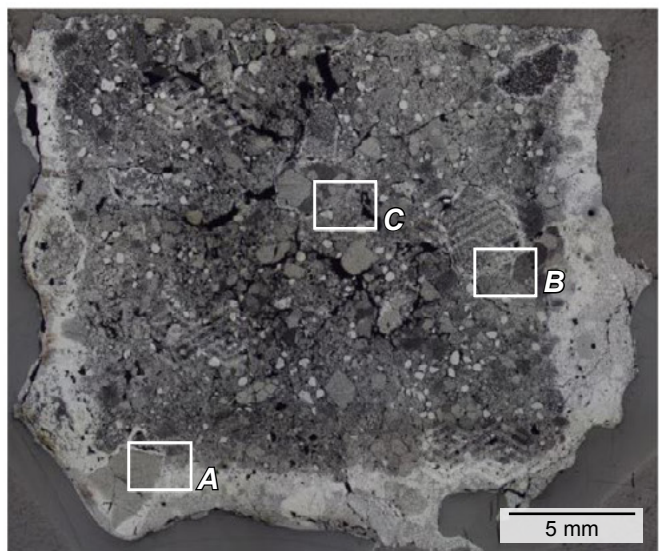
A field trial in the lower vessel of a RH degasser confirmed and extended the results observed in the laboratory scale investigations. Magnesia-chromite bricks with the Flexosphere technology were installed as a panel in the lower vessel wear lining directly above one of the legs and the standard magnesia-chromite bricks were used to line an equivalent area above the other leg (Figure 7). Figure 8 shows a schematic section of the RH degasser, where the refractory with the Flexospheres technology is represented in blue and the standard product is marked in yellow. As the lining above the up leg usually experiences higher stresses than that above the down leg, the steel direction was switched after each leg/snorkel campaign to guarantee a uniform distribution of the wear rate. Typically, one lower vessel wear lining campaign comprises two leg/snorkel campaigns at this customer.

During the trial, relative measurements of the lower vessel lining were performed after the first leg/snorkel run and indicated a 11% performance increase of the Flexosphere-containing bricks compared to the standard magnesia-chromite material. At the end of the lower vessel campaign, absolute brick measurements could be made as the lining was dismantled and revealed a 14% performance improvement with the new development. Overall, when variables such as measurement tolerances and swapping the up and down legs were taken into consideration, it was concluded that the Flexosphere material had an improved performance of 5–15% compared to the standard magnesia-chromite bricks.

Conclusion

The holistic approach that combined laboratory investigations as well as a field trial at one of RHI Magnesita's customers enabled the development of an innovative magnesia-chromite product. The Flexosphere technology improves the corrosion resistance and flexibility against thermal shock of magnesia-chromite bricks, resulting in a product suitable for applications under aggressive conditions such as the tuyere area in copper furnaces and the RH degasser used in the steel industry.

Figure 8.

Section of the RH degasser lower vessel lining showing the magnesia-chromite Flexosphere product on the left (blue) and the standard magnesia-chromite bricks on the right (yellow).

Figure 7.

Standard magnesia-chromite bricks installed above the left leg and magnesia-chromite with the Flexosphere technology installed above the right leg in the RH degasser vessel.
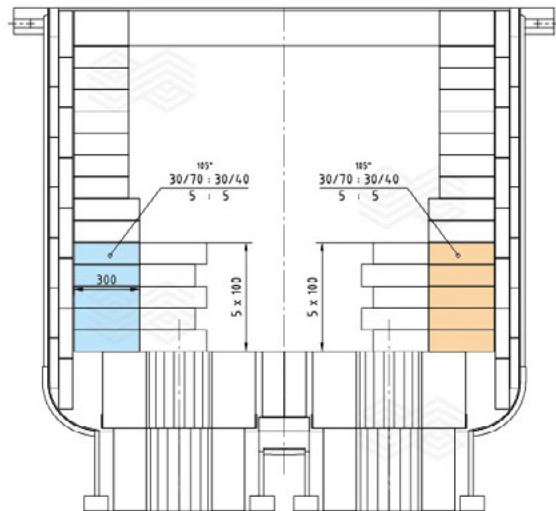
Reprint permission

References

[1] Routschka, G. and Wuthnow, H. *Praxishandbuch Feuerfeste Werkstoffe*; Vulkan-Verlag, 2017, 117–124.

[2] Poirier, J. and Rigaud, M. *Corrosion of Refractories: The Fundamentals. FIRE Compendium Series*; Göller Verlag, 2017, 1–18, 33–37.

[3] Geith, M., Jörg, S. and Krischanitz, R. Spinospheres Technology—An Advanced Technology to Improve Cement Rotary Kiln Brick Properties. Presented at 17th Unified International Technical Conference of Refractories (UNITECR), Chicago, USA, Sept. 14–17, 2021.

[4] Geith, M., Jörg, S. and Krischanitz, R. Influence of Flexibilizers on Basic Cement Rotary Kiln Brick Properties. Presented at the 15th Unified International Technical Conference of Refractories (UNITECR), Santiago, Chile, Sept. 27–30, 2017.

[5] Reynaert, C., Sniezek E. and Szczerba, J. Corrosion Tests for Refractory Materials Intended for the Steel Industry—a Review. *Ceramics Silikaty*. 2020, 64, 1–9.

Authors

Francesca Capó Tous, RHI Magnesita, Leoben, Austria.
Bernd Neubauer, RHI Magnesita, Leoben, Austria.
Laura Rechberger, RHI Magnesita, Leoben, Austria.
Daniela Mancini Fonseca, RHI Magnesita, Rotterdam, Netherlands.
Jürgen Schmidl, RHI Magnesita, Vienna, Austria.
Dean Gregurek, RHI Magnesita, Leoben, Austria.
Corresponding author: Francesca Capó Tous, Francesca.Capotous@rhimagnesita.com

Return to Content

Alexander Leitner, Simone Neuhold, Stefan Heid, Daniela Gavagnin, Pia Maria Meschik, Raffael Stastny, Barbara Zocratto and Matheus Naves Moraes

Enhancing Refractory Recycling: The Role of Automated Sensor-Based Sorting Systems

Elevating refractory recycling rates to unprecedented levels necessitates enhanced quality control. While manual sorting significantly contributes to improved material quality, it has reached its practical limitations and falls short in providing essential data for quality monitoring. The adoption of automated sensor-based sorting stands as a key driver in advancing recycling efficiency, enabling the processing of material fractions previously untapped. RHI Magnesita's activities, notably in the Horizon Europe ReSoURCE project, have established a robust foundation for the forthcoming implementation of automated sorting technology. This imminent advancement is anticipated to redefine standards in circular mineral quality. The article presents an overview of recent developments, addresses the ongoing challenges, and outlines the anticipated future of sorting technologies in the realm of refractory processing.

Introduction

RHI Magnesita is at the forefront of enhancing refractory recycling rates and has made significant progress to reach the 2025 target of 15% [1]. However, the adoption of advanced technologies [2], such as automated sensor-based sorting technologies will ensure future continuous growth of the recycling business. This innovative approach exceeds the conventional manual sorting techniques by accurately analysing particles using advanced sensors, thereby enabling data-driven decisions regarding their potential reapplication. These advancements serve to invalidate the preconception that recycled materials are inferior, fostering greater trust and acceptance of circular materials in the future. By addressing challenges such as limited available feedstock, the traditional manual sorting of only larger particles without chemical insights, and a lack of comprehensive post-sorting data, automated sensor-based sorting stands as a pivotal solution. This article describes RHI Magnesita's pioneering developments in automated sensor-based sorting systems for recycling refractories, highlighting a significant advance toward resource sustainability.

Development of an Automated Sensor-Based Sorting System

Automated sensor-based sorting provides multiple benefits over traditional manual methods [3–6]. Manual sorting is constrained by the physical limitations of human operators, who can only handle large particles (i.e., >80 mm) to maintain an economical throughput (Figure 1). This restriction inherently caps the volume of material that can be processed within a given time. In contrast, automated systems equipped with advanced sensors and rapid ejection mechanisms can process smaller particles ranging from 5–80 mm, significantly expanding the accessible volume of source materials.

Furthermore, automated sorting provides detailed specifications of each particle. By utilising technologies such as laser-induced breakdown spectroscopy (LIBS) for elemental chemistry analysis and hyperspectral imaging (HSI) for mineral phase composition, the sorting process ensures a consistently high-quality output with valuable data that can be leveraged in future product developments. This reduces the incidence of downcycling, where materials are

Figure 1.

Overview of manual recycling processing steps.
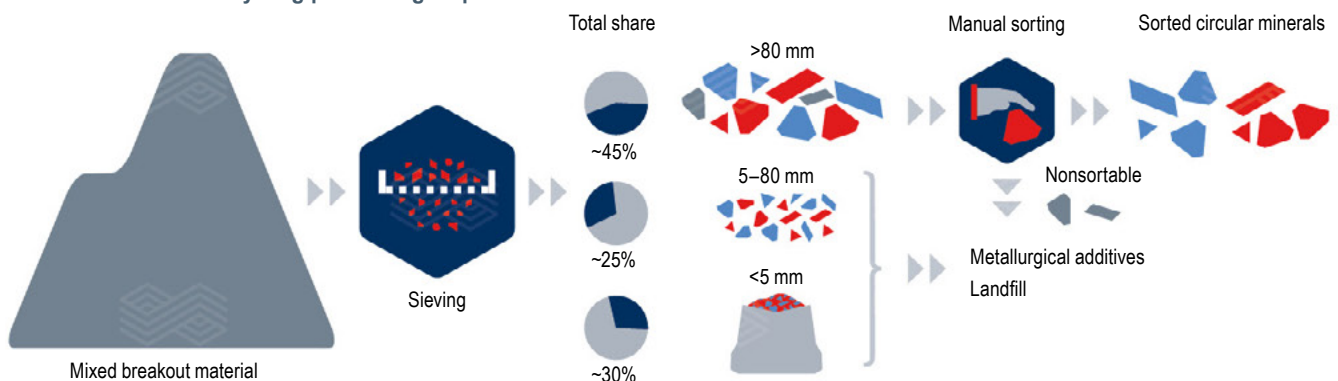
reused in lower value applications than originally intended, as well as the environmental implications and costs of landfilling.

The preliminary design of the mobile automated sensor-based sorting equipment, capable of sorting up to 10 tonnes/hour of spent refractories, is shown in Figure 2. The feedstock will be loaded into a hopper by a wheel-loader. Subsequently, the particles will be automatically singularised, characterised by sensors, and sorted, depending on their characteristics, either by pick and place robots or an air ejection system at the end of the conveyor.

The equipment design enables mobility and replication across different locations. As the cost of generating circular materials is substantially affected by transport distances, mobile sorting units will be used to achieve economic viability by minimising logistical expenses.

ReSoURCE: A European Horizon Project

Automated sorting entails complex processes, necessitating a holistic approach that incorporates feedback loops due to upstream and downstream interdependencies. As achieving optimal outcomes requires collaborative efforts among various experts, the ReSoURCE (Refractory Sorting Using

Revolutionizing Classification Equipment) Horizon Europe project was initiated [7]. The framework of this European programme provides an ideal setting to establish well-defined development agreements, significantly accelerate progress, and provides substantial benefits to all partners involved. Within this collaborative environment, understanding across different technology sectors is enhanced, leading to the development of cutting-edge, tailor-made solutions. Additionally, the involvement of academic institutions ensures that best practices are applied throughout all processes. Featuring a total budget of ~€8.5 million, of which ~€7.0 million are funded by grants, enables the challenge to be tackled in an effective manner. Table I outlines the partners and their respective roles in the ReSoURCE project, illustrating the diverse contributions and expertise in this integrated initiative.

Sensor Combination

The integration of three distinct sensors in the equipment aims to redefine the standards for robust sorting (Figure 3). This multi-sensor approach not only increases the effectiveness of the sorting process but also enriches the data quality, paving the way for more sophisticated recycling operations.

Figure 2.

Mobile automated sensor-based sorting equipment based on transportable 40-foot containers.
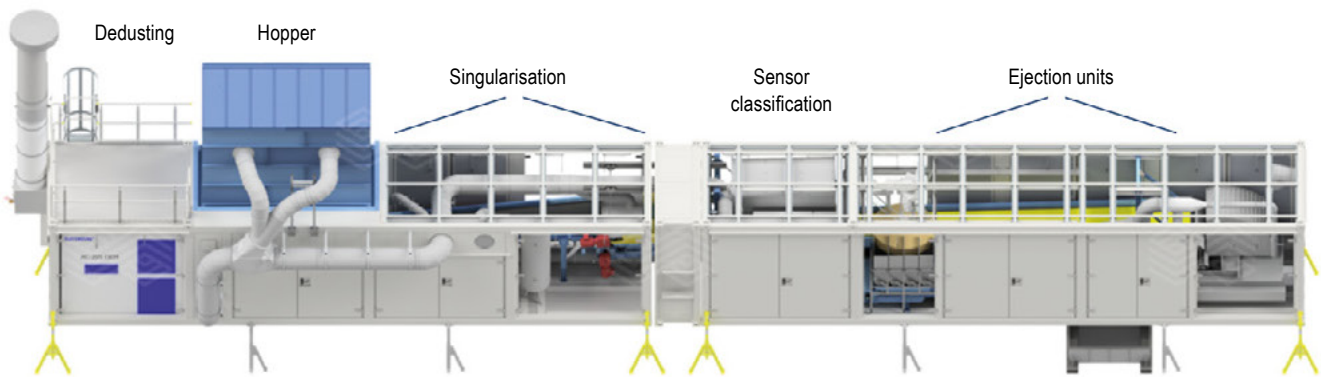

Figure 3.

Overview of the sensor combination to be used in the ReSoURCE equipment. Abbreviations include laser-induced breakdown spectroscopy (LIBS), artificial intelligence (AI), hyperspectral imaging (HSI), and region of interest (ROI).
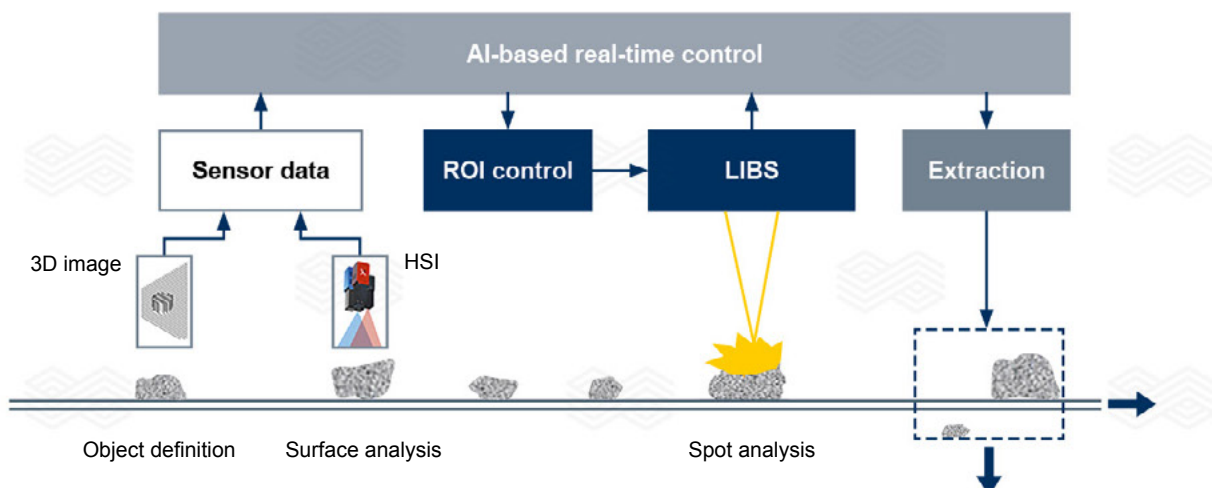
Table I.

ReSoURCE consortium members and their key roles in the project. Abbreviations include laser-induced breakdown spectroscopy (LIBS), artificial intelligence (AI), hyperspectral imaging (HSI), life cycle analysis (LCA), and techno-economic analysis (TEA).

	Partner	Key role	Nationality
RHI MAGNESITA	RHI Magnesita (Coordinator)	Refractory recycling and production	AUT
LSA Laser Analytical Systems & Automation	LSA GmbH	Development of LIBS unit and automation	GER
Fraunhofer ILT	Fraunhofer-Institute for Laser Technology	AI-based sensor data combination and analysis	GER
SINTEF	SINTEF	Powder technology for fine fractions	NOR
MONTAN UNIVERSITÄT LEOBEN	Chair of Mineral Processing	Optimised preprocessing	AUT
	Chair of Waste Processing Technology and Waste Management	Waste characterisation and process optimisation	AUT
INNOLAS LASER INC	InnoLas Laser GmbH	Customised laser development	GER
neo NORSK ELEKTRO OPTIKK AS	Norsk Elektro Optikk	HSI provider and developer	NOR
cpi	CPI Ltd.	LCA, TEA, and nonrefractory applications	UK
Crowdhelix COLLABORATION INTELLIGENCE	Crowdhelix	Stakeholder management and cross-linking	IRL

Initially, a 3D camera plays a crucial role by pinpointing the exact location of each sample on the conveyor belt while also mapping the complete topology of the particle. This is vital for scanning fractured particles with irregular surfaces. The 3D camera helps identify the geometrically ideal regions on these uneven surfaces for conducting LIBS measurements. Optimally, the laser should hit the sample perpendicular to the test surface to ensure high accuracy and low noise levels. In addition, analysis of surface features on the fracture surfaces by the 3D camera contributes to the sorting process. For example, it can facilitate preliminary classification—either confirming the particle's suitability for recycling or excluding it. In some cases, it might even refine existing sorting classes, enhancing the overall efficiency and precision of the sorting system.

Secondly, two HSI cameras play a critical role by capturing the spectral signature of each particle in the range of 400–2500 nm. This technology extends far beyond traditional image analysis, enabling precise visualisation of optical features with a spatial resolution of 384 pixels for the first camera and 1800 for the second. By interpreting reflectance curves obtained from the HSI, it is possible to gather information about the bonding system and identify specific mineral phases. Such information is invaluable for enhancing quality monitoring in refractory recycling, as it provides crucial insights into the material's composition [8].

Moreover, HSI data is instrumental in assessing the mid-scale homogeneity of samples—typically spanning a few centimetres. This capability is particularly significant because it helps mitigate a major limitation of LIBS, which can only analyse small spots on the material (i.e., tested volumes usually in the range of a few hundred μm^3). In determining the material heterogeneity, HSI aids directing the LIBS to the most relevant regions for targeted analysis. It also plays a crucial role in detecting nonrefractory materials, such as attached process media like slag or clinker, that might be present on the sample.

In summary, the broader imaging scope of HSI offers various advantages, including the ability to classify materials directly into specific sorting categories based on underlying models. By integrating these insights, HSI contributes to a more nuanced and effective sorting process, providing visual surface information as a basis for the subsequent selection of coordinates for the LIBS measurement.

Finally, LIBS measurements will be executed at optimal positions, as determined by the data from the 3D camera and HSI sensors (see Figure 3). LIBS plays a pivotal role by analysing the elemental chemistry of each particle [4,9]. This capability is fundamental for classifying materials based on their chemical composition, which is a primary specification that circular minerals must meet for recycling purposes.

Due to its high sensitivity to nearly all elements in the periodic table, LIBS can be utilised to further refine the sorting process. It enables the establishment of new sorting classes with more precise elemental limits. Following each sorting campaign, LIBS not only categorises materials but can also provide quantitative data regarding the levels of specific elements within each particle (Figure 4). This information is crucial for targeted applications in products and can also provide the basis for blending strategies at later stages. Additionally, LIBS is particularly useful for identifying contamination gradients or harmful substances in used bricks. By targeting the precrushing and liberation of infiltrated zones, automated sorting can isolate material volumes requiring special treatment, thereby reducing them, leading to more economical processing costs.

All data collected from the three sensors will be continuously analysed to identify ways to streamline the sensor setup. Furthermore, using the information gained from this initial setup, the goal is to develop more cost-efficient equipment in the future, optimising both technological and economic aspects of the refractory recycling processes.

Advanced Sensor Setups Tailored to Refractory Applications

Currently, sensor and analysis technologies available on the market do not fully meet the specific needs of refractory recycling. For instance, existing LIBS systems are predominantly optimised for sorting metal scrap. This presents a significant challenge for refractory materials, which typically feature a highly heterogeneous microstructure. Unlike metals, where representative volumes are only a few hundred micrometres cubed, coarse ceramic refractories have larger representative volumes, sometimes exceeding 5 mm in terms of the individual raw material components. This size difference means that a random sample may not accurately represent the total chemistry of the refractory product, as indicated in Figure 5.

Furthermore, refractories often possess contamination layers or nonrepresentative layers that can exceed 1 mm due to process media, dust, and oxidation effects. Therefore, efficiently sorting these particles requires a laser capable of quickly ablating any coating material before the measurement pulse analyses the sample. Furthermore, the precision in detecting certain elements is crucial as even minimal levels of contamination can severely impact refractory performance.

To address these challenges, the ReSoURCE project is developing a novel laser source in collaboration with InnoLas (Germany). This advanced technology achieves higher energy levels suitable for testing larger volumes and incorporates tailored pulse modulation to enable both cleaning and analysis pulses within short repetition times. The two new lasers being developed increase the maximum energy level from 150 mJ to up to 430 mJ as well as

Figure 5.

LIBS measurement spots on a 50 mm diameter test cylinder of a basic refractory brick.

Periclase
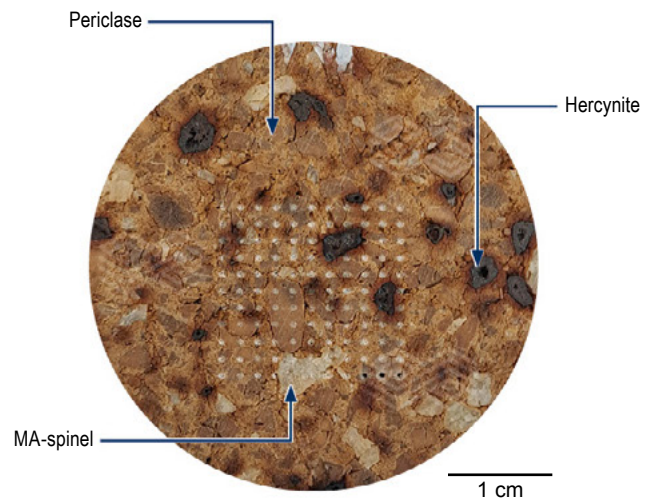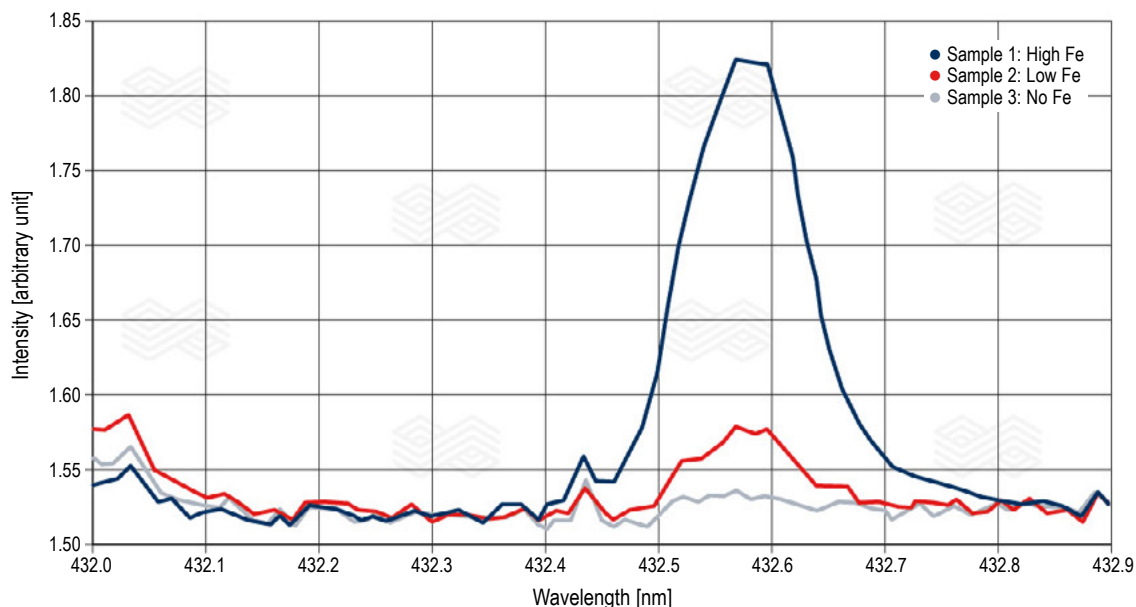
Hercynite

MA-spinel

1 cm

Figure 4.

LIBS spectra showing the Fe peaks for three refractory samples, indicating the different Fe levels detected.

increase the measurement rate up to 400 Hz, when used at lower energy levels. Additionally, a novel spectrometer design and novel optics developed by LSA GmbH (Germany) will enable higher resolution (in the range of 50–150 pm), particularly for critical elements.

Given the chemical complexity of refractories, AI-based algorithms are being employed to enhance the accuracy and efficiency of data analysis. This cutting-edge approach not only improves sorting accuracy but also ensures that recycled materials meet stringent quality standards.

Calibration—The Key to Robust Sorting

The current sorting classes used in recycling operations often feature broad specifications. This is partly due to limitations in the precision of existing sorting technologies but can also result from a deliberate choice to accommodate the infrastructure capabilities at recycling plants. As a result, a wide variety of products, and consequently an even greater diversity of raw materials, are grouped into each

sorting class. This diversity poses significant challenges in calibrating the sorting machinery effectively.

For the LIBS technology, an initial calibration step involves using a variety of raw materials to pinpoint individual peak positions in the spectrum. So far, just in the ReSoURCE project more than 20 primary raw materials and 100 circular mineral samples have been tested, analysed, and categorised. These identified peaks will be crucial for later stages, where they will help differentiate between various recycling classes. Furthermore, the precision of these measurements was remarkably high, with an average classification accuracy of far more than 90% being achieved for all investigated product types (Table II).

To classify materials based on spectral data gathered with the HSI, models such as pixel class majority are being trained and applied on the samples. To establish a solid ground truth within the project, absorption spectra of over 350 crushed circular mineral samples, raw materials, and possible impurities (e.g., slag and clinker) have been recorded. The first results show a promising average classification accuracy of the HSI data (Table III).

The effectiveness of these spectral features, proven by their high accuracy, has also been applied to the classification of circular minerals. An initial outline of this application demonstrates the potential for enhancing the precision and efficiency of sorting practices in refractory recycling, paving the way for more tailored and effective recycling processes.

Table II.

Classification accuracy of different product types by LIBS.

Product type	Classification accuracy [%]
Alumina-silica—low Al_2O_3	98
Alumina-silica—medium Al_2O_3	96
Alumina-silica—high Al_2O_3	96
Magnesia spinel	94
Fired magnesia	93
Alumina-magnesia-carbon	92
Magnesia-carbon with antioxidants	93
Magnesia-carbon without antioxidants	91

Table III.

Example of a confusion matrix based on the pixel class majority of different product types determined by HSI, showing only a minimum number of the samples were incorrectly classified (red shading) even with the nonoptimised model.

Actual refractory class	Sample number	Predicted refractory class		
		Magnesia spinel	Hercynite low Fe	Hercynite high Fe
Magnesia spinel	30	30 (100%)		
Hercynite low Fe	36	3 (8.3%)	33 (91.7%)	
Hercynite high Fe	70			70 (100%)

Conclusion

The advancements in automated sensor-based sorting technologies are set to revolutionise refractory recycling. These systems go beyond replicating manual sorting by significantly enhancing precision and efficiency. The ability to specifically target materials that require treatment ensures economic benefits, particularly when refractory producers provide direct input on sorting criteria. Moreover, extensive data collection and subsequent big data analysis are instrumental as they not only facilitate streamlining equipment features but also lay the foundation for future technological developments. In addition, this strategic approach ensures that only necessary material treatments are applied, optimising both resource usage and economic outcomes in the refractory industry.

Acknowledgment

References

[1] RHI Magnesita 2023 Sustainability Report. https://www.rhimagnesita.com/wp-content/uploads/2024/04/rhim-sustainability-report-2023-final-2.pdf

[2] Moraes, M., Leitner, A., Nogueira, G., Zocratto, B., Heid, S. and Mühlhäußer, J. Technical Challenges for Refractory Recycling and Innovative Processing Solutions. *Bulletin*. 2023, 33–38.

[3] Knapp, H., Horckmans, L., Bouillot, F., Fricke-Begemann, C., Makowe, J., Ducastel, A. and Stark, A. Sensor-Based Identification of Spent Refractory Bricks. RWTH Aachen University Publications. 2015. https://publications.rwth-aachen.de/record/479445/files/64_SENSOR-BASED%20 IDENTIFICATION%20OF%20SPENT%20REFRACTORY%20BRICKS%202015.pdf

[4] Horckmans, L., Nielsen, P., Dierckx, P. and Ducastel, A. Recycling of Refractory Bricks Used in Basic Steelmaking: A Review. *Resources, Conservation and Recycling*. 2019, 140, 297–304.

[5] Müller, S., Müller, A., Döring, I. and Palzer, U. Sorting of Construction and Demolition Waste for Coarse Fractions. Proceedings of the 9th Sensor-Based Sorting & Control Conference. Aachen, Germany, April 13–14 2022, 105–112. https://biblio.ugent.be/publication/8749858/file/8749862. PDF#page=106

[6] Tong, Y. *Technical Amenability Study of Laboratory-Scale Sensor-Based Ore Sorting on a Mississippi Valley Type Lead-Zinc Ore*. Master's Thesis, University of British Columbia, Canada, 2012. https://open.library.ubc.ca/media/download/pdf/24/1.0073277/1

[7] https://www.project-resource.eu

[8] Bonifazi, G., Capobianco, G., Palmieri, R. and Serranti, S. Hyperspectral Imaging Applied to the Waste Recycling Sector. *Spectroscopy Europe*. 2019, 31, 8–11.

[9] Pedarnig, J.D. *Application of Laser-Induced Breakdown Spectroscopy to the Analysis of Secondary Materials in Industrial Production. In: Laser Spectroscopy for Sensing: Fundamentals, Techniques and Applications*; Woodhead Publishing: Sawston, 2014, 496–521.

Authors

Alexander Leitner, RHI Magnesita, Leoben, Austria.
Simone Neuhold, RHI Magnesita, Leoben, Austria.
Stefan Heid, RHI Magnesita, Leoben, Austria.
Daniela Gavagnin, RHI Magnesita, Leoben, Austria.
Pia Maria Meschik, RHI Magnesita, Radenthein, Austria.
Raffael Stastny, RHI Magnesita, Vienna, Austria.
Barbara Zocratto, RHI Magnesita, Rotterdam, the Netherlands.
Matheus Naves Moraes, RHI Magnesita, Contagem, Brazil.
Corresponding author: Alexander Leitner, Alexander.Leitner@rhimagnesita.com

Return to Content

Roland Krischanitz, Peter Steinkellner and Martin Geith

Advancing Sustainable Practices in Refractories for the Cement Industry

The refractory industry plays a pivotal role in various high-temperature industrial processes, such as cement and nonferrous metal production, steelmaking, and glass manufacturing. As environmental concerns intensify, there is a growing imperative to adopt sustainable practices within the refractory industry. For example, in recent years RHI Magnesita started to develop recycling options for magnesia spinel bricks used for lining cement rotary kilns, resulting in a quite extensive low carbon (LC) product portfolio, the ANKRAL LC-Series. The most recently released product, ANKRAL RS-LC, has the highest recycling content implemented so far (i.e., up to 50%), which lowers the carbon footprint by close to 50% compared to the standard product. This paper describes three case studies with products from the LC-Series, highlighting the latest results of ANKRAL RS-LC. The ANKRAL LC-Series contributes to the growing body of knowledge supporting integration of recycled materials in critical industrial processes, promoting a circular economy, and aligning with global efforts to reduce CO_2 emissions.

Introduction

RHI Magnesita set the goal to reduce 15% of its scope 1, 2, and 3 emissions by 2025 [1] and aspires to becoming CO_2 neutral in the future. To achieve this ambitious target, a commitment was made in 2019 to invest €50 million in new and emerging technologies aimed at reducing CO_2 emissions across various processes. In addition to substantial investments, RHI Magnesita was also the first to display the carbon footprint of refractory products on its technical data sheets [2], enabling benchmarking of different concepts according to their carbon footprint. Based on this information, customers can now incorporate sustainable aspects into their product decision-making.

The use of recycled materials to substitute primary raw materials plays a central role in carbon footprint reduction. Furthermore, products that require basic refractory raw materials can benefit significantly in this context because compared to many other refractory materials, basic raw materials have a substantial carbon footprint. This is attributed to the fact that basic raw materials are mostly derived from carbonates and to transform them into refractory oxides they need to be calcined, during which a significant amount of geogenic CO_2 is released. This process occurs at temperatures of up to 1000 °C and requires substantial fuel input, causing further greenhouse gas (GHG) emissions. Additionally, to produce refractory materials with high density and stability at elevated temperatures, an additional step is necessary, which can involve either a sintering or melting process. Sintering requires temperatures of up to 2000 °C, while melting takes place at temperatures above 2800 °C.

Depending on the type of kilns and fuel used, CO_2-specific emissions can range from around 1.4–5.2 tonne of CO_2 equivalent per tonne of raw material (t CO_2e/t) [3]. However, other approaches for producing sintered or fused magnesia do not result in a lower carbon footprint, as the complex production process (e.g., wet route) of seawater or brine-based magnesia types results in the same level of GHG emissions compared to magnesite-based ones [3]. As a vertically integrated company, the production of sintered magnesia and dead burned magnesia, as well as dead

burned doloma is responsible for around 85% of RHI Magnesita's scope 1 CO_2 emissions [3]. On the one hand, this is due to the scarcity of alternative primary raw materials available in the market that can serve as substitutes and on the other hand it highlights that using recycled materials within a circular economy is essential.

Refractory products, when in use, are exposed to various wear mechanisms, making the reprocessing process extremely complex in most cases [4]. This complexity is particularly evident in the cement industry, where over the past few decades the use of alternative fuels has significantly increased infiltration of alkali salts into the refractory lining. The concept of fuel switching, which involves transitioning from conventional fossil fuels to alternative fuels with improved CO_2 ratings, varies globally. While Central Europe has made significant progress with substitution rates of up to 100%, other regions like China, Africa, and the Middle East are still relatively early in this transition. Nevertheless, RHI Magnesita has managed to develop a product portfolio with a reduced carbon footprint, the ANKRAL LC-Series, based on recycled bricks from cement rotary kilns.

From Spent Refractories to Circular Raw Materials

At the end of their lifespan, worn out refractory bricks were typically disposed of or landfilled, potentially incurring additional costs for operators. However, these materials are a valuable source of raw materials, which can be repurposed to create new refractory products. Removing used bricks from the kiln involves standard procedures and machinery, without any additional steps. Before debricking, any coatings or build-ups on the lining should be removed. Depending on the type of magnesia (e.g., low or high iron content) and flexibiliser (e.g., spinel or hercynite), the bricks are separated onsite into predefined categories to control the chemical characteristics of the subsequently generated circular raw materials. A well-defined sourcing concept, as well as an adequate reconditioning process, is key to guarantee excellent and stable product properties [5].

Once the material has arrived at a recycling hub, the conversion from spent refractories to circular raw material

begins. This process consists of several sorting and classification steps and starts with chemical analysis to verify the nature and type of collected material. After manual sorting (Figure 1), where any foreign objects (e.g., steel anchors and wood) are also removed, the material is subjected to a patented cleaning process in which the largest share of unavoidable alkali salt infiltrations from the cement process are removed. This treatment requires a certain effort in terms of energy and time; however, it is essential to achieve the desired product properties. After crushing the material, the new circular raw material is used to produce ANKRAL LC-Series bricks.

One of RHI Magnesita's priorities is developing fully automated identification and separation of used materials, including sensors specifically designed to meet the challenges of refractory recycling (see page 41). Currently, pilot equipment is being implemented in Austria that will completely change the status quo of spent refractory sorting [4].

Innovative Low-Carbon Series

With the ANKRAL LC-Series, RHI Magnesita has successfully implemented the principles of a circular economy in the production of magnesia spinel bricks for the cement industry. The LC-Series (low carbon) incorporates up to 50% recycled materials. Designed with a significantly reduced carbon footprint, these products aim to assist cement producers in lowering emissions within their supply chain while maintaining technical specifications. To meet the growing demand for sustainable refractories, RHI Magnesita offers a range of LC products, including ANKRAL Q1-LC, ANKRAL R8-LC, ANKRAL Q2-LC, ANKRAL RC-LC, and ANKRAL ZE AF-LC. The different products of the LC-Series have been widely used globally in central burning and transition zones under various operational conditions since their market launch in 2020. During this time, the series has gained recognition as a well-known brand, particularly in Europe.

The primary goal in creating the ANKRAL LC-series was to incorporate circular raw materials, thereby reducing the carbon footprint, while ensuring that product properties remained uncompromised. Although the technical data sheet values for conventional ANKRAL bricks and their corresponding LC-Series counterparts may not be identical, both can be effectively used in the same applications and achieve the same level of performance. Rigorous laboratory tests, combined with meticulous sourcing and raw material processing, guarantee consistent performance even under demanding conditions, which has been proven in numerous applications.

The latest development in the field of sustainable products is ANKRAL RS-LC, where the circular raw material content has been increased up to a remarkable 50%. Despite this high recycling rate, a product with outstanding properties was developed. The brick has an exceptional refractoriness under load (RuL T0,5 > 1700 °C), which is comparable to products based on primary raw materials (Figure 2). Additionally, due to sophisticated processing methods, the brick exhibits a remarkably low content of secondary phases, providing excellent resistance against chemothermal wear. The positive results of this development have already been confirmed in practical applications.

Figure 1.

Manual sorting at a recycling hub, which will be fully automated in the future.

Figure 2.

Technical data sheet of ANKRAL RS-LC.

Technical data sheet

RHI MAGNESITA

ANKRAL RS-LC

General information	
Classification	Magnesia-spinel product type MSp80 ISO 10081-2
Main raw material components	Fused spinel, High grade sintered magnesia
Bonding type	Ceramic
Main Application(s)	Sintering and transition zones
Type of brick	Fired
Mortar to use	ANKERFIX CRP

Environmental indicators			
Product Carbon Footprint	1,431	[t CO2e/t prod.]	ISO 14067

The Carbon Footprint of the Product (CFP) has been calculated following the principles of ISO 14067.

Chemical analysis					
MgO	Al$_2$O$_3$	Fe$_2$O$_3$	CaO	SiO$_2$	
85,8%	11,0%	0,5%	1,4%	0,8%	

Determination on fired substance (1025 °C / 1877 °F) acc. to ISO 12677

Physical properties				
Bulk Density		2,90	[g/cm^3]	ISO 5017
Apparent Porosity		18,0	[vol%]	ISO 5017
Cold Crushing Strength		60,0	[N/mm^2]	ISO 10059-1
Thermal Expansion	500 °C / 932 °F	0,51	[%]	EN 993-19
	750 °C / 1382 °F	0,84	[%]	EN 993-19
	1000 °C / 1832 °F	1,20	[%]	EN 993-19
Refractoriness under Load T$_{0,5}$		1700	[°C]	ISO 1893
Res. to Thermal Shocks Air		> 100	[cycles]	EN 993-11
Thermal Conductivity	500 °C / 932 °F	4,30	[W/mK]	Dr. Klasse
	750 °C / 1382 °F	3,50	[W/mK]	Dr. Klasse
	1000 °C / 1832 °F	3,00	[W/mK]	Dr. Klasse

The indicated values are standard values, i.e. values taken over a longer representative period of time according to either valid test standards or internal test methods. They may not be regarded as committed specifications and therefore not as guaranteed properties. We reserve the right to further technical developments and new editions of technical product information.
Colour deviations of the product may occur due to the nature of the raw materials used, however they are not an indication of inferior performance or quality.

Revision: 02. JUL. 2024

ANKRAL RS-LC 1 / 1

Case Study A—ANKRAL ZE AF-LC

Plant A operates a precalciner kiln (Ø 3.8 m x 59 m long) with a capacity of approximately 1900 tonnes per day (tpd) in Central Europe and an alternative fuel (AF) rate of beyond 90% (including plastics and sewage sludge). ANKRAL ZE AF-LC was installed in January 2022 between 15 m and 17 m in the upper part of the central burning zone (CBZ), where high thermal load in combination with occasional clinker melt infiltration and coating loss are the typical wear mechanisms. After completing a full campaign of one year, the lining was inspected again in January 2023. This revealed a very uniform wear and a residual thickness of 170–180 mm (Figure 3). At the next opportunity to enter the kiln in January 2024, the lining showed a similar appearance, with a residual thickness of 140–160 mm. By mid-2024, at the time of writing this article, the bricks were already in their third campaign, with high expectations for completing a third year. The results of this successful trial confirm ANKRAL ZE AF LC's full equivalency to any other iron-rich CBZ brick on the market.

Case Study B—ANKRAL Q1-LC

The kiln at Plant B (precalciner, Ø 4.0 m x 60 m long with a capacity of 2200 tpd) is another example of a European kiln running with substitution rates close to 100% (e.g., refuse-derived fuels, solvents, and biomass). ANKRAL Q1-LC was installed in the lower transition zone (LTZ) between 6.4 m and 8.4 m, followed by ANKRAL Q1 between 8.4 m and 10 m. In previous campaigns, this area was lined completely with the conventional ANKRAL Q1, achieving lifetimes of one year despite high chemothermal load and proximity to the tyre. After one full year in operation, the Lining Evaluation Scan (LES) showed a residual thickness of 140–170 mm and rather uniform wear in the installation area of the LC-series bricks (Figures 4 and 5). The corresponding standard brick performance was largely the same, confirming that the product development goal of not compromising the product properties by adding circular raw material was fully met. Based on these results, the operator decided to enlarge the installation area of ANKRAL Q1-LC in future campaigns.

Figure 3.

ANKRAL ZE AF-LC in the CBZ between 15 m and 17 m, (a) before and (b) after a one-year campaign.
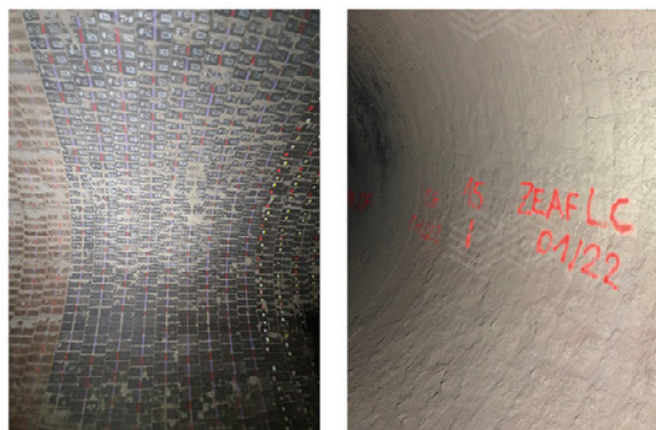
(a)   (b)

Case Study C—ANKRAL RS-LC

The plant for case study C is operating a modern precalciner kiln (Ø 5.2 m x 77 m with a capacity of approximately 6000 tpd) in Southern Europe. It is using a fuel mix consisting of coal/pet coke and residue derived fuel (i.e., sewage sludge and tyre chips), reaching AF rates of more than 60%. The refractory lining of this kiln is exposed to high chemothermal stress and increased mechanical load from the centre tyre and in the outlet area. In addition, the lining is affected by frequent kiln stops.

Figure 4.

ANKRAL Q1-LC in the LTZ, lined between 6.4 m and 8.4 m, after one year in operation.

Figure 5.

Installation of ANKRAL Q1-LC (6.4 m–8.4 m) and ANKRAL Q1 (8.4 m–10 m) after one year in operation.

In March 2023, ANKRAL RS-LC was installed in the remote upper transition zone of this kiln between 40.5 m and 45.5 m (Figure 6). A LES in September of the same year (after approximately 6 months of service) revealed that the brick was in perfect condition, showing no signs of wear and still having the original thickness (Figure 7). Another inspection in January 2024, which again included LES, basically

showed the same results (Figure 8). Both lining evaluation scans performed by RHI Magnesita in September 2023 and January 2024 showed that the lining area of ANKRAL RS-LC was in perfect condition, without any spalling and with uniform residual thicknesses beyond 200 mm from the original 220 mm (Figure 9).

Figure 6.

Installation of ANKRAL RS-LC between 40.5 m–45.4 m.

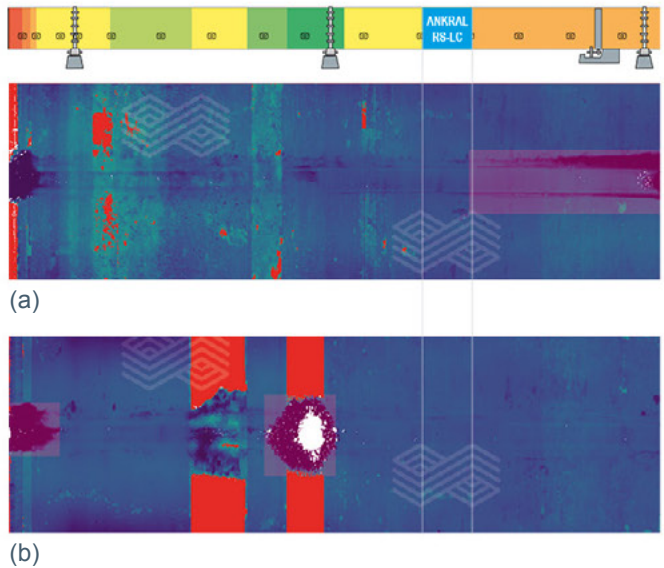**Figure 8.**

Image taken during a further inspection in January 2024, showing the ANKRAL RS-LC lining area with no significant wear (LES image).

Figure 7.

ANKRAL RS-LC in September 2023 after 6 months in operation, showing original residual thicknesses without prewear areas.

Figure 9.

Lining evaluation scans in (a) September 2023 and (b) January 2024.

(a)

(b)

Another opportunity to inspect the lining arose in April 2024, during a further kiln stoppage. At this time, the ANKRAL RS-LC had been in service for more than 12 months and still did not show signs of massive wear (Figure 10). After the first year of service, the customer confirmed that the bricks were still in satisfactory condition and is very confident that they will remain in operation for at least another year.

Figure 10.

Inspection of the ANKRAL RS-LC lining area in April 2024, showing no significant wear.

Sustainable Refractories

The product portfolio of the ANKRAL LC-Series includes products designed to address the challenges of modern clinker production across all relevant kiln sections that require magnesia spinel bricks. The focus of further developments is to optimise the sourcing, preparation, and production process to incorporate even higher amounts of circular raw materials [4], reduce the carbon footprint, and contribute to a sustainable refractory industry. The priority focus for R&D is on a fully automated identification and separation of recycled materials. Currently, RHI Magnesita is developing pilot equipment that is being implemented in Austria and will completely change the status quo of spent refractory sorting.

References

[1] RHI Magnesita 2023 Sustainability Report. https://www.rhimagnesita.com/wp-content/uploads/2024/04/rhim-sustainability-report-2023-final-2.pdf

[2] Joos-Bloch, M., Rechberger, L., Haider, C., Moulin-Silva, W., Wucher, J. and Drnek, T. Product Carbon Footprint of Refractory Products. *Bulletin*. 2023, 39–44.

[3] Ribeiro, T., Bonadia, P., Gueguen, E., Maier, F. and Drnek, T. Alternatives to Reduce the Carbon Footprint in Refractory Raw Material Production Processes. *Bulletin*. 2021, 16–21.

[4] Moraes, M., Leitner, A., Nogueira, G., Zocratto, B., Heid, S. and Mühlhäußer, J. Technical Challenges for Refractory Recycling and Innovative Processing Solutions. *Bulletin*. 2023, 33–38.

[5] Steinkellner, P. Developing Sustainable Refractory Solutions. *International Cement Review*. September 2023, 94–96.

Authors

Roland Krischanitz, RHI Magnesita, Vienna, Austria.
Peter Steinkellner, RHI Magnesita, Vienna, Austria.
Martin Geith, RHI Magnesita, Leoben, Austria.
Corresponding author: Roland Krischanitz, Roland.Krischanitz@rhimagnesita.com

José Alvaro Previato Sardelli, Sérgio Eustáquio Soares and Gláucio Galdino Martins

Microstructural Design Optimisation of Magnesia–Chromite Bricks for RH Degassers: Determining an Optimal Balance Between Thermal Shock and Corrosion Resistance

Magnesia-chromite bricks are widely used in RH degassers due to their outstanding corrosion and abrasion resistance in critical environments. Among the different types of magnesia-chromite bricks, rebonded bricks, characterised by a high fused magnesia-chromite (FMC) content, are particularly preferred in snorkel and throat areas of RH degassers. However, rebonded bricks exhibit lower thermal shock resistance compared to direct-bonded bricks (i.e., based on sintered magnesia and chrome ore). To address this limitation, semi-rebonded bricks have emerged as a potential solution to fulfil these constraints. While the literature has explored the characteristics of these three distinct classes of magnesia-chromite bricks, only a limited number of studies have evaluated the microstructural effects on physical, thermomechanical, and corrosion resistance properties. Therefore, this study aimed to determine the optimal amount of FMC grains to achieve a suitable balance between the required properties. Experimental tests were conducted to assess the impact of increasing amounts of fused grain on the most influential properties of magnesia-chromite bricks. The findings indicated that an optimal quantity of fused grains could be identified, where the physical and thermomechanical properties were improved without compromising corrosion and abrasion resistance, and that these properties could be further enhanced by optimising the grain size distribution (GSD). This study highlights the importance of microstructural differences in formulation design and the selection of appropriate raw materials and GSD to achieve comparable properties to rebonded bricks without influencing essential application requirements.

Introduction

Magnesia-chromite refractories are widely used in various industries due to their exceptional thermal stability, minimal thermal expansion, and resistance to thermal shock. They are particularly favoured in applications such as RH degassers, rotary cement kilns, and nonferrous copper converters [1]. Compared to magnesia-based counterparts, they offer superior thermal shock resistance and corrosion resistance to acidic and basic slags, especially fayalitic slags [1–3]. To improve slag penetration resistance, it is crucial to densify the bricks, reduce apparent porosity, while maintaining thermal shock resistance. This can be achieved through microstructure design, focusing on fostering direct bonding between the refractory grains, including secondary spinel phases and fused magnesia-chromite (FMC), along with a carefully tailored grain size distribution (GSD).

The principal constituents of magnesia-chromite bricks, customised to specific applications, include sintered magnesia, fused magnesia, chrome ore, and FMC. These raw material compositions facilitate categorising magnesia-chromite bricks into three discrete classes: Direct-bonded, semi-rebonded, and rebonded. Each classification presents distinct advantages and constraints, requiring detailed alignment with the specific requisites of the intended application. Notably, direct-bonded bricks exhibit superior thermal shock resistance, but comparatively inferior corrosion resistance compared to rebonded bricks, with the semi-rebonded class filling an intermediate position within this range.

In direct-bonded bricks, the bonding mechanisms between sintered magnesia and chrome ore grains are determined by temperature-driven reactions during the firing process. At 1500 °C, a liquid phase forms around the chrome ore grains, subsequently infiltrating the adjacent magnesia matrix, enabling diffusion of Fe_2O_3, Cr_2O_3, and Al_2O_3 from the chrome ore into the magnesia at 1670 °C. Finally, at 1750 °C, complete dissolution of the chrome ore occurs, precipitating spinel-like exsolution phases within the MgO structure [4]. This behaviour is beneficial for thermal shock resistance owing to the microcracking induced by interdiffusion of chrome ore components into the magnesia matrix.

In the context of RH degassers, magnesia-chromite bricks primarily comprise FMC and are typically classified as rebonded bricks. The main bonding process occurs during the FMC electrofusion process, followed by firing the bricks at temperatures exceeding 1700 °C to form rebonded refractories. The FMC consists mainly of periclase and a solid solution spinel $[(Fe,Mg)(Fe,Al,Cr)_2O_4]$, resulting from the fusion of various spinel structures (AB_2O_4-type phases), where A represents a divalent cation and B a trivalent one [5–7]. This complex structure, characterised by interstices and vacancies, enables the formation of solid solutions with broad solubility ranges and ionic radii ranging from 0.44–1.00 Å [5,8]. Consequently, these bricks exhibit excellent resistance to corrosion and slag infiltration. Additionally, preferentially oriented microcracks within the FMC grains enhance the material's flexibility and resistance to thermal shock damage. The FMC features a periclase matrix with

embedded spinel precipitates, typically around 15 µm in size, exhibiting a consistent pattern with {110} planes as revealed by electron backscatter diffraction, aligning with the Zener-Stroh crack mechanism [9]. Figure 1 provides a visual representation of the FMC parameters described.

The semi-rebonded classification of magnesia-chromite bricks involves combining FMC with the microcracking phenomena promoted by the direct-bonded behaviour that occurs between sintered magnesia and chrome ore grains during the firing process. This unique combination has emerged as a promising approach to impart the necessary properties crucial for certain applications. The primary objective of the investigations presented in this paper were to determine the optimal amount of FMC grains necessary to achieve a balanced equilibrium between thermal shock resistance and corrosion resistance, while maintaining the physical and thermomechanical integrity of the material.

Additionally, a secondary aim of the study was to evaluate a new GSD to enhance the microstructure achieved with the optimal amount of FMC.

Materials and Methods

Laboratory magnesia-chromite bricks were formulated utilising Alfred's model incorporating a customised particle size distribution coefficient tailored to the FMC content in the semi-rebonded formulation under investigation. Additionally, a novel GSD was developed and assessed to enhance the key properties of these materials during application. A spectrum of compositions ranging from low to high FMC content was systematically explored (Table I). To ensure comparison across all FMC compositions and mitigate any potential interference during firing, uniform binder systems and sintering additives were incorporated across all compositions.

Figure 1.

Morphology and elemental mapping of the FMC microstructure assessed by scanning electron microscopy coupled with energy dispersive spectroscopy [9].

Element content [wt%]	
Fe	3.9
Cr	45.6
Al	3.3
Mg	13.0
O	34.2

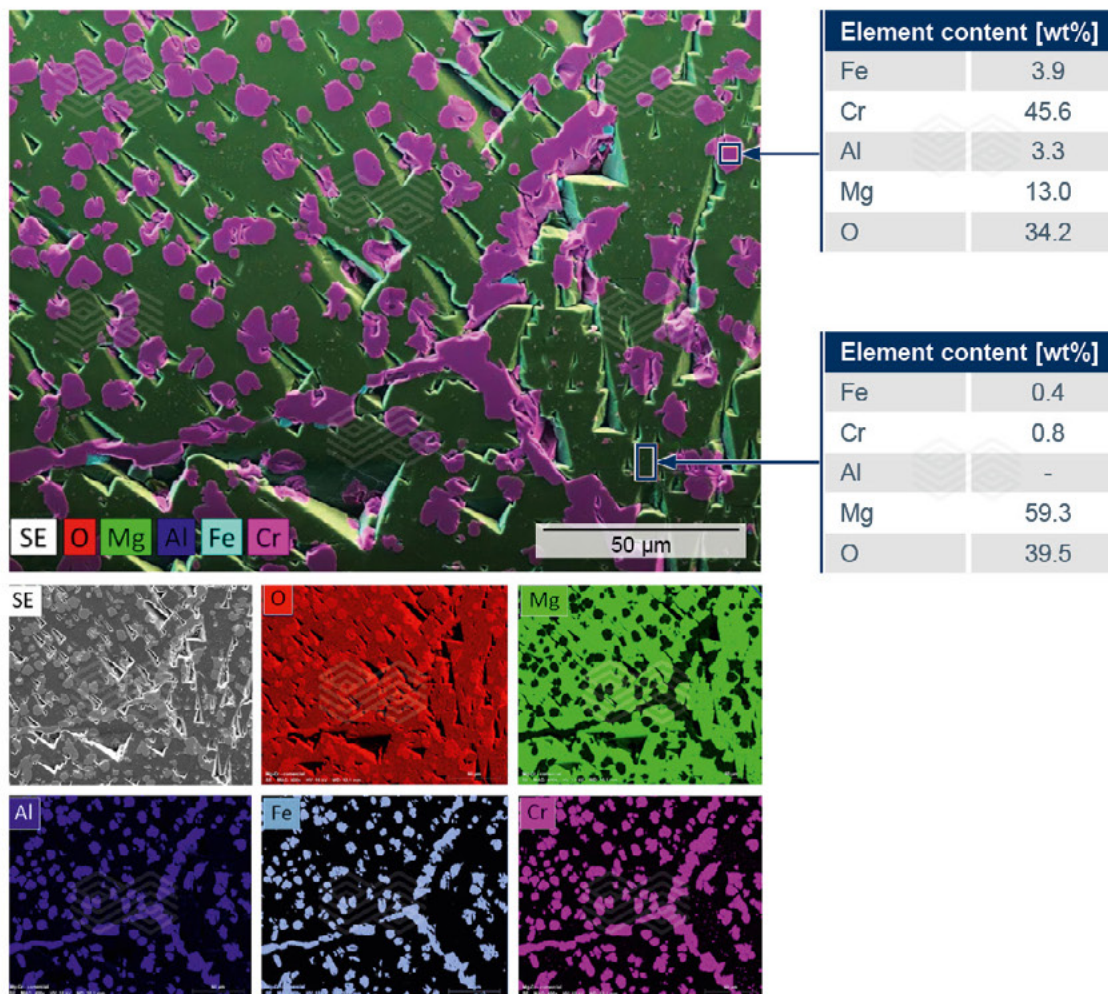| Element content [wt%]	
Fe	0.4
Cr	0.8
Al	-
Mg	59.3
O	39.5

Table I.

Compositions evaluated during the semi-rebonded magnesia-chromite brick development.

Grain size distribution	Raw materials	A	B	C	D	E	F
Standard GSD	FMC content	+	++	+++	++++	+++++	++++++
New GSD	FMC content	+	++	+++	++++	+++++	++++++

All formulations were homogenised in roller mixers and hydraulic presses were used to shape 160 x 85 x 63 mm^3 bricks that were subsequently fired at temperatures above 1700 °C in an industrial tunnel kiln. Bulk density and apparent porosity were determined using a liquid immersion method in water, according to the ABNT NBR 6220 standard. Cold modulus of rupture was evaluated using a KRATOS KE (3 tonnes) and cold crushing strength was carried out with a KRATOS ECC (Brazil) using a 100 kN load cell (JIS, R-2206, Brazil) on cylindrical 50 x 50 mm^3 specimens. Hot modulus of rupture was carried out on bars (152 x 25 x 25 mm^3) placed in an electric furnace with a continuous sample feeding system coupled to a mechanical press (KRATOS K500/2000, Brazil). The permeability test was conducted according to ASTM C577 and abrasion resistance was measured following ASTM C704. Microstructure analysis by optical microscopy was carried out using a Carl Zeiss microscope (AXIO-Imager model). The thermal shock resistance test was conducted on 152 x 25 x 25 mm^3 bars using a water-cooled copper plate. The decrease of elastic modulus was followed for 5 thermal shock cycles (ΔT = 700 °C) (ABNT NBR 13202) utilising ultrasound equipment (Emodumeter, James Instruments, USA). Based on the ultrasound velocity and density of each sample, the elastic modulus was calculated as well as the residual elastic modulus at the end of 5 cycles. Additionally, the residual modulus of rupture was measured after the 5th cycle. The corrosion tests were performed at 1700 °C in an induction furnace, using steel and fayalitic slag added every 30 minutes for 5 hours, and 8 samples were evaluated simultaneously.

Laboratory Trial Results

To assess the impact of different levels of FMC and the two GSDs on bulk density and apparent porosity, 3 samples of each magnesia-chromite brick composition were tested. Based on the results obtained, it was apparent that increasing the FMC content led to an overall rise in bulk density, coupled with a decline in apparent porosity for both GSDs examined (Figure 2). Furthermore, alongside the benefits of increasing the high-grade raw material content on these properties, the new GSD emerged as a pivotal factor for increasing bulk density and decreasing porosity, apart from at the lowest level of FMC addition.

To visually examine the different brick compositions, optical microscopy was performed and micrographs of compositions featuring the standard GSD are provided in Figure 3. The images clearly demonstrate how each composition's microstructure changes with the addition of higher FMC levels; most notably the porosity decreases, leading to improved densification.

Figure 2.

Bulk density (BD) and apparent porosity (AP) of the different magnesia-chromite brick compositions with increasing amounts of FMC and two GSDs. The lines between the AP values are for visual guidance.
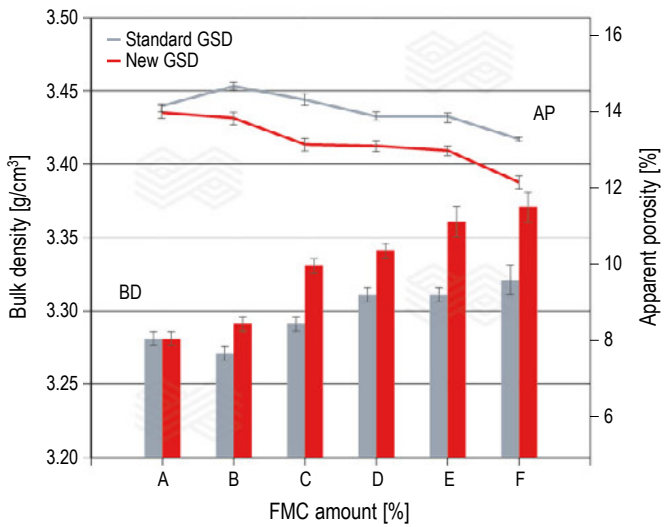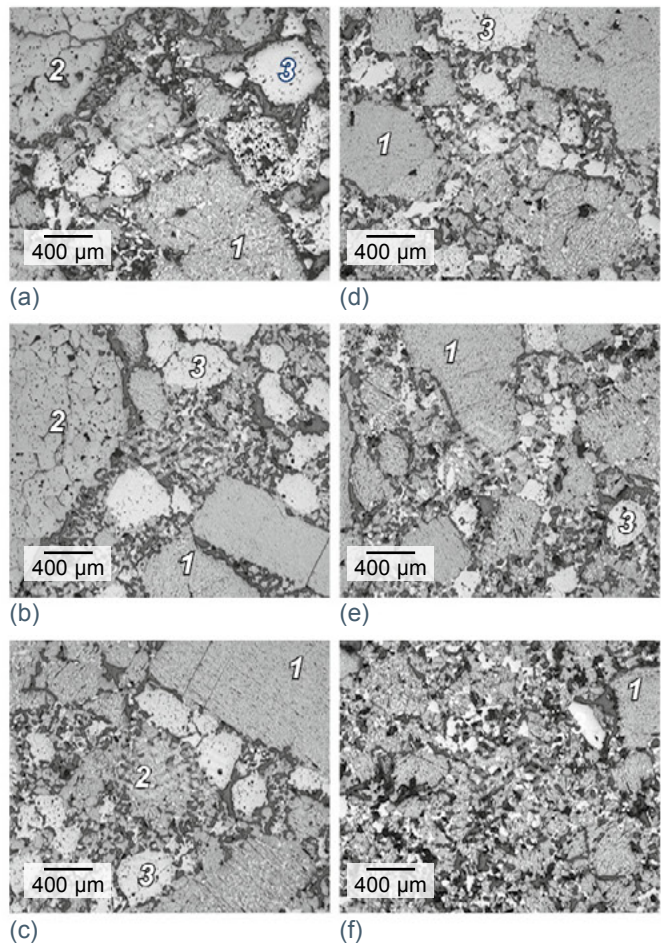

Figure 3.

Comparative microstructural evaluation of fired magnesia-chromite bricks with different FMC content and the standard GSD. The images (a–f) correspond to the increased addition of FMC as detailed in Table I. FMC (1), sintered magnesia (2), and chromite (3) are indicated.
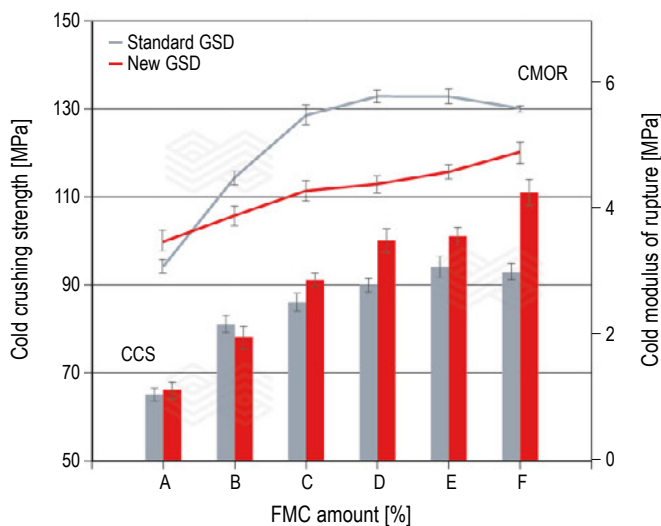
In order to explore the influence of FMC content and GSD on cold mechanical properties, the cold crushing strength and cold modulus of rupture were measured for 3 samples of each magnesia-chromite brick composition. The results presented in Figure 4 show that both properties increased with FMC content for both GSDs. However, regarding the cold crushing strength, discernible differences in values between the two GSD only emerged from composition D onwards, with the magnitude of difference increasing with FMC content. In summary, it appeared that the novel GSD effectively optimised microstructural packing, resulting in highly favourable outcomes for practical applications when combined with higher amounts of FMC. In contrast, a similar trend was not observed for the cold modulus of rupture. Although at the lowest FMC content no distinction was observed between the GSDs, for all other compositions the standard distribution exhibited a higher cold modulus of rupture compared to the new GSD.

To assess the influence of FMC addition and GSD on thermomechanical properties, the hot modulus of rupture test was conducted on 3 samples of each brick composition at test temperatures of 1250 °C, 1400 °C, and 1485 °C (Figure 5). At 1250 °C, the hot modulus of rupture showed an upward trend with the increasing addition of FMC, irrespective of the GSD, indicating incorporation of FMC had a beneficial effect on this thermomechanical property, while the GSD did not significantly influence the obtained values. With an elevation of the test temperature to 1400 °C, the hot modulus of rupture was lower than at 1250 °C, but also rose with increasing amounts of FMC, in a similar manner for both GSDs, until a certain content was reached (i.e., composition D), whereupon this upward trend stabilised. It is established that at 1400 °C, liquid phase formation originating from in situ generated silicate minerals (e.g., monticellite and merwinite) is more prevalent in the material's microstructure, which would account for the observations. At a testing temperature of 1485 °C all the samples showed the lowest hot modulus of rupture, with similar values irrespective of FMC content and GSD.

The microcracking effect induced by direct-bonding reactions within the magnesia-chromite brick matrix is an approach to enhance thermal shock resistance, when appropriately balanced against corrosion by slag and molten metal. To examine the influence of FMC content and GSD on thermal shock behaviour, 3 samples of each magnesia-chromite brick composition were heated to 725 °C, held for 30 minutes, and rapidly cooled to room temperature. After each thermal cycle, the elastic modulus was determined and after 5 cycles the residual elastic modulus was calculated. In addition, the cold modulus of rupture was measured at the end of the 5 cycles and the residual cold modulus of rupture determined. The residual elastic modulus results (Figure 6)

Figure 5.

Hot modulus of rupture (HMOR) of the different magnesia-chromite brick compositions with increasing amounts of FMC and two GSDs, tested at 1250 °C, 1400 °C, and 1485 °C. The bars correspond to the standard GSD at the three test temperatures and the squares, triangles, and circles to the new GSD at 1250 °C, 1400 °C, and 1485 °C, respectively. The lines connecting the HMOR values of the new GSD are for visual guidance.

Figure 4.

Cold crushing strength (CCS) and cold modulus of rupture (CMOR) of the different magnesia-chromite brick compositions with increasing amounts of FMC and two GSDs. The lines connecting the CMOR values are for visual guidance.
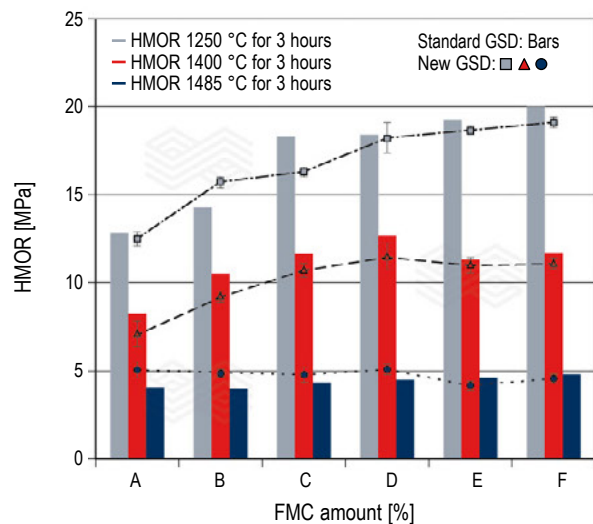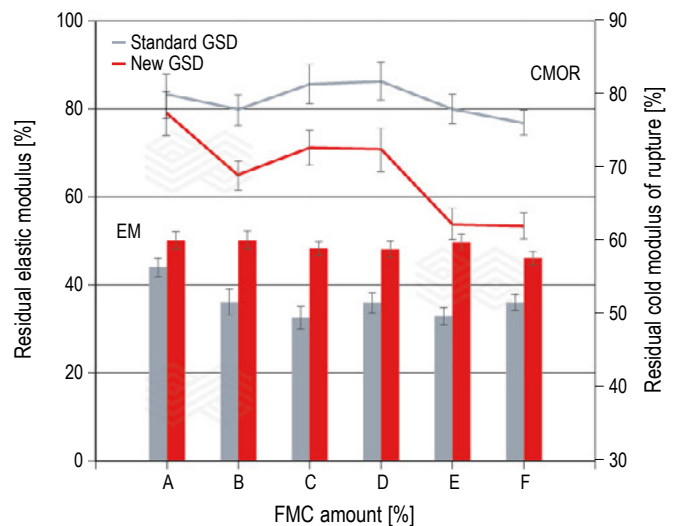

Figure 6.

Residual elastic modulus (EM) and residual cold modulus of rupture (CMOR) of the different magnesia-chromite brick compositions with increasing amounts of FMC and two GSDs after 5 thermal shock cycles (i.e., 725 ºC to room temperature). The lines connecting the residual CMOR values are for visual guidance.

indicate that increasing the FMC content was not detrimental to the thermal shock behaviour and that the new GSD positively impacted this property. However, the residual cold modulus of rupture showed a decreasing trend with increased FMC addition, which was more pronounced with the standard GSD.

Having determined that the thermal shock resistance was not detrimentally affected in materials featuring high FMC levels corresponding to direct-bonded compositions, it was essential to evaluate the impact of FMC addition on other pertinent properties, notably corrosion resistance. However, a critical aspect to enhancing this essential property entails understanding the material's permeability and abrasion characteristics, which in conjunction with chemical corrosion are key factors contributing to the compromised performance of magnesia-chromite bricks. Figure 7 shows the permeability and abrasion values obtained for 3 samples of each magnesia-chromite brick composition, indicating the permeability slightly decreased with FMC addition, irrespective of the GSD, and that abrasion was notably lower for both GSDs with increasing FMC content.
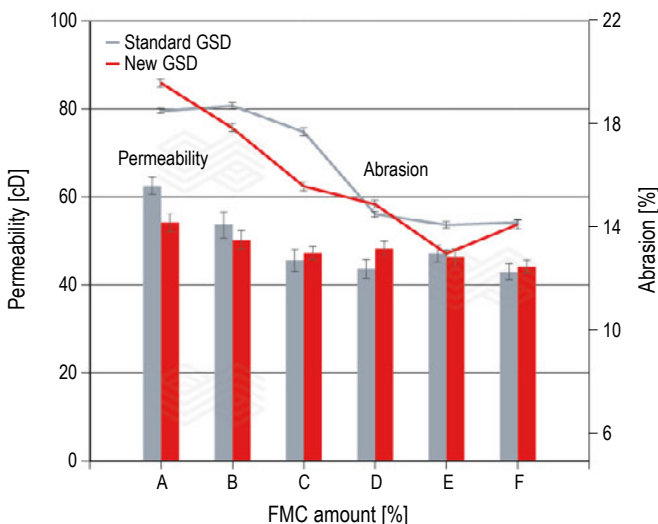
The final analyses performed on all the different magnesia-chromite brick compositions were corrosion tests conducted at 1700 °C for 5 hours with steel and fayalitic slag. It is important to mention that it was not possible to evaluate all 12 brick compositions simultaneously due to the experimental setup; however, multiple tests were conducted and wear in both the steel and slag zones was assessed. The results presented in Figure 8 show that in both the slag and steel zones, typically an increased FMC content positively influenced the corrosion resistance, with a significant benefit observed for the new GSD in the slag zone.

Plant Implementation Results

Following the culmination of research and development activities aimed at creating a new magnesia-chromite grade endowed with optimal properties and an engineered

microstructure, composition D was selected for plant trials. One-tonne mixes of both the standard and new GSD were processed in an industrial mixer, pressed into RH degasser throat shapes, and fired according to standard plant procedures. Subsequently, the properties of five bricks for each GSD were determined and the results compared to those of the laboratory-produced bricks (Table II). In the

Table II.

Comparison of the results obtained for laboratory and plant trial bricks produced using composition D with either the standard or new grain size distribution (GSD).

Composition D Properties	Laboratory trial bricks		Plant trial bricks	
	Standard GSD	New GSD	Standard GSD	New GSD
BD [g/cm^3]	3.31	3.34	3.34	3.36
AP [%]	13.90	13.13	13.37	12.37
CCS [MPa]	90	100	133	125
CMOR [MPa]	5.8	4.4	8.3	8.7
HMOR 1250 °C [MPa]	18.4	18.2	18.0	17.2
HMOR 1400 °C [MPa]	12.7	11.5	9.9	13.7
HMOR 1485 °C [MPa]	4.5	5.1	4.4	5.3
Abrasion [%]	14.5	14.9	8.0	7.7
Permeability [cD]	43.5	48.1	36.3	37.8
Thermal shock resistance (ΔT = 700 °C)				
Residual EM [%]	36.0	48.1	47.0	48.0
Residual CMOR [%]	72.3	83.0	72.4	81.8
Corrosion test (induction furnace at 1700 °C for 5 hours)				
Metal line [%]	6.19	4.72	5.50	5.76
Slag line [%]	52.08	32.30	42.79	39.35

Figure 8.

Corrosion of the different magnesia-chromite brick compositions with increasing amounts of FMC and two GSDs observed in the slag and steel zones after 5 hours at 1700 °C in an induction furnace. The bars correspond to corrosion of the standard GSD in the slag and steel zones and the triangles and squares to corrosion of the new GSD in the slag and steel zones, respectively. The lines connecting the corrosion percent of the new GSD are for visual guidance.

Figure 7.

Permeability and abrasion of the different magnesia-chromite brick compositions with increasing amounts of FMC and two GSDs. The lines connecting the abrasion values are for visual guidance.
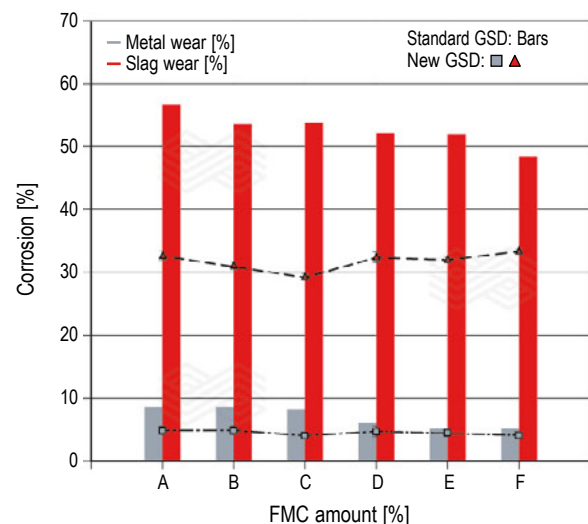
majority of cases, properties of the plant trial bricks were either equivalent or better than the laboratory-produced bricks, with the only notable exceptions related to the hot modulus of rupture. Furthermore, properties of the plant trial bricks with the new GSD were typically better than the standard GSD. Microscopy was also performed and showed that bricks produced in the plant with the new GSD had a dense microstructure (Figure 9). Consequently, composition D featuring the new GSD (i.e., RADEX TB016) was selected for field trials in the throat area of RH degassers at six Brazilian customers.

Customer Trial Results

Currently, only one of the six Brazilian customers has completed field trials with the developed material. In this case, the initial test was carried out in the outlet throat (down leg) of the RH degasser. Throughout this campaign, which ran for 78 heats and ended based on the customer's program, the field trial was documented in detail, as shown in Figures 10–12. Given that the outlet throat typically experiences lower stresses than the inlet throat (up leg), conducting a field trial in the less demanding region was an

Figure 9.
Microstructural evaluation of RADEX TB016, a fired magnesia-chromite brick produced during the plant trial (i.e., composition D) with the new GSD. The images (a–c) show a dense microstructure and FMC (1), sintered magnesia (2), and chromite (3) are indicated.

(a)   (b)   (c)
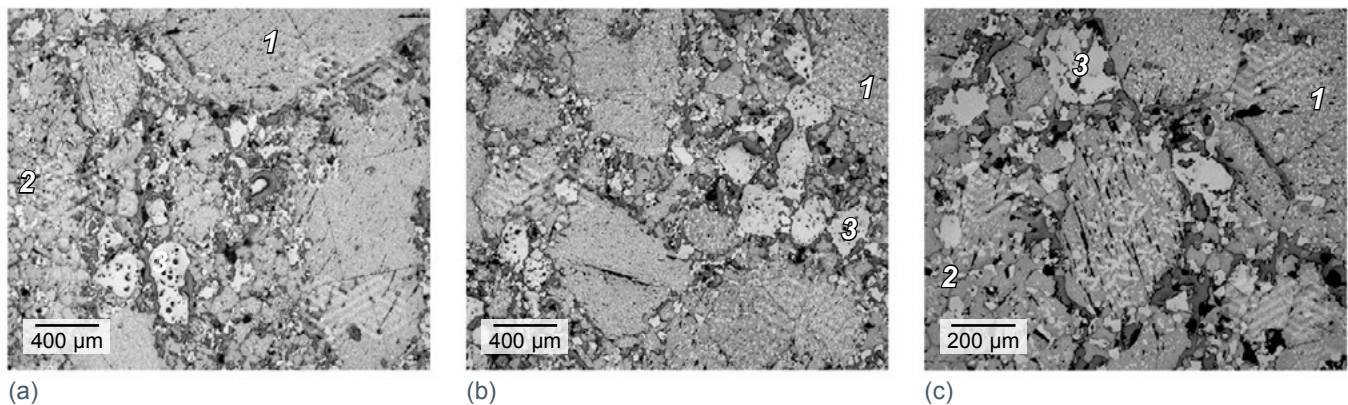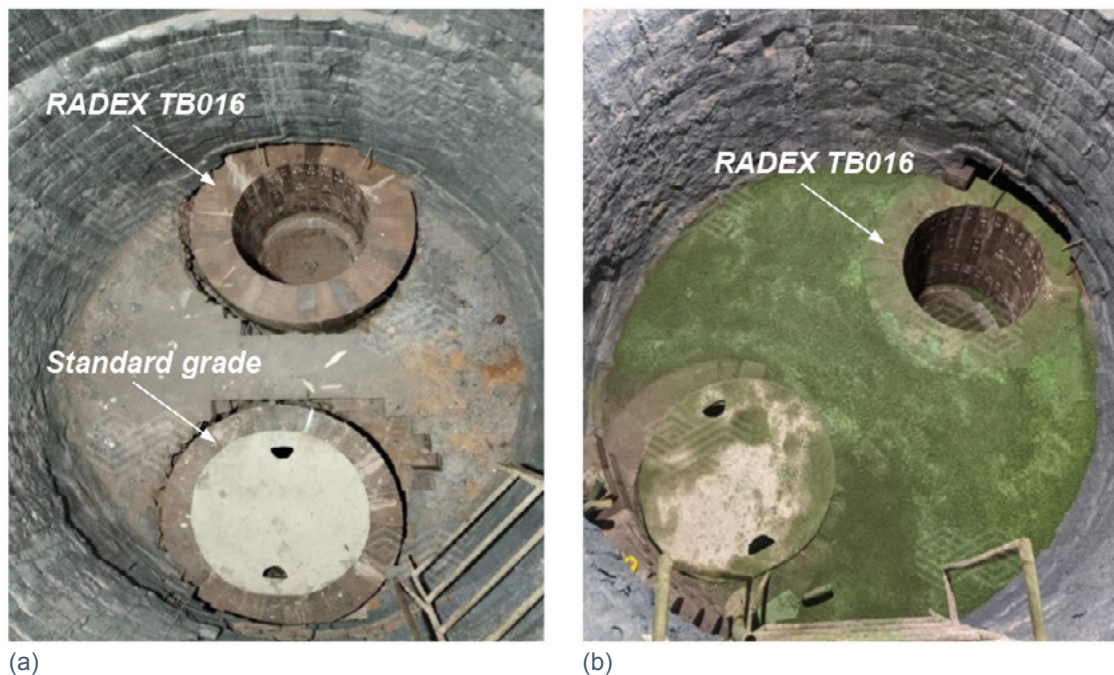
Figure 10.
RH degasser showing (a) installation of RADEX TB016 in the outlet throat and a standard magnesia-chromite grade in the inlet throat and (b) completed installation.

(a)   (b)

appropriate first step to evaluate the new grade. During the trial, the RADEX TB016 exhibited minimal wear with residual thicknesses ranging from 225 mm (initial brick dimension) to 190 mm. Furthermore, the RADEX TB016 bricks showed significantly less wear compared to the standard magnesia-chromite bricks from another supplier used to line this area. Figure 11 shows the visual appearance of the outlet throat lined with RADEX TB016 during the campaign. The

calculated wear rate of RADEX TB016 was 0.385 mm/hour, indicating a potential throat lifetime of up to 415 heats with this new grade, while maintaining a minimum safety thickness of 60 mm. Following the initial field trial, RADEX TB016 was successfully implemented in the inlet throat for a campaign of 104 heats, which ended according to the customer-defined process.

Figure 11.

Images of the RH degasser outlet throat region lined with the RADEX TB016 at (a) 22 heats, (b) 34 heats, (c) 52 heats, and (d) 78 heats during the campaign.

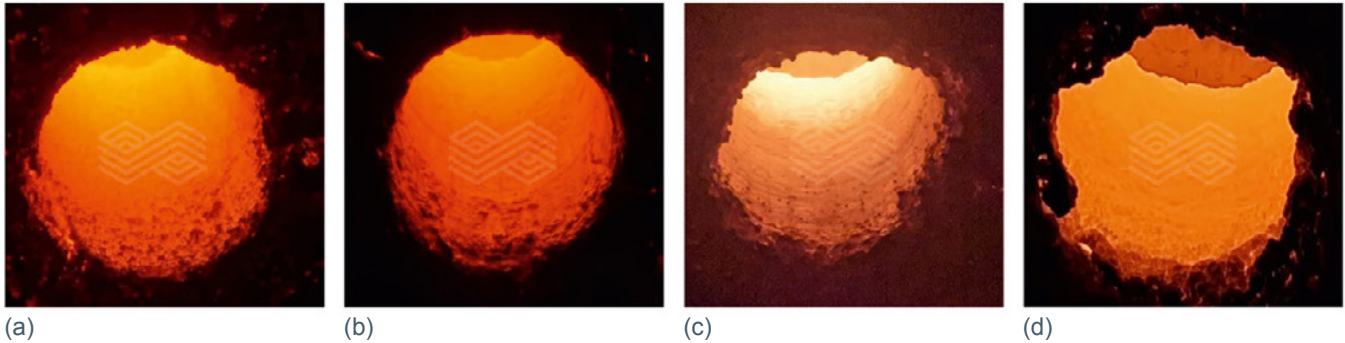(a)   (b)   (c)   (d)

Figure 12.

(a) lining disassembly of the outlet throat region lined with RADEX TB016 enabling measurement of (b) the residual brick thicknesses that ranged from 190–195 mm.

(a)   (b)

Conclusion

Magnesia-chromite bricks, incorporating increasing amounts of FMC as a substitute for sintered magnesia and chrome ore, were produced on a laboratory scale and comprehensively evaluated. In addition, the impact of two distinct GSDs on the various magnesia-chromite brick compositions was also assessed. The results indicated that regarding essential properties for magnesia-chromite brick applications, the addition of FMC enhanced these properties, underscoring the importance of rebonded magnesia-chromite bricks for various demanding applications. Furthermore, the other parameter investigated in this study demonstrated the potential for property enhancement not only through high-quality raw materials but also by optimising the GSD. Following extensive comparative analysis of numerous compositions during the developmental phase, composition D was chosen for plant trials with both the standard and new GSD. Although most of the properties measured for the bricks produced with both GSDs in the plant were better than the laboratory-scale equivalent, particularly notable improvements were observed with the new GSD. Consequently, composition D featuring the new GSD (i.e., RADEX TB016) was selected for field trials at six Brazilian steel plants in the RH degasser. Recently, trials at one customer were completed and showed excellent performance of RADEX TB016 in the outlet and inlet throats, with the potential to increase the RH degasser's lifetime. In conclusion, the newly developed magnesia-chromite grade, RADEX TB016, further extends RHI Magnesita's portfolio of high-performance refractory grades for RH degassers.

References

[1] Azhari, A., Golestani-Fard, F. and Sarpoolaki, H. Effect of Nano Iron Oxide as an Additive on Phase and Microstructural Evolution of Mag-Chrome Refractory Matrix. *J. Eur. Ceram. Soc.* 2009, 29, 2679–2684.

[2] Goto, K. and Lee, W. E. The "Direct Bond" in Magnesia Chromite and Magnesia Spinel Refractories. *J. Am. Ceram. Soc.* 1995, 78, 1753–1760.

[3] Alper, A.M. (Ed.). *High Temperature Oxides*; Academic Press: New York, 1970.

[4] Guo, Z. and Ma, Y. Bonding Mechanisms of Basic Refractories for RH Snorkels. Presented at the 16th United International Technical Conference on Refractories (UNITECR), Yokohama, Japan, Oct. 13–16, 2019.

[5] Landy, R.A. *Magnesia Refractories. In: Refractories Handbook*; CRC Press, 2004, 109–149.

[6] Xu, T., Xu, Y., Li, Y., Sang, S., Wang, Q., Zhu, T., Nath, M. and Zhang, B. Corrosion Mechanisms of Magnesia-Chrome Refractories in Copper Slag and Concurrent Formation of Hexavalent Chromium. *J. Alloy. Compd.* 2019, 786, 306–313.

[7] Zhu, D., Yang, C., Pan, J., Zhang, Q., Shi, B. and Zhang, F., Insight into the Consolidation Mechanism of Oxidized Pellets Made from the Mixture of Magnetite and Chromite Concentrates. *Metall. Mater. Trans. B.* 2016, 47, 1010–1023.

[8] Brosnan, D.A. *Corrosion of Refractories. In: Refractories Handbook*; CRC Press, 2004, 39–78.

[9] Borges, O. H., Coury, F. G., Muche, D. N. F. and Pandolfelli, V. C., Eco-Friendly Design of Complex Refractory Aggregates as Alternatives to the Magnesia-Chromite Ones. *J. Eur. Ceram. Soc.* 2023, 43, 6536–6549.

Authors

José Alvaro Previato Sardelli, RHI Magnesita, Contagem, Brazil.
Sérgio Eustáquio Soares, RHI Magnesita, Contagem, Brazil.
Gláucio Galdino Martins, RHI Magnesita, Contagem, Brazil.
Corresponding author: José Alvaro Previato Sardelli. Jose.Sardelli@rhimagnesita.com

Return to Content

Rainer Neuböck, Gerald Nitzl, Christoph Eglsäer and Reinhard Ehrengruber

Clean Steel Casting Technology

Refractories and flow control systems for clean steel casting are technology drivers because the demands on steel cleanliness are permanently increasing. Clogging and nonmetallic inclusions in steel not only contribute to additional costs but also have an impact on the continuous casting process due to product downgrades and increased scrap rates. Since low pressures and high turbulence during liquid steel transfer from the ladle to the mould create sources of potential contaminations, special solutions to minimise nonmetallic inclusion formation are required as well as efficient ways to remove them. This starts in the ladle with specialised purging plugs for improved inclusion flotation and ends in the continuous casting mould with modelling to optimise liquid steel flow. Furthermore, in between these two process steps there are refractory systems in the RHI Magnesita product portfolio that can contribute to maintaining high cleanliness of the liquid steel on its journey from a batch process in the ladle to the continuous casting operation in the mould.

Introduction

The term "clean steel" is commonly used to describe steels with low levels of soluble elements (e.g., sulphur, phosphorous, nitrogen, oxygen, and hydrogen), residual elements (e.g., copper, lead, zinc, and magnesium), and above all to define steels with a low frequency of failure due to defects related to nonmetallic inclusions [1]. Both clogging and nonmetallic inclusions affect steel cleanliness and plant productivity in a negative way and in many cases these phenomena are interconnected. For example, clogging in the casting channel affects flow performance and reduces sequence length, while inclusions in the final product can lead to higher scrap rates or downgrading the cast steel. This not only has a negative impact on the conversion costs (Figure 1) but additional resources and energy are required when the steel must be reproduced due to high scrap rates. A fully integrated steel plant generates approximately two tonnes of CO_2 (scope 1 and 2) per tonne of steel [2] and in regions with carbon pricing schemes the cost of these emissions is expected to increase, further exemplifying why the yield improvement of prime quality steel is so important.

Product Portfolio from the Ladle to the Mould

At the continuous caster, a sequence of ladles is poured into the tundish and converted into a continuous process. The liquid steel is then distributed to one or more strands where it solidifies in the mould. As shown in Figure 2, RHI Magnesita can offer all refractory consumables and flow control systems in the complete continuous casting domain.

Clogging and nonmetallic inclusions can form due to contact of the liquid steel with air, refractories, and slag; therefore, controlling these side reactions is key to casting clean steels. As low pressure and high liquid steel turbulence accelerate contact reactions (Figure 3), areas of low pressure need special solutions to protect the liquid steel from detrimental air ingress into the casting channel. This can be achieved by adopting innovative sealing, shrouding, and inert gas shielding approaches. On the other hand, high levels of turbulence can lead to unwanted refractory erosion and slag emulsification, which can be minimised by reducing and dissipating the turbulence using flow modifiers in the tundish and specially designed subentry nozzles for the mould.

Figure 1.

Clogging and nonmetallic inclusions: Influencing factors on total conversion costs.
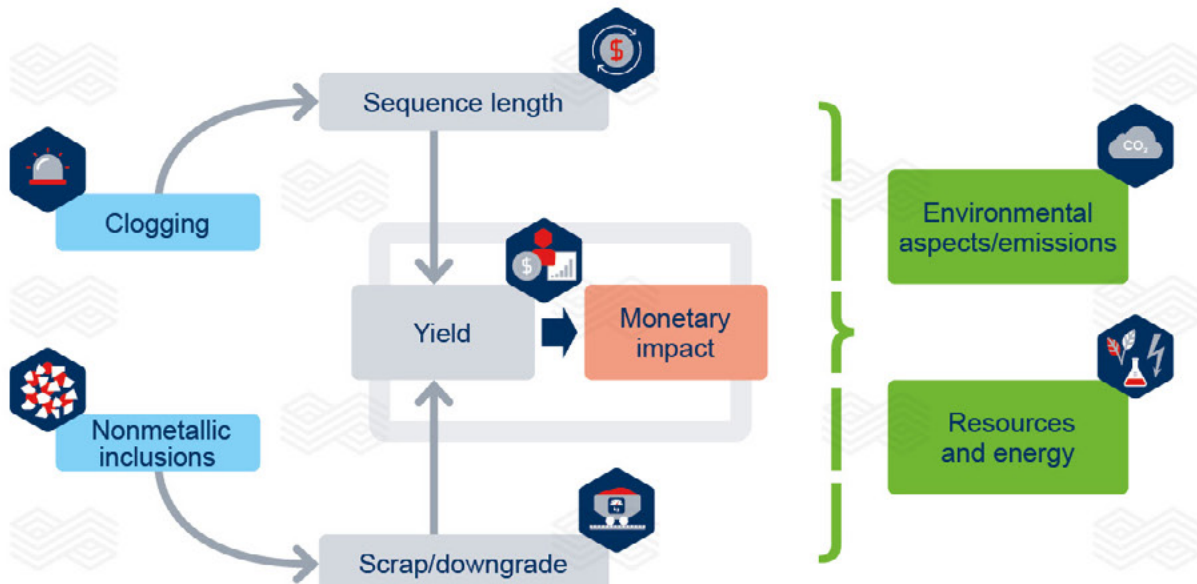
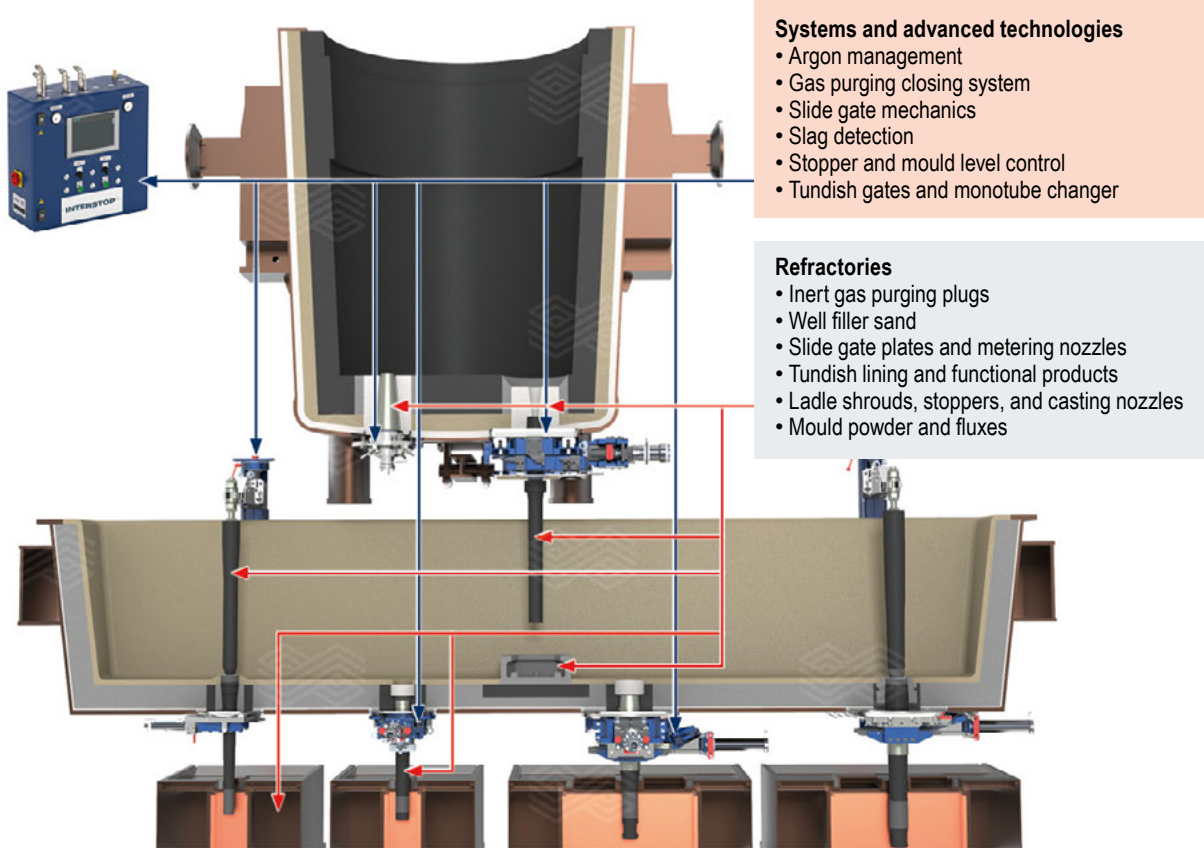**Figure 2.**

Product portfolio from the ladle to the mould.

Systems and advanced technologies
• Argon management
• Gas purging closing system
• Slide gate mechanics
• Slag detection
• Stopper and mould level control
• Tundish gates and monotube changer

Refractories
• Inert gas purging plugs
• Well filler sand
• Slide gate plates and metering nozzles
• Tundish lining and functional products
• Ladle shrouds, stoppers, and casting nozzles
• Mould powder and fluxes

Figure 3.

Potential sources of steel contamination.

		Pressure	Turbulences
1	Ladle	High	High/low
2	Ladle gate	High/low	High
3	Ladle shroud	Low	High
4	Tundish	High	High/low
5	Nozzle	Low	High
6	Mould	High/low	High/low

Clogging/nonmetallic inclusions → **Casting and product defects**
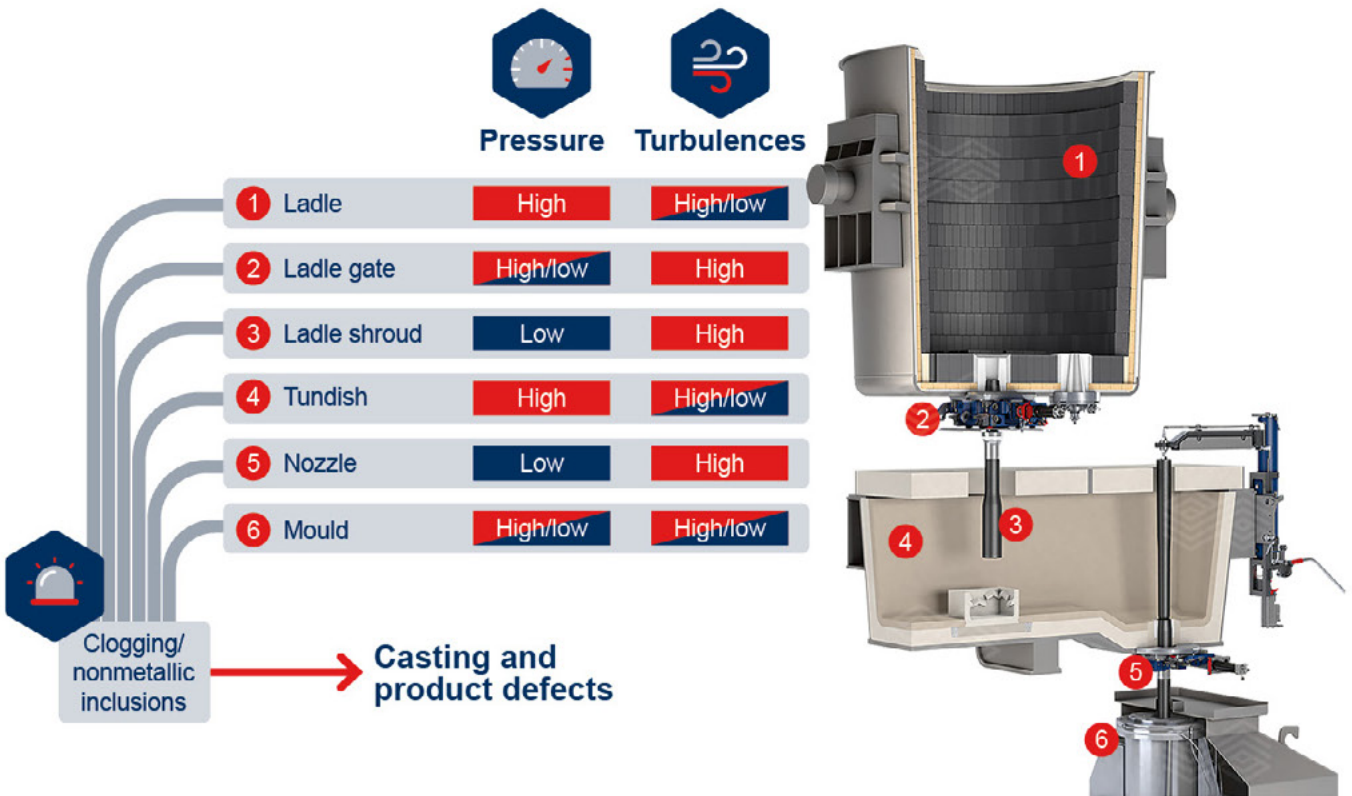
Ladle Operation

A key to clean steel casting is steel cleanliness in the ladle, which requires the temperature and nonmetallic inclusion load in the melt to be accurately controlled and every ladle in the casting sequence to be as reproducible as possible. This can be effectively achieved using inert gas purging with hybrid plugs [3], a technology that generates both the high gas flow rates required for rapid metallurgical treatment and melt homogenisation as well as fine bubbling for inclusion flotation while avoiding reoxidation at the meniscus. Using water modelling experiments it has been possible to determine the relationship between gas flow rates and bubble size for different inert gas purging plugs and visualise the high number of bubbles generated by hybrid plugs (Figure 4).

The main features and benefits of hybrid plugs are:

- Multicomponent plug combining random and directional porosity.
- Excellent flow rate adjustability.
- High volume of fine bubbles at low flow rates.
- 100% opening rate.
- Integrated safety indicator.
- Low service costs.
- Supports continuous and discontinuous operations as well as high ladle bottom lifetimes.

An important challenge with inert gas purging is to control the bubble size distribution at low argon flow rates. Especially at the beginning of the gas purging process, a dense slag cover on the steel bath surface makes it very difficult for the operator to define the correct flow rate. Furthermore, if gas purging is excessive the formation of an open eye on the steel surface can create issues with unwanted reoxidation and the formation of nonmetallic inclusions.

To address this issue, RHI Magnesita has been investigating the vibrational patterns of different inert gas plugs as an approach to characterise gas purging behaviour. This is achieved by installing an acceleration sensor on the outer gas pipe of the purging plug and online analysis of the vibration signals using special fast Fourier transformation algorithms to generate the relative bubble size (i.e., bubble index) (Figure 5). The aim of this technology is that the bubble index will indicate to the operator the actual purging

Figure 4.

Hybrid purging plug performance visualised using water modelling experiments. (a) relationship between bubble size, bubble number, and gas flow rate and (b) comparison of a hybrid and slot plug.
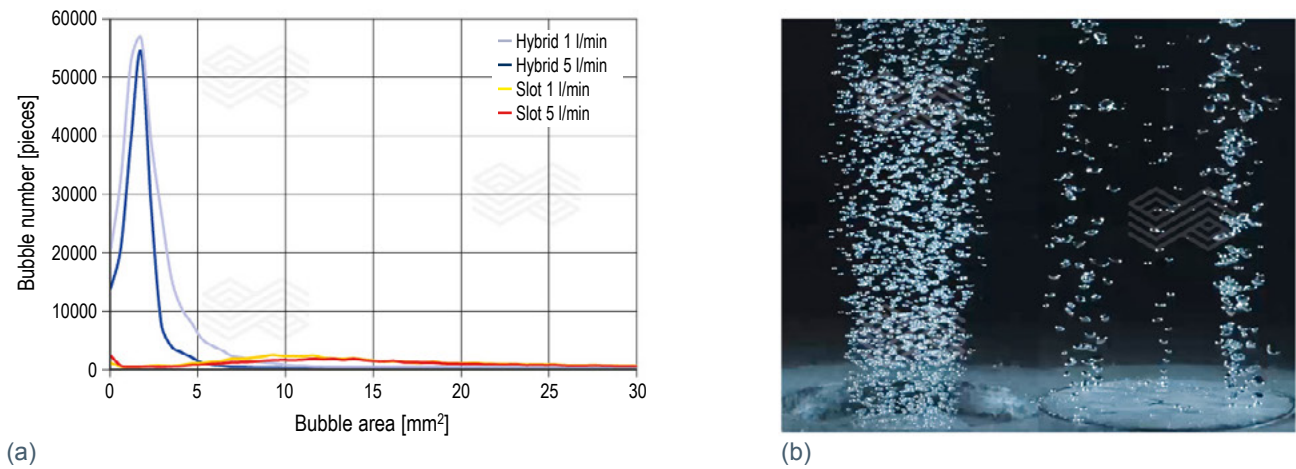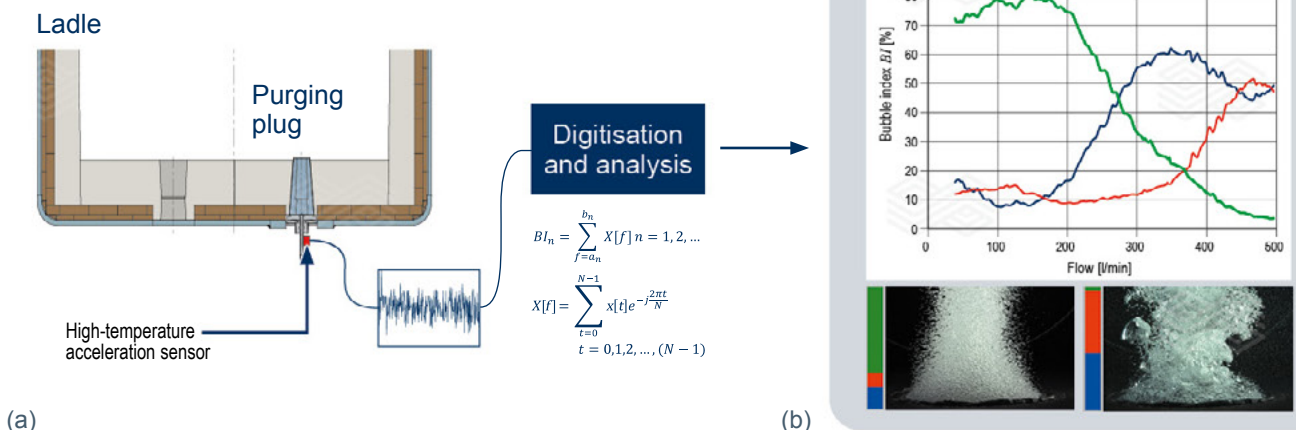

(a)

(b)

Figure 5.

Technological approach to characterise inert gas purging plug behaviour. (a) acceleration sensor on the outer purging plug gas pipe and (b) online analysis of the vibration signals.

$$BI_n = \sum_{f=a_n}^{b_n} X[f] \; n = 1, 2, \dots$$

$$X[f] = \sum_{t=0}^{N-1} x[t] e^{-j\frac{2\pi t}{N}}$$
$$t = 0, 1, 2, \dots, (N-1)$$

(a)

(b)

performance, even when the liquid steel surface is not visible during the purging process [4]. This technology will help to improve the consistency of inert gas purging control, also under different purging plug wear conditions. The main characteristics of this technology include:

- An acceleration sensor mounted on the purging plug gas pipe.
- The signal is digitised and converted into a frequency spectrum.
- An algorithm transforms the frequency spectrum into a bubble index.
- The relative bubble size distribution can be visualised.
- Purging plug performance can be optimised.

Ladle to Tundish Transfer

With steel transfer from the ladle to the tundish, a batch operation becomes a continuous process. To maintain an almost constant steel level in the tundish, a slide gate mounted on the ladle bottom controls the quantity of liquid steel flowing through the ladle shroud into the tundish. Due to the negative pressure below the throttling of the ladle gate system, a strong pressure drop occurs in the steel stream [5].

A typical setup for the new automation-ready gate is shown in Figure 6 [6,7]. This INTERSTOP SX ladle gate system provides not only excellent operational performance, but an improved cost benefit compared to other gate systems. Furthermore, the system can be upgraded at any time with various technical features including:
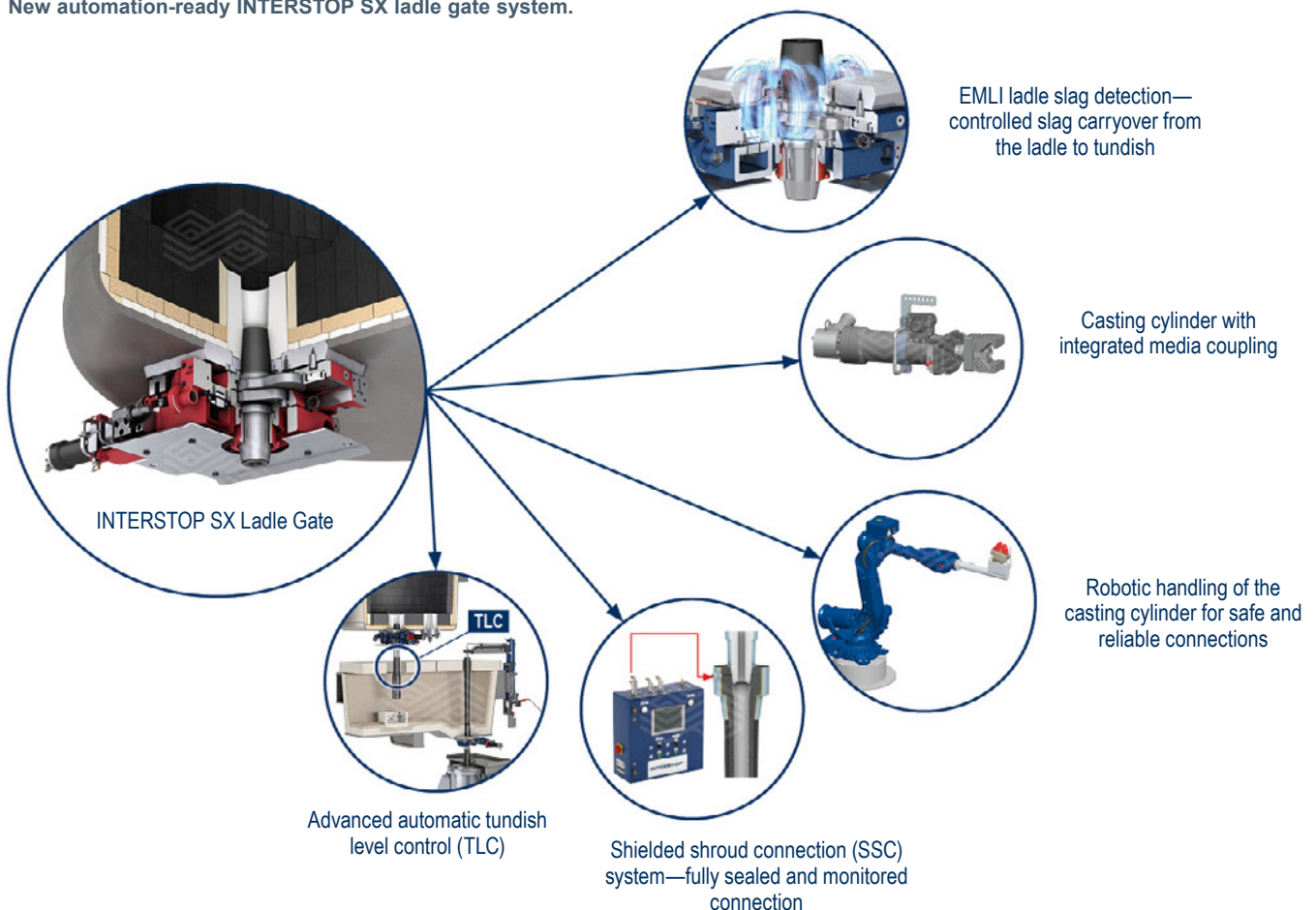
- Electromagnetic slag detection system (EMLI) to minimise ladle slag carryover.
- Casting cylinder with automation-ready media couplers.
- Robotic handling system for safe ladle gate operations.
- Shielded shroud connection (SSC) systems to minimise air aspiration into the casting channel.
- Advanced automatic tundish level control (TLC) for smooth operation.

Furthermore, as refractories such as ladle slide gate plates must resist extremely high thermal shocks due to cold starts, RHI Magnesita offers a wide range of high-performance grades that are appropriate for different gate systems and plate sizes [8].

The main purpose of a ladle shroud is to avoid steel oxidation during its transfer from the ladle into the tundish. High turbulences in the casting channel, which are created by high ferrostatic pressure and severe slide gate throttling practise, require special refractory solutions. In order to avoid erosion and potential holing in the steel impingement area of the ladle shroud, a high erosion resistant inner liner is required. Such a reinforcement liner concept is often necessary for big slab caster reverse taper or bell shrouds.

Figure 6.
New automation-ready INTERSTOP SX ladle gate system.

EMLI ladle slag detection—controlled slag carryover from the ladle to tundish

Casting cylinder with integrated media coupling

Robotic handling of the casting cylinder for safe and reliable connections

INTERSTOP SX Ladle Gate

Advanced automatic tundish level control (TLC)

Shielded shroud connection (SSC) system—fully sealed and monitored connection

When opening the steel flow with a new ladle, an immersed opening ensures avoiding reoxidation of the steel stream. In addition, it reduces the risk of tundish cover powder emulsifiaction. Such shrouds, due to their longer shape and bigger exit diameters (to avoid blow-back), are approximately 50% heavier than standard shrouds (Figure 7).

Thermomechanical stresses, which can result from the ladle shroud contact to the collector nozzle, need special refractories reinforced with metal cans to ensure safe and reliable operation with minimal nitrogen pickup [9]. Typical shrouds with a reinforced throat and inner liner are shown in Figure 7. The key features and benefits of high-performance ladle shrouds include:

- Immersed opening possible for bell and reverse taper shrouds.
- Very good thermal shock resistance for cold starts.
- Resistance against high manipulator upthrust forces.
- Metal can support.
- Argon shielding possible.
- Less transition slabs.
- Outstanding oxidation resistance in the throat for oxygen lancing.
- Wear-resistant liner.
- Slagline reinforcement possible.

In addition to the above-mentioned topics, sealing and inert gas shielding at the ladle shroud connection to the collector nozzle are important [10]. Although different design solutions for sealing and shielding are available to ensure stable and safe operation, during process improvements sealing must be regarded as the first priority and shielding as the second.

Tundish Operation

When steel flows through the ladle shroud into the tundish, the turbulent kinetic energy needs to be dissipated to avoid refractory wear and the direction of steel flow must be optimised to improve residence time and inclusion flotation. Furthermore, the steel flow needs to be controlled to feed all strands with the same steel quality and temperature. Simulation tools like water modelling in combination with computational fluid dynamics enable different TUNFLOW impact pots to be designed for the required tundish geometry and throughput (Figure 8). These shapes need to be customised to achieve maximum performance and the lowest conversion costs during tundish operation [11,12]. In summary, the advantages of TUNFLOW impact pots are:

- Designed to the customer's requirements using state-of-the-art simulation technologies.
- Barriers to eliminate kinetic energy.
- Design to promote plug flow.
- Support the flotation of nonmetallic inclusions by enhancing residence time and flow direction.
- High anti-splash properties.
- Reduced slag emulsification.
- Less surface turbulence and reoxidation.
- Cold start capabilities.

Figure 7.

High-performance ladle shrouds.

Figure 8.

(a) computational fluid dynamics to examine tracer concentration in the tundish and (b) TUNFLOW designs.
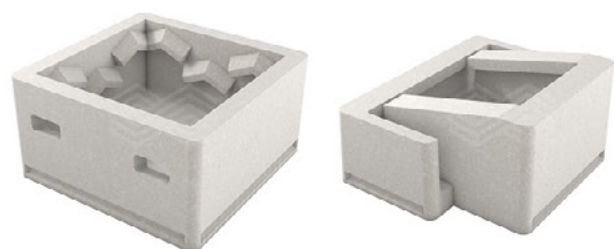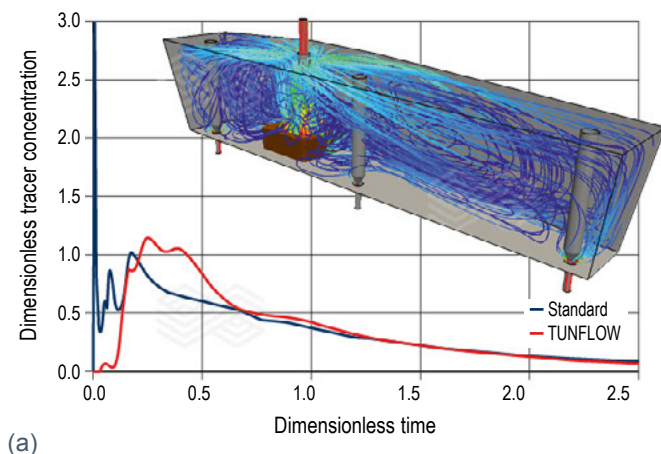
Additional refractory advances in the tundish area include energy-saving lining technologies that reduce the CO_2 footprint due to a decreased gas consumption for heat-up procedures, such as sol-bonded mixes for the permanent lining and cold-setting (i.e., self-hardening) wear lining mixes (see page 68). Besides the environmental and energy saving benefits, the self-hardening mixes (e.g., ANKERTUN SH) result in faster relining and better availability of the tundish fleet [13,14].

In addition to TUNFLOW impact pots and tundish lining using energy-saving mixes, thermodynamic simulations (e.g., FactSage) can be used to optimise steel/refractory/tundish slag interactions for minimum steel contamination. As a result of combining all these approaches, the overall cost per tonne of cast steel can be reduced.

INTERSTOP's new slide gate systems for tundish operation incorporate sealed housing and inert gas purging to avoid air ingress at the junction between the plates. This development not only results in improved steel cleanliness, less clogging, and increased sequence length, but also widens the product portfolio [15]. Furthermore, for slab casters an integrated monotube changer provides additional safety and the possibility for long sequence casting. Very important features to achieve stable mould level performance are (Figure 9):

- Accurate regulation of the cylinder and slide gate.
- Advanced mould level control system and sensors.
- Controlled argon feeding for the gate system and casting channel.
- Wear-resistant refractory shrouding system.

All these components can be assembled according to the special needs and requirements.

Argon Purged Stoppers for Slab Casting

Argon purged stoppers are widely used for casting Al-killed steel grades to minimise nonmetallic inclusions precipitating on the casting nozzle inner surface. However, as nonhomogeneous argon bubble injection has been shown to result in severe mould level fluctuations and contribute to surface defects, the Slot Hole Plug (SHP) stopper nose design was developed (Figure 10) [16,17]. In addition to reducing sliver defects on the slab surface, the SHP stopper technology results in a stable gas feed and fine bubble distribution to capture inclusions whenever they flow into the casting channel. This even distribution of fine bubbles reduces mould level perturbations caused by unwanted bubble bursting effects on the steel meniscus in the mould and flow pattern changes from bubbly- to slug-flow can also be minimised with improved argon purging strategies. Ultra low carbon (ULC) steel grades have been shown to benefit the most from using the SHP argon stopper technology.

Figure 9.

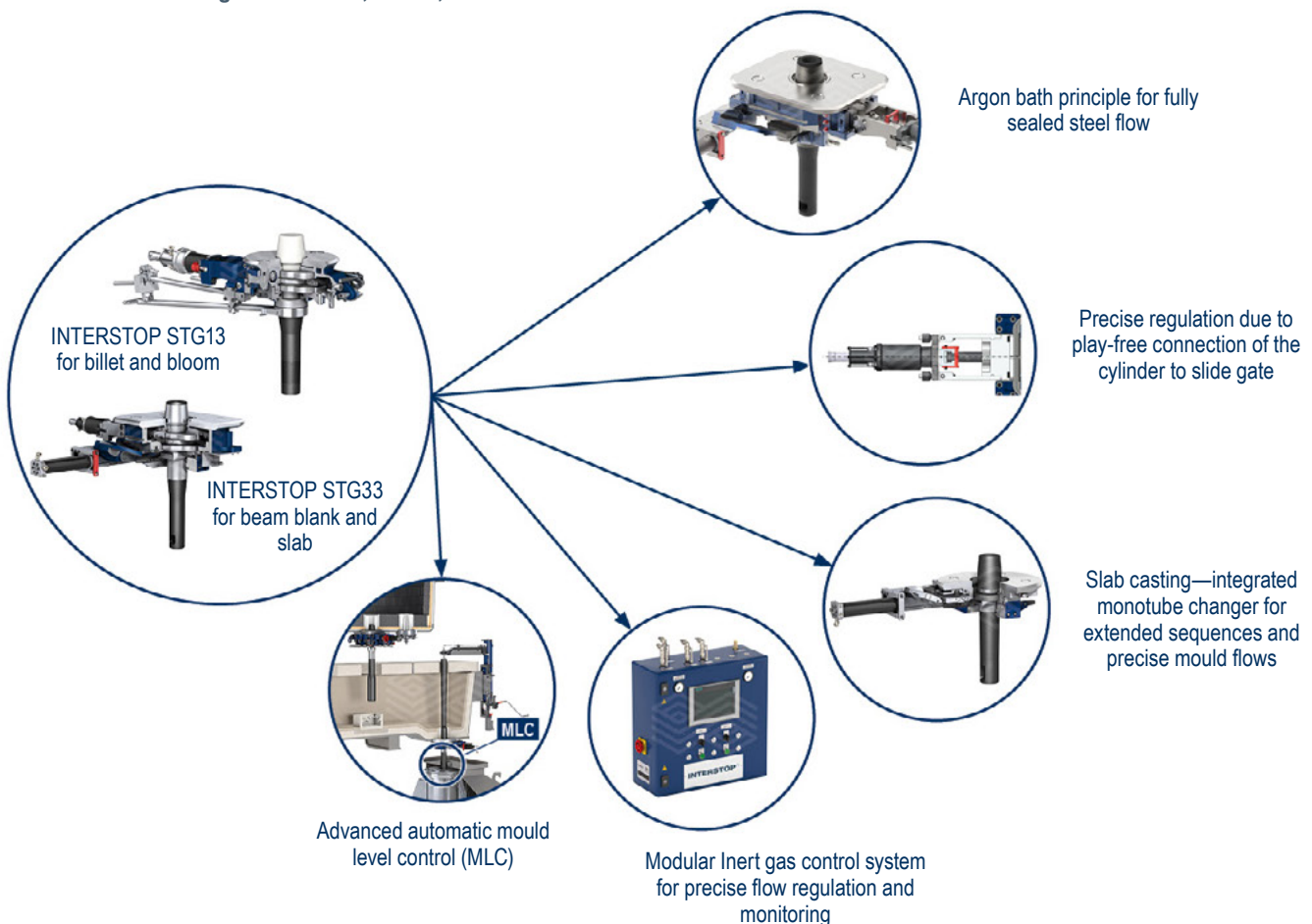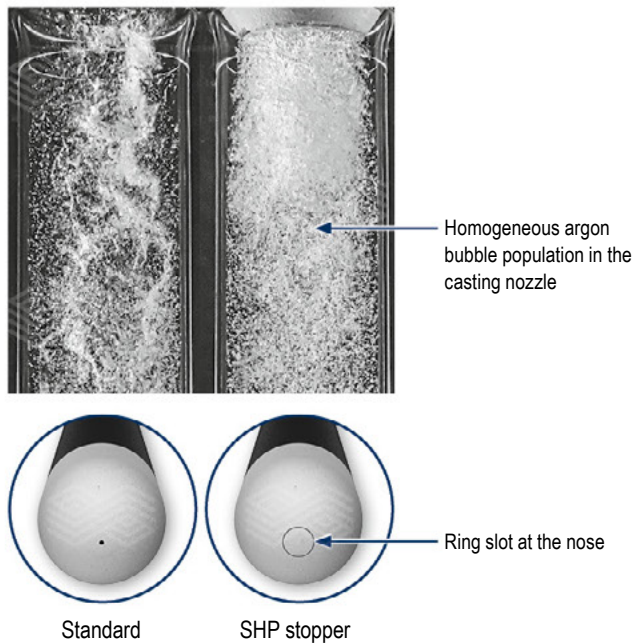**Sealed tundish slide gates for billet, bloom, and slab casters.**

INTERSTOP STG13 for billet and bloom

INTERSTOP STG33 for beam blank and slab

Argon bath principle for fully sealed steel flow

Precise regulation due to play-free connection of the cylinder to slide gate

Slab casting—integrated monotube changer for extended sequences and precise mould flows

Advanced automatic mould level control (MLC)

Modular Inert gas control system for precise flow regulation and monitoring

Figure 10.

Comparison of a standard and SHP stopper for argon purging.

Homogeneous argon bubble population in the casting nozzle

Ring slot at the nose

Standard   SHP stopper

High-Performance Refractories for Anticlogging

In addition to the aforementioned high-performance systems and refractories available from RHI Magnesita for clean steel applications, clogging in the casting channel can be further minimised by:

- Combining argon purged refractories. For example, using the direct purging mononozzle technology in combination with an argon purged stopper (Figure 11) [18].
- Incorporating special liners with anticlogging properties in the inner bore of casting nozzles (Figure 12) [19,20].

Conclusion

The formation of nonmetallic inclusions and refractory clogging during steelmaking have detrimental effects on steel cleanliness and conversion costs. Therefore, RHI Magnesita has developed a comprehensive portfolio of flow control systems and refractories for clean steel casting. Using state-of-the-art equipment, a range of products has been designed showing excellent thermomechanical properties and corrosion resistance required for demanding

Figure 11.

(a) direct purging mononozzle and (b) combining an argon purged stopper and the direct purging mononozzle technology.

(a)   (b)

Figure 12.

Cut products showing an anticloggging inner liner in the bore.
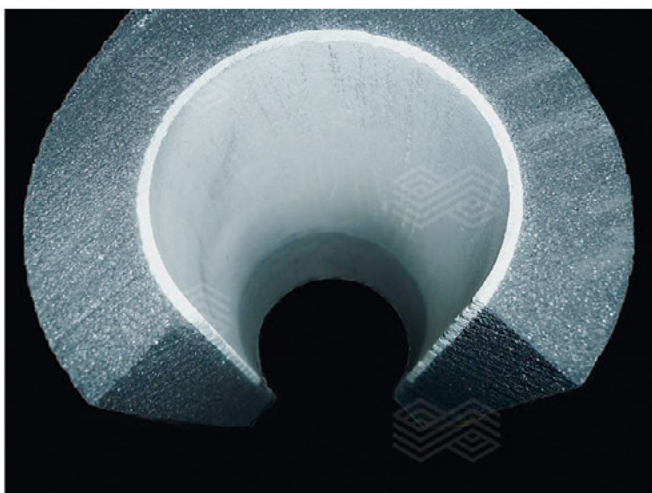
applications. In addition, optimising numerous operational parameters in the continuous casting process can also contribute to steel cleanliness and less clogging, such as improving the refractory preheat cycle, product installation, casting nozzle design [21–23], and sealing the gas feeding lines [10]. Overall, an optimum result can only be achieved by trying to address all influencing factors summarised in this article [24]. Factfinding plays a key role in identifying the highest potentials for improvement in the process chain from the ladle to the mould. Furthermore, customising solutions available in RHI Magnesita's portfolio can contribute to metallurgical and process advances, leading to a more efficient operation that includes energy savings and a reduced CO_2 footprint.

References

[1] https://www.sidenor.com/wp-content/uploads/2017/06/SID_WHITEPAPER_ACEROS_LIMPIOS_EN.pdf

[2] Smith, R. and Ordosch, A. Steel CO_2 Dashboard. October 2020. CRU International Ltd., London, UK.

[3] Trummer, B., Fellner, W., Viertauer, A., Kneis, L. and Hackl, G. A Water Modelling Comparison of Hybrid Plug, Slot Plug and Porous Plug Designs. *RHI Bulletin*. 2016, 1, 35–38.

[4] Trummer, B., Manhart, C. and Fellner, W. Vibrational Determination of Gas Purging Regime and Efficiency in a Water Model and Validation by a High-Speed Camera. *Bulletin*. 2020, 50–54.

[5] Hackl, G., Fellner, W., Heinrich, H. and Bühlmann, R. New Slide Gate Water Model Facility. *RHI Bulletin*. 2017, 1, 60–63.

[6] Ehrengruber, R., Baumgartner, G., Steins, A. and Renggli, R. Latest INTERSTOP Ladle and Tundish Systems Ready for Robotic Handling. *Bulletin*. 2021, 48–52.

[7] Ehrengruber, R., Bühlmann, R., Schmidt, V. and Persson, M. Influence of the Trends Robotics and Digitalisation on Ladle Slide Gate Development. *China Refractories*. 2021. 30, 30–34.

[8] Müller, M.A., Sherriff, R. and Wiesel, M. Development of Slide Gate Refractories Based on the Investigation of Wear Mechanisms. *RHI Bulletin*. 2007, 1, 39–42.

[9] Pinto, J., Freire, R., Resende, R. and Martins, D. Ladle Shroud Design Optimisation through Numerical Modelling. *Bulletin*. 2019, 46–50.

[10] Ehrengruber, R., Excellence in Inert Gas Control Systems for the Steel Industry. *RHI Bulletin*. 2015, 1, 7–15.

[11] Arth, G., Meurer, D., Kappel, M., Loop, P. and Petritz, B. Tundish Technology and Processes: Ladle to Mould Systems and Solutions (Part III). *Bulletin*. 2018, 64–70.

[12] Resende, A., Lukesch, G., Hackl, G. and Meurer, D. Tundish Refractory Design Optimisation Through Mathematical and Physical Modelling. *Bulletin*. 2021, 1, 60–65.

[13] Kirschen, M., Badr, K., Cappel, J. and Drescher, A. Intelligent Refractory Systems: A Cost Effective Method to Reduce Energy Consumption and CO_2 Emissions in Steelmaking. *RHI Bulletin*. 2010, 2, 43–49.

[14] Sorger, R. and Petritz, B. New Cold-Setting Mixes for Tundish Wear Linings. *RHI Bulletin*. 2011, 1, 54–58.

[15] Heinrich, B., Cousin, J-D., Bühlmann, R. and Ehrengruber, R. New INTERSTOP Sealed Tundish Gate for Billet and Bloom Casting, *Bulletin*. 2022, 29–33.

[16] Nitzl, G., Liu, X., Liu, Q., Shen, J. and Tang, Y. New Argon Stopper Technology for Slab Casting. *China Refractories*. 2021, 30, 41–44.

[17] Krumpel, G., Fuchs, R., Posch, W., Michelitsch, A. and Hackl, G. Optimized Argon Supply from Tundish to Mold using the SHP stopper. Proceedings of METEC and 2nd ESTAD, Düsseldorf, Germany, June 15–19, 2015.

[18] Seitz, P., Nitzl, G., Fauhl, M. and Botvinikova, O. New Direct Purging NC Technology for Slab Casting. *Bulletin*. 2021, 54–58.

[19] Seitz, P., Tang, Y. and Nitzl, G. Refractory Tubes with Innovative Liner Technology for Flow Control and Clean Steel Applications. *Bulletin*. 2020, 42–48.

[20] Dösinger, H., McFarlane, C., Nitzl, G., Tang, Y. and Hackl, G. Anticlogging Solutions for Isostatically Pressed Submerged Nozzles. *RHI Bulletin*. 2015, 1, 84–87.

[21] Hackl, G., Tang, Y., Nitzl, G., Chalmers, D., Dorricott, J. and Heaslip, L. Design Optimization of Submerged Entry Nozzles Using Simulation Technology. *RHI Bulletin*. 2014, 1, 47–53.

[22] Hackl, G., Tang, Y., Nitzl, G., Schurmann, D., Willers, B. and Eckert, S. GYRONOZZLE – An Innovative Submerged Entry Nozzle Design for Billet and Bloom Casting. *Bulletin*. 2019, 52–57.

[23] Hackl, G., Nitzl, G., Tang, Y., Eglsäer, C. and Krumpel, G. Novel Isostatically Pressed Products for the Continuous Casting Process. *RHI Bulletin*. 2015, 1, 78–83.

[24] Raidl, G. and Cappel, J. The Basics of Clean Steel in Continuous Casting. ARCS-13, Ispat Bhawan, SAIL, Ranchi, India, June 26–28, 2013.

Authors

Rainer Neuböck, RHI Magnesita, Leoben, Austria.
Gerald Nitzl, RHI Magnesita, Vienna, Austria.
Christoph Eglsäer, RHI Magnesita, Vienna, Austria.
Reinhard Ehrengruber, RHI Magnesita Switzerland AG, Hünenberg, Switzerland.
Corresponding author: Christoph Eglsäer, Christoph.Eglsaeer@rhimagnesita.com

Return to Content

Markus Fasching, Stefan Eder, Bernhard Griessler and David Wappel

Sustainable Tundish Lining—Reducing Energy Consumption and CO$_2$ Emissions While Achieving Cost Savings

As the most relined vessel in a steel plant, the tundish can be very time-consuming and work-intensive regarding lining frequence, drying, and preheating. Therefore, when it comes to the modern tundish lining, it is important to supply refractory products that are cost-efficient, time saving, as well as sustainable. In this regard, the combination of sol-bonded permanent linings and cold-setting wear linings are state-of-the-art for tundish applications because these refractories not only enable a reduction of the CO$_2$ footprint and energy consumption, but also the possibility of faster lining installation requiring less manpower. Additional environmental benefits are also possible by switching the primary raw materials to a more local source or even substituting a proportion with recycled materials. This paper provides a description of RHI Magnesita's sustainable tundish lining recommendations, including case studies that exemplify the achievable savings that support green steel production.

Introduction

With respect to sustainability and cost efficiency, CO$_2$ emission reduction, energy consumption as well as CO$_2$ emission allowance and energy costs are becoming increasingly more important, with both the steel and refractory industries challenged to achieve change. This article focuses on the tundish, as the most relined unit in the steel plant, to demonstrate how RHI Magnesita products decrease energy consumption and CO$_2$ emissions and how this translates into cost benefits for the customer.

In continuous casting, the tundish serves as a reservoir for distributing molten steel to the moulds while also fulfilling essential metallurgical functions. The vessel comprises a steel shell and anchors, with an insulation layer, permanent lining, and wear lining (Figure 1). In this article refractories for the permanent lining are described that highlight the

multiple advantages of using sol-bonded castables for this application, including energy savings. Furthermore, the various wear lining approaches are reviewed with a focus on cold-setting (i.e., self-hardening) mixes, which also provide benefits including reduced CO$_2$ emissions through a decreased gas requirement and increased tundish availability.

To quantify the savings that can be achieved by adopting sol-bonded and cold-setting mixes, trials were conducted in various steel plants to determine the gas and CO$_2$ emission allowance costs per tonne of installed refractory mix. Prompted by the substantial natural gas price increases that started in 2021, the case studies presented in this article using 2024 gas and CO$_2$ emission allowance costs clearly demonstrate the advantages of using sol-bonded and cold-setting mixes.

Figure 1.

Schematic of the various layers in a tundish, detailing different options for the insulation, permanent lining, and wear lining.
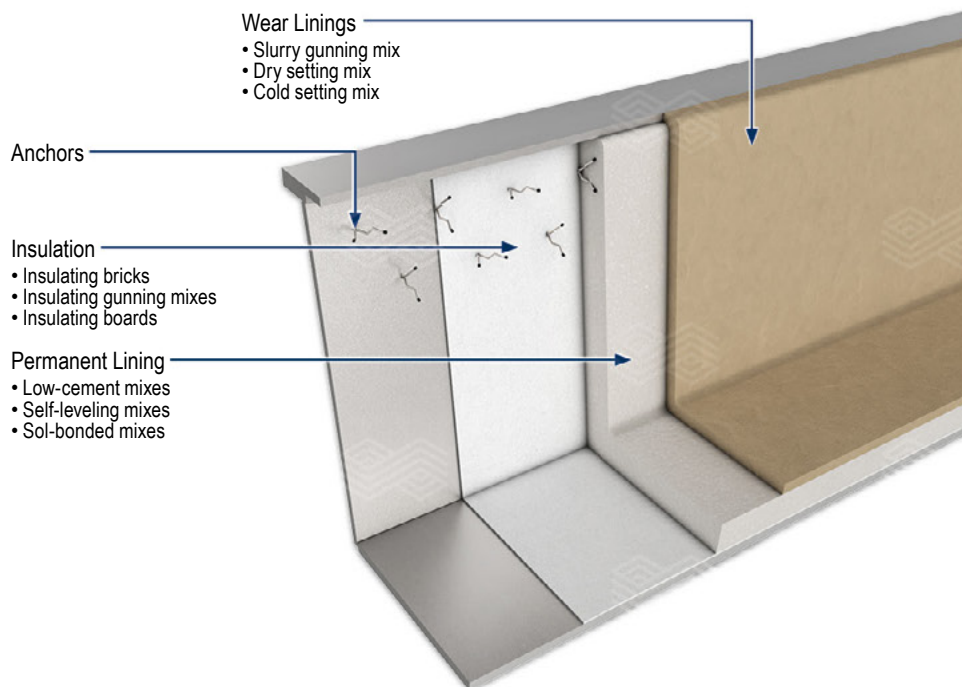
Tundish Permanent Lining

Typically known as the permanent or safety lining, this refractory layer is the last defence to prevent a breakout of liquid steel through the tundish steel shell; therefore, the aim is to minimise any wear and keep it in operation for as long as possible. Ideally, and with appropriate maintenance practices, the lifetime can be extended to years. Currently, the most commonly used refractories for the permanent lining are hydraulically bonded low cement castables (LCC), which are mainly composed of mullite-rich raw materials or bauxite.

For a standard LCC, 7% water is added during mixing and the castable is applied using a template equipped with vibrators. During processing the water reacts with calcium aluminate phases to form hydrates, which result in the necessary bonding and the template can be removed after dimensional stability has been reached (~24 hours). For safe operation and to prevent a vapour burst the added water must then be removed. Since the undried cement-bonded castable is dense and has low gas permeability, the first heat up must be performed very carefully and slowly so initially the physically bonded water can evaporate, followed by release of the chemically bonded water with increasing temperature [1]. For a 150 mm thick permanent lining, this time- and energy-consuming drying can take ~55 hours, with a stepwise temperature increase to 600–700 °C (Figure 2a).

Renowned for their easy and fast heat-up procedure, sol-bonded mixes are a sustainable alternative for the permanent lining. Processed in a similar manner to LCCs, the binder is added during the mixing procedure in the form of a liquid sol (i.e., DIVASIL) that contains nano-sized silica particles [1]. As with LCCs, sol-bonded castables can be applied using a template equipped with vibrators, although free-flowing and gunnable versions are also available for additional flexibility. After setting, water in the sol-bonded mix is not chemically bonded and as a result the main water component in the gel structure is easily removed at very low temperatures. A comparison of the vaporisation rates for a sol-bonded mix and a LCC is shown in Figure 3. This thermogravimetric analysis clearly shows that the sol-bonded mix reaches zero vaporisation at 100–110 °C while the LCC does not release all the water until 450 °C. In addition, the pore size distribution of sol-bonded castables results in a high permeability even at low temperatures, which further facilitates dehydration. As a result, the drying time of a 150 mm thick sol-bonded lining can be reduced to ~20 hours (see Figure 2b), increasing tundish availability and decreasing gas demand. There is also an option to avoid any gas consumption by using alternative heat sources such as electric drying.

Figure 2.

Recommended drying procedure for a 150 mm thick (a) LCC and (b) sol-bonded mix. The temperatures refer to the tundish chamber (e.g., castable surface).
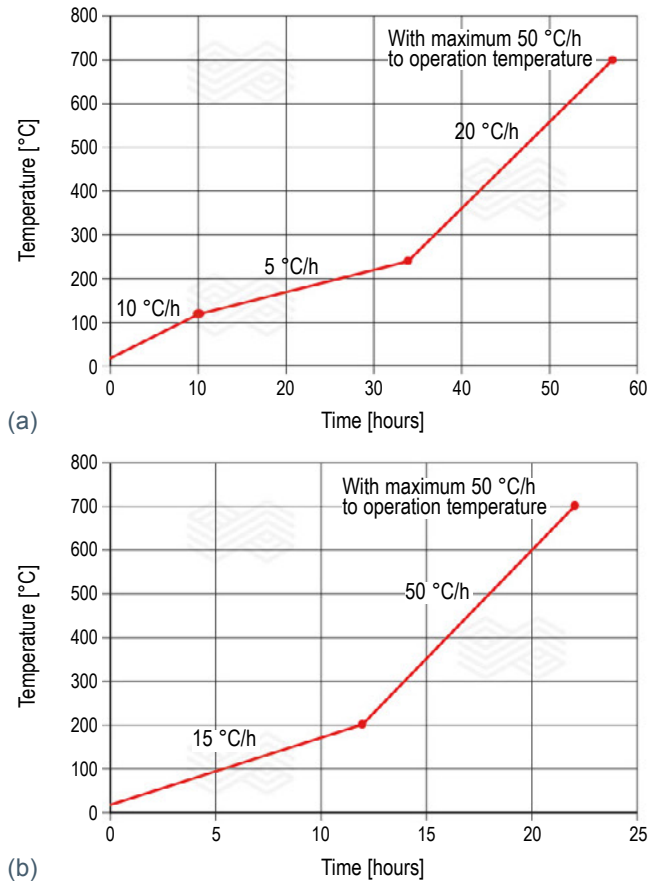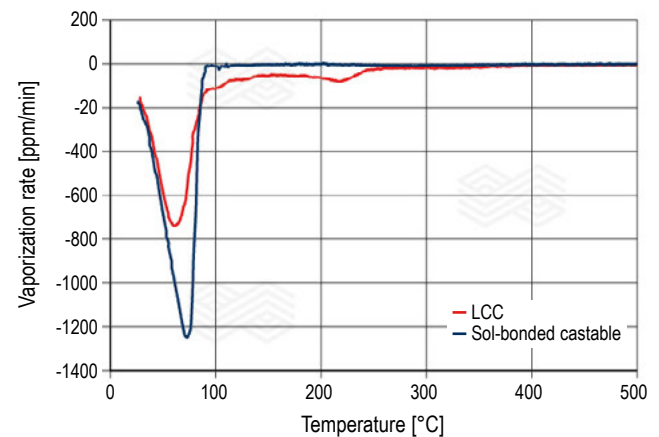

(a)

(b)

Figure 3.

Vaporisation rates of a sol-bonded mix and LCC determined using thermogravimetric analysis [1].

In summary, the main advantages of sol-bonded mixes include:

- Fast and easy heat-up procedure.
- Decreased gas demand for drying and the associated CO_2 emission reductions.
- Option for drying with green electricity.
- Increased tundish availability.
- Various application methods (i.e., vibrating, self-flowing, and gunning mixes).
- Longer shelf life than LCCs as the dry mix does not contain binder.
- Reduced sensitivity to incorrect dosing of the mixing liquid.
- Higher refractoriness compared to equivalent LCCs.
- Longer operational lifetime than LCCs.

There is a wide range of sol-bonded mixes available from RHI Magnesita and the positive experiences regarding performance, installation, and handling over the years have resulted in their increasing application in diverse areas by multiple industries (e.g., steel, cement, and nonferrous). Table I details the chemical composition and main raw materials of three sol-bonded castables recommended for the tundish permanent lining.

Tundish Wear Lining

To withstand casting sequences that can be over 100 hours, the alumina silica based permanent lining is protected by a sacrificial basic refractory wear lining. Unlike the permanent lining, the wear lining is directly exposed to various chemical and thermomechanical wear mechanisms during steel casting (e.g., from slags and cover powders). Consequently, it must be removed after use (via deskulling or tilting) and

replaced. Over the last decades, three main technologies have become the industrial standard for wear lining applications, namely:

- Slurry gunning mixes.
- Dry-setting mixes.
- Cold-setting mixes.

As the most conventional type of wear lining, slurry gunning mixes require ~20–35% water content to reach a pumpable consistency. After continuous water addition, the wet mix is conveyed to a collecting hopper and then pumped through a hose to the nozzle. Compressed air, injected directly at the front end of the spraying nozzle, propels the mix towards the target area (e.g., tundish wall). Characterised by their broad flexibility in terms of the desired lining thickness, slurry gunning mixes are still the primary tundish wear lining mix type used in most steel plants. Due to the relatively high water addition, a drying process is crucial prior to steel casting, which can take place at a controlled drying station in ~3–5 hours. To decrease or even eliminate this drying step, RHI Magnesita developed the FAST TO CAST gunning mixes [2].

Dry-setting and cold-setting mixes are widely used alternatives to slurry gunning mixes. For dry-setting mixes, the dry mix is filled into a gap between the template and the permanent lining. During curing at 200–300 °C, the organic or inorganic binders are thermally activated and result in a stable wear lining after ~1–2 hours of total preparation. In contrast, cold-setting mixes are applied via a continuous mixing machine, for example the ANKERTUN CS machine shown in Figure 4, whereby the addition of 1–3% water initiates a chemical cold-setting reaction. Simultaneously, the
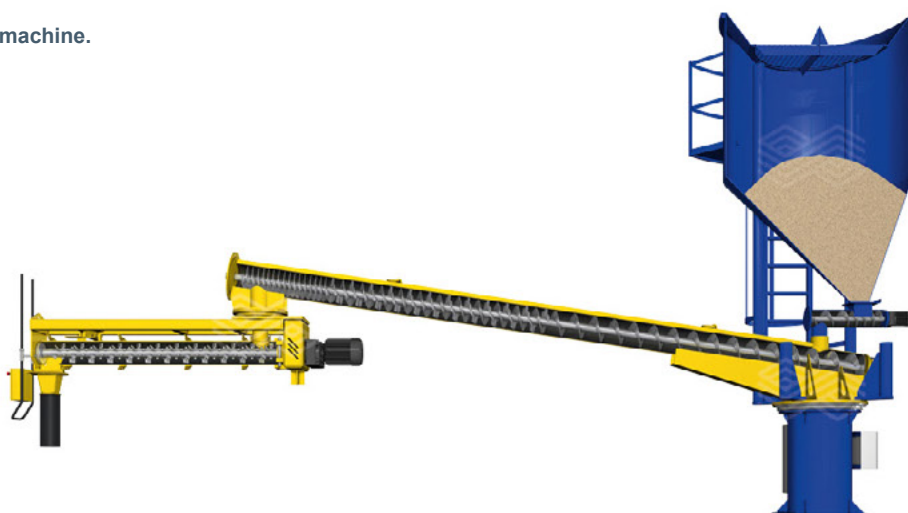
Table I.

Examples of sol-bonded castables for the tundish permanent lining.

Grade	Al_2O_3 [wt.%]	SiO_2 [wt.%]	Fe_2O_3 [wt.%]	TiO_2 [wt.%]	MgO [wt.%]	CaO [wt.%]	Na_2O [wt.%]	Main raw material	Installation method
DIDOFLO SB B89-6	89.0	7.5	1.0	1.5	0.1	0.8	-	Bauxite	Self-flowing
COMPAC SOL M64-6	66.0	29.0	0.9	2.6	-	-	0.1	Mullite	Vibrating
COMPAC SOL B88-6	87.0	8.5	1.2	2.1	0.1	0.8	-	Bauxite	Vibrating

Figure 4.

ANKERTUN CS machine.

mix is filled into a gap between a vibratable template and the permanent lining. After approximately 30–60 minutes the mix hardens without further actions, such as temperature treatment. After template removal, a cold-setting lining can be used directly for steel casting as the added water is already at a reasonably low level. Since no drying or preheating cycles must be applied to cold-setting tundish linings, the total gas consumption and associated CO_2 emissions can be reduced to a bare minimum.

Cold-setting mixes can be defined as mixes that set or harden at room temperature without any external heat, as a result of starting a chemical reaction during the mixing process. Typically, this is achieved by using either a two-component binder system based on the well-known reaction of liquid sodium silicate with a hardener or the patent protected self-hardening (SH) system where only minimal water is required to activate binding. For the wear lining case study examples in this article, the focus is on ANKERTUN SH mixes as they represent an environmentally friendly, state-of-the-art tundish lining solution where the liquid additive is free of chemicals.

The SH binder consists of a solid acid component, in combination with a solid inorganic basic material. This SH binder is mixed with the desired refractory raw materials (e.g., sintered magnesia and olivine) in a dry state before

delivery to the customer. During application at the customer and due to the slight water addition, the SH binder forms a metal-organic complex leading to the formation of binder bridges with the refractory material. At this stage the water is in a nonchemically bonded form and can easily evaporate from the lining at ambient temperature [3]. The chemical composition and main raw materials in commonly used ANKERTUN SH wear lining grades are detailed in Table II.

Principally, the benefits that can be achieved by using ANKERTUN SH mixes and the ANKERTUN CS machine are:

- Minimised total lining time compared to other technologies.
- Setting without an external heat supply.
- Reduced energy consumption and the associated CO_2 emissions.
- Increased tundish availability.
- Easy application and working conditions.
- Minimal material waste.
- Minimal cleaning effort due to the machine's automatic cleaning mode.
- Nontoxic, phenol and silica free binding agents.
- Only water required—no storage and handling of other liquids.
- Cold start practice possible.

Table II.

Examples of ANKERTUN SH mixes recommended for the tundish wear lining.

Grade	MgO [wt.%]	CaO [wt.%]	SiO$_2$ [wt.%]	Fe$_2$O$_3$ [wt.%]	Al$_2$O$_3$ [wt.%]	Main raw material
ANKERTUN SH10	93.2	3.0	2.9	0.6	0.1	Low-iron sintered magnesia
ANKERTUN SH40	90.0	4.2	2.1	2.8	0.4	Sintered magnesia
ANKERTUN SH60	88.6	4.2	1.2	5.2	0.6	Sintered magnesia

Tundish Lining Case Studies—Combining Cost Efficiency and Sustainability

Gas costs and CO_2 emission allowance prices

In 2021, natural gas prices increased dramatically due to various reasons such as the Ukraine war [4]. As this energy source is primarily used to dry tundish linings and preheat the vessel, the case studies described in this section were initiated to accurately determine the financial benefits that can be achieved using sol-bonded and cold-setting ANKERTUN SH mixes. Despite the recent decline in gas prices, for example in Europe (Figure 5), the studies clearly show the cost savings that can be achieved per tonne of installed refractory with these lining technologies as well as the reduced susceptibility to future fuel price volatilities. Additionally, as approximately 2 kg of CO_2 are emitted for every cubic metre of gas consumed [5], the reduced gas consumption also has a positive environmental impact as well as an economic advantage in regions with carbon pricing schemes. As the European Union Emission Trading System (EU ETS) is the world's first and largest carbon market [6], the EU CO_2 emission allowance price was used to calculate the monetary implications. Although this allowance price has fluctuated during the last years (Figure 6), since the EU ETS is based on a "cap and trade"

principle, CO_2 allowance costs are predicted to increase over time and become even more relevant regarding these types of cost calculations. For the studies, April 2024 natural gas and CO_2 allowance prices of €26.2/MWh and €61.1/tonne CO_2, respectively, were used.

Permanent lining comparison

For the permanent lining case study, three customers were selected to compare the costs associated with drying either LCC or sol-bonded linings. The maximum drying temperature and time, tundish capacity, as well as the amount of mix per lining at each customer are provided in Table III. In the case of customer C, a direct comparison could be made as the lining technology was recently changed from LCC to sol-bonded mixes. Regarding gas consumption, it is important to state that the equipment for tundish lining is often on the same gas loop as the ladle preheating stands or other gas consuming equipment. Therefore, the gas consumption for the lining drying was measured indirectly and it was necessary to make certain assumptions for any missing customer data, including whether the equipment was new or old as well as the tundish dimensions and lining thickness. Using this approach, figures for the specific gas consumption (m^3/tonne$_{refractory}$) to dry the permanent lining were

Figure 5.

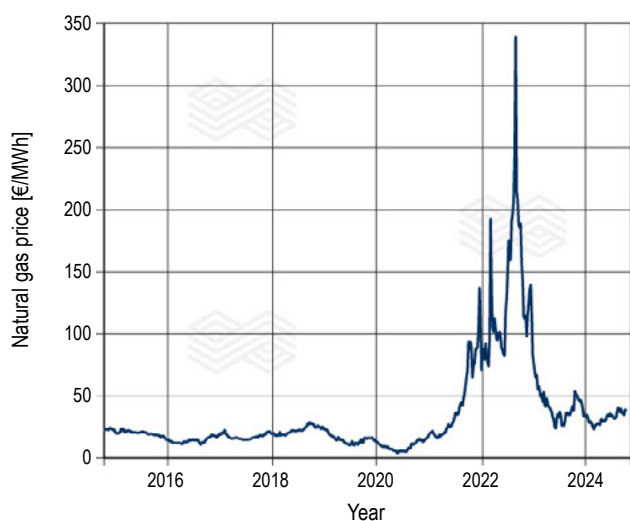**Natural gas price (€/MWh) development in Europe (Netherlands) [7].**

Figure 6.

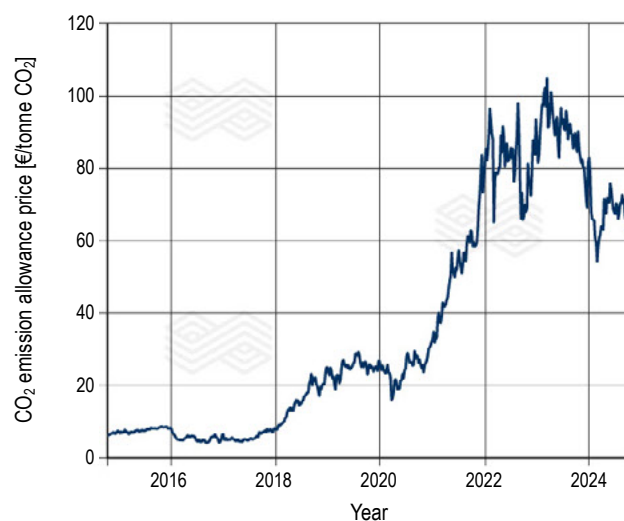**CO_2 emission allowance price (€/tonne CO_2) development in Europe [8].**

Table III.

Details of the permanent lining type, maximum drying temperature and time, tundish capacity, and amount of installed refractory for the three customers.

Customer	Tundish mix	Maximum drying temperature [°C]	Maximum drying time [hour]	Tundish capacity [tonne]	Mix amount per lining [tonne]
A	LCC	500	70	25	7.5
B	Sol-bonded	750	30	20	8.5
C	LCC	500	75	30	15.0
C	Sol-bonded	700	15	30	15.0

determined that show sol-bonded mixes required significantly lower amounts of gas (Figure 7). For example, a gas saving of 70% was achieved at customer C by changing from LCCs to sol-bonded mixes and there is the possibility to further decrease this by optimising the drying curve, as illustrated by customer B. In this case, after improving the drying schedule at customer B, an 86% lower specific gas consumption was achieved compared to customer A using LCCs, although the amount of mix installed per lining was similar.

To determine the financial implications, the emitted CO_2, as well as the gas and CO_2 emission allowance costs per tonne of installed refractory were calculated from the specific gas consumption (Table IV). A value of 0.0105 MWh/m³ was used to convert the gas consumption (m³) to MWh. These results indicate that ~€45/tonne_refractory can be saved by

changing the permanent lining from a LCC to a sol-bonded mix (Figure 8), as well as a time saving of 60 hours in the case of customer C.

Wear lining comparison

In the wear lining case study, the focus was on comparing traditional slurry gunning with the cold-setting ANKERTUN SH mixes. Two of the customers selected were also part of the permanent lining evaluation, while the third customer D provided a direct comparison of the lining technologies as both mix types are used in this steel plant. Details of the wear lining type, maximum drying temperature, maximum preheat temperature, tundish capacity, and amount of installed refractory for the three customers are given in Table V. The gas consumption for drying the slurry gunning wear linings and preheating the tundishes was

Figure 7.

Specific gas consumption (m³/tonne_refractory) required to dry LCCs and sol-bonded (SOL) permanent linings at the different customers.
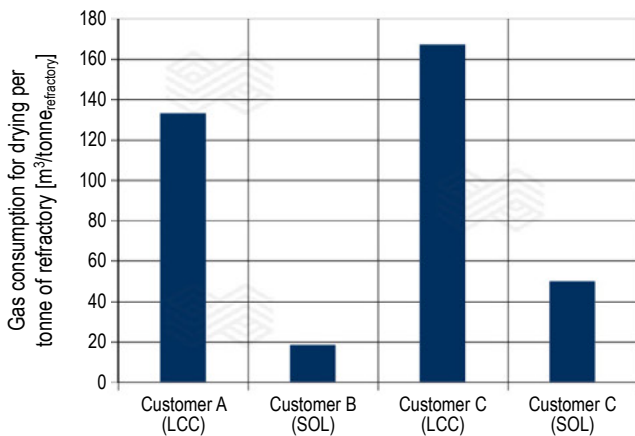

Figure 8.

Comparison of the specific gas and CO_2 emission allowance costs (€/tonne_refractory) resulting from drying LCCs and sol-bonded (SOL) permanent linings at the different customers.
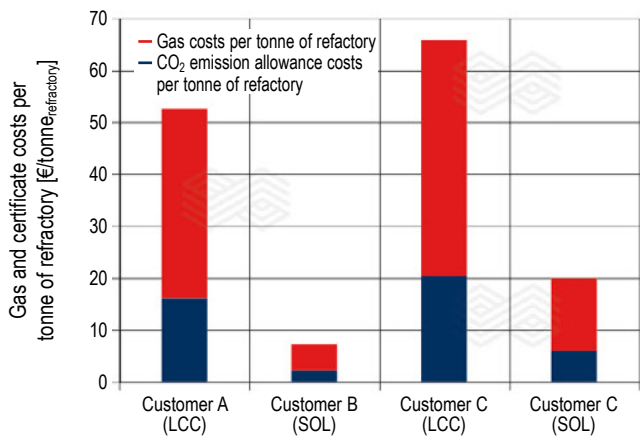

Table IV.

Specific gas consumption, emitted CO_2, as well as the specific gas and CO_2 emission allowance costs (€/tonne_refractory) at the different customers.

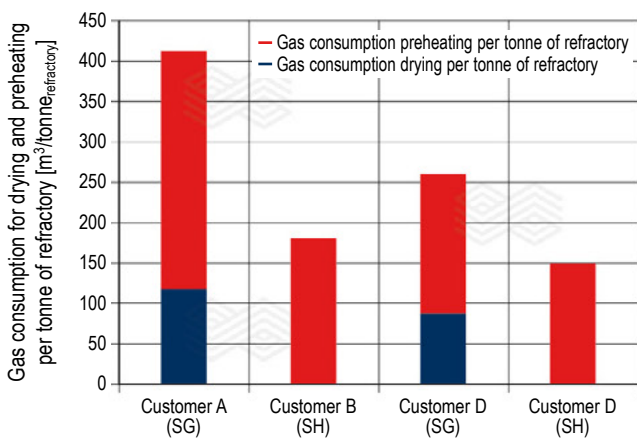| Customer	Tundish mix	Gas consumption [m³/t_refractory]	Emitted CO_2 [t_{CO_2}/t_refractory]	Gas costs [€/t_refractory]	CO_2 emission allowance costs [€/t_refractory]
A	LCC	133.33	0.27	36.68	16.29
B	Sol-bonded	18.82	0.04	5.18	2.30
C	LCC	166.67	0.33	45.85	20.37
C	Sol-bonded	50.00	0.10	13.76	6.11

Table V.

Details of the wear lining type, maximum drying temperature, maximum preheat temperature, tundish capacity, and amount of installed refractory at the different customers.

Customer	Tundish mix	Maximum drying temperature [°C]	Maximum preheat temperature [°C]	Tundish capacity [tonne]	Mix amount per lining [tonne]
A	Slurry gunning	600	1200	25	1.7
B	Self-hardening	-	1100	20	2.5
D	Slurry gunning	400	1000	35	3.0
D	Self-hardening	-	1000	35	3.5

directly measured as it was possible to ensure that no other equipment on the same gas line was concurrently in operation. Figure 9 shows that a >40% specific gas consumption saving was achieved with the ANKERTUN SH mixes, as no lining drying step was required and the preheating time was slightly shorter than for slurry gunning mixes. Following calculation of the emitted CO_2, and gas and CO_2 emission allowance costs per tonne of refractory (Table VI), potential savings ranging from €40/tonne$_{refractory}$ up to €90/tonne$_{refractory}$ were determined for ANKERTUN SH mixes, depending on the specific preheat practice (Figure 10). Furthermore, since it is possible to use the ANKERTUN SH mixes with a cold start practice at the caster, the specific gas consumption and financial savings can be considerably more.

In conclusion, the case studies show that sol-bonded and ANKERTUN SH mixes can significantly reduce the specific gas consumption required in the tundish area for drying and preheating, thereby providing both financial and environmental benefits. Furthermore, since certain steps during the tundish turnaround cycle are shorter or can be eliminated, tundish availability is also increased by using these refractory technologies. For example, comparison of typical time schedules for slurry gunning and ANKERTUN SH mixes, from wear lining installation to transfer to the casting platform, show that 210 minutes can be saved using ANKERTUN SH mixes (Table VII), with additional time savings possible from implementing a cold start practice.

Figure 9.

Specific gas consumption (m^3/tonne$_{refractory}$) required to dry and preheat tundishes lined with slurry gunning (SG) mixes and ANKERTUN SH mixes at the different customers.

Figure 10.

Comparison of the specific gas and CO_2 emission allowance costs (€/tonne$_{refractory}$) resulting from drying and preheating tundishes lined with slurry gunning (SG) and ANKERTUN SH mixes at the different customers.
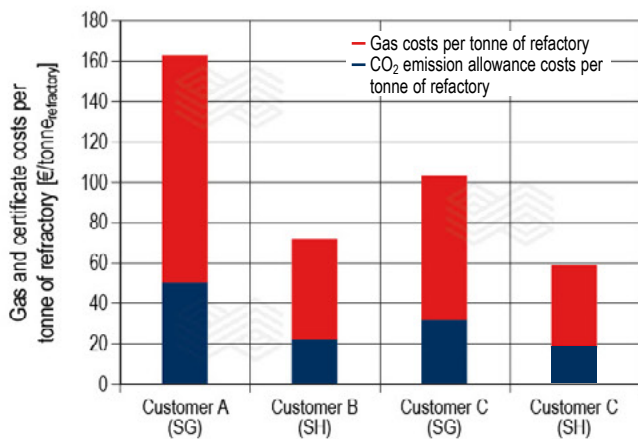

Table VI.

Specific gas consumption, emitted CO_2, as well as the specific gas and CO_2 emission allowance costs (€/tonne$_{refractory}$) at the different customers.

Customer	Tundish mix	Gas consumption [m^3/$t_{refractory}$]	Emitted CO_2 [t_{CO_2}/$t_{refractory}$]	Gas costs [€/$t_{refractory}$]	CO_2 certificate costs [€/$t_{refractory}$]
A	Slurry gunning	411.76	0.82	113.28	50.32
B	Self-hardening	180.00	0.36	49.52	22.00
D	Slurry gunning	259.99	0.52	71.53	31.77
D	Self-hardening	148.57	0.29	40.87	18.16

Table VII.

Time schedule comparison of slurry gunning and ANKERTUN SH mixes from wear lining installation to crane transfer to the caster [9].

Step	Operation	Slurry gunning mix Time [minutes]	ANKERTUN SH mix Time [minutes]
1	Wear lining installation	30	30
2	Drying at ambient temperature	60	-
3	Drying at ~500 °C	180	-
4	Hardening	-	30
5	Further installation of equipment (e.g., stopper)	30	30
6	Crane transfer to casting platform	10	10
	Total	**310**	**100**

Tundish Mixes—Additional Decarbonisation Initiatives

Greenhouse gas (GHG) emissions, such as CO_2, are subdivided into three categories [10]:

- Scope 1: Direct emissions of an organisation (e.g., fuel combustion).
- Scope 2: Indirect emissions of an organisation directly associated with the provision of energy (e.g., emissions from a coal electricity power plant).
- Scope 3: Indirect emissions upstream or downstream of an organisation (e.g., purchased raw materials and third-party transport).

In the case of sol-bonded and ANKERTUN SH mixes, the decreased natural gas consumption directly impacts scope 1 emissions at the steel plant. However, there are additional decarbonisation initiatives that enable scope 3 emissions to be tracked and decreased.

Product carbon footprint and recycling

In line with RHI Magnesita's corporate climate strategy, it was decided to create 100% transparency regarding the GHGs emitted during refractory production. Therefore, the product carbon footprint (PCF) of our products is calculated in accordance with the principles of ISO 14067 and disclosed on the technical data sheets (Figure 11). The PCF covers all GHG emissions from upstream sources and the direct manufacturing of a product (i.e., cradle-to-gate) [10], enabling customers to make purchasing decisions based on this sustainability criterion. Furthermore, RHI Magnesita is committed to reducing the GHG intensity of its products by becoming more circular and using recycled raw materials. This has resulted in the tundish mix portfolio including grades that contain appropriate amounts of circular raw materials, which have a decreased PCF while maintaining the required performance.

Local-for-local

With a global network of 47 main production sites, RHI Magnesita follows a local-for-local strategy by using production facilities located as close as possible to the customer. This translates into scope 3 benefits, as third-party transport to the customer can be minimised. In addition, by operating our own raw material production sites across several continents, the uncertainties and volatility of

raw material supply and price fluctuations can be mitigated. However, when considering raw materials for tundish wear mixes, local raw material sources can differ from standard raw materials available on the world market (Table VIII). To establish the most cost efficient and sustainable usage at the customer, the local raw material compositions must be considered and the grades optimised for individual customer applications. This might lead to rethinking well-known standard concepts based on Chinese raw material sources, opening up the possibility to use high-quality local raw materials with slightly different chemical compositions and colours.

Figure 11.

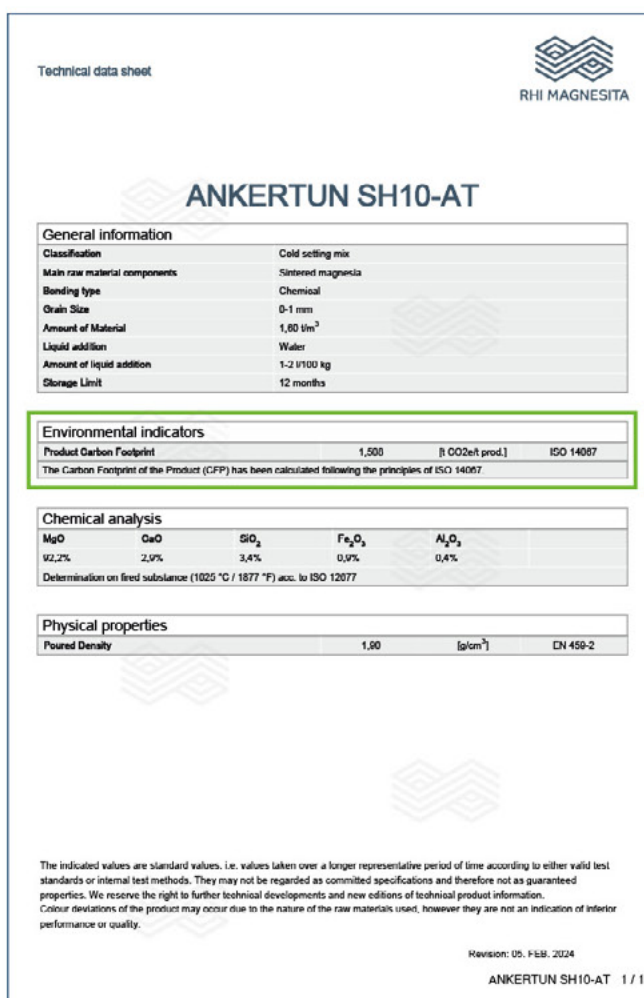**Technical data sheet detailing the product carbon footprint.**

Table VIII.

Comparison of the chemical composition of different locally produced RHI Magnesita magnesia raw materials with Chinese dead burned magnesia (DBM) available on the world market.

Raw material source	Austria (Europe)	Brazil (South America)	Türkiye (Europe)	Chinese DBM 9010 (world market)
MgO [wt.%]	70–91	~94.5	>93	90–93
CaO [wt.%]	2–25	~0.5	~3.0	~2.5
SiO$_2$ [wt.%]	<1.5	~1.5	~3.5	~4
Fe$_2$O$_3$ [wt.%]	4–6	~2.3	~0.5	~1.2
Description	High iron (and lime)	Medium iron	Low iron	

Conclusion

RHI Magnesita is committed to sustainability, which includes developing decarbonisation initiatives for our customers [11]. This article presents case studies that demonstrate CO_2 emission reductions and cost savings can be achieved in the tundish area by adopting permanent and wear lining technologies that require less drying and preheating. For example, by changing the permanent lining refractory at a customer from a LCC to a sol-bonded mix, the drying time was reduced by 60 hours and the natural gas consumption was decreased by 70%. At current gas prices this translates to a financial saving of ~€30/tonne$_{refractory}$. However, in 2022, when the average gas price in the Netherlands was €133.5/MWh (see Figure 5), this would have equated to a saving of ~€160/tonne$_{refractory}$. Furthermore, in regions with carbon pricing schemes, additional costs savings can be achieved due to the corresponding decrease in CO_2 emissions, which at a current allowance price of €61.1/tonne CO_2 equates to a further ~€14/tonne$_{refractory}$ for the customers using sol-bonded mixes.

The wear lining case studies show that by changing the lining method from slurry gunning to cold-setting ANKERTUN SH mixes it is possible to achieve gas costs savings of ~40–55% per tonne of installed refractory, with additional financial benefits in the same range due to reduced CO_2 emission allowance costs. Furthermore, even higher savings are possible by optimising the preheating schedule or using a cold start practice. Using the figures determined for customer D, who is currently using both wear lining technologies in parallel, it was calculated that annual gas and CO_2 emission allowance savings of €53655 and €23817, respectively, can be achieved using the ANKERTUN SH mix, considering 3.5 tonnes of mix per lining and 500 lining per year, with additional process efficiency improvements due to the decreased time between wear lining installation and transfer to the casting platform. In addition, there are supplementary approaches customers can take to reduce their CO_2 footprint related to the tundish, which include taking advantage of lining mixes that contain recycled materials and have a reduced carbon footprint as well as the local-for-local strategy using our high-quality raw materials.

References

[1] Blajs, M., von der Heyde, R., Fritsch, P. and Krischanitz, R. COMPAC SOL – The New Generation of Easy, Safe, and Fast Heat-Up No Cement Castables. *RHI Bulletin*. 2010, 1, 13–17.

[2] Kerr, J., Almeida, P., Wappel, D., Borges, R., Naves, M. and Olvera, F. Innovative Spray Tundish Mix for Energy Savings and CO_2 Footprint Reduction. *Bulletin*. 2023, 61–65.

[3] Sorger, R. and Petritz, B. New Cold-Setting Mixes for Tundish Wear Linings. *RHI Bulletin*. 2011, 1, 54–58.

[4] Drnek, T. Energie in Europa. Aktuelle Situation und Ausblick. *Berg- und Hüttenmännische Monatshefte*. 2023, 168, 373–379.

[5] https://www.eeagrants.gov.pt/media/2776/conversion-guidelines.pdf

[6] https://climate.ec.europa.eu/eu-action/eu-emissions-trading-system-eu-ets_en

[7] https://tradingeconomics.com/commodity/eu-natural-gas

[8] https://tradingeconomics.com/commodity/carbon

[9] Silbergasser, H. Green Tundish Lining Technology. Presented at the 8th International Iron & Steel Symposium, Izmir, Turkey, May 26–27, 2022.

[10] Joos-Bloch, M., Rechberger, L., Haider, C., Moulin-Silva, W., Wucher, J. and Drnek, T. Product Carbon Footprint of Refractory Products. *Bulletin*. 2023, 39–44.

[11] RHI Magnesita 2023 Sustainability Report. https://www.rhimagnesita.com/wp-content/uploads/2024/04/rhim-sustainability-report-2023-final-2.pdf

Authors

Markus Fasching, RHI Magnesita, Vienna, Austria.
Stefan Eder, RHI Magnesita, Leoben, Austria.
Bernhard Griessler, RHI Magnesita, Vienna, Austria.
David Wappel, RHI Magnesita, Leoben, Austria.
Corresponding author: Markus Fasching, Markus.Fasching@rhimagnesita.com

Return to Content

Christian Rodrigues, Menghuai Wu, Abdellah Kharicha, Anton Ishmurzin, Gernot Hackl, Clemens Lind, Mathias Chintinne, Zilong Qiu, Annelies Malfliet and Muxing Guo

Development and Application of a Computational Fluid Dynamics Model to Study Slag Freeze Lining

Freeze lining (FL), a protective layer of solidified slag, holds significant economic value in industrial processes. It protects furnaces and refractory linings from corrosive molten slag and acts as a thermal barrier to minimise energy consumption. To improve our understanding of FL formation, an international collaboration was established. It united academic researchers from the Universities of Leoben (Austria) and Leuven (Belgium) with industry partners RHI Magnesita and Aurubis-Beerse. This collaborative effort has led to the development of a novel computational fluid dynamics (CFD) model capable of simulating FL formation across various applications. Extensive validation confirmed the model's robustness and versatility. This model provides a solid foundation for further fundamental research on FL formation and paves the way for more efficient and cost-effective industrial processes.

Introduction

In the high-temperature world of pyrometallurgy, furnaces often rely on a self-forming protective layer called freeze lining (FL). FL technology has proven successful in various industrial processes, including copper, lead, and ilmenite smelting, zinc fuming, aluminium production (Hall-Heroult process), and in steelmaking [1–7]. However, despite its proven industrial importance, the mechanisms governing FL formation are not fully understood. While laboratory experiments have provided valuable insights into FL microstructure development and growth characteristics, current models haven't been able to comprehensively capture these findings. To bridge this gap, a collaborative research project was undertaken to develop a computational fluid dynamics (CFD) model framework capable of simulating FL formation based on prevalent knowledge. The model was validated against a laboratory experiment (i.e., finger experiment) and industrial processes (i.e., electric smelting furnace and slag fuming furnace).

Model Validation Through Finger Tests

To analyse FL formation under controlled conditions, a laboratory experiment, also known as the finger experiment, was conducted at KU Leuven (Figure 1a). This experiment involved introducing a gas-cooled probe into a slag bath, inducing FL formation that grew outward from the probe's surface over time. The crucible containing the slag could be set to static (natural convection) or rotating (forced convection) conditions. During the experiment, the slag bath temperature before and during probe immersion, FL thickness over time, and heat fluxes were monitored. The CFD results of the equivalent experimental setup are illustrated in Figure 1b and depict the simulated solid fraction distribution (f_s) at three different moments during immersion of the probe into the slag and the FL shape evolution over time. The colour gradient varies from dark blue for the molten slag (also set as transparent in the outer regions), transitioning to a mushy zone (partially solidified slag), and ending with dark red for fully solidified slag (FL). Figure 1c compares the evolution of the measured FL thickness with

the simulation results and demonstrates a good quantitative agreement. This validation confirmed the model's accuracy in a controlled environment.

Figure 1.

(a) schematic of finger experiment, (b) simulation results showing the slag solid fraction distribution, indicating the FL shape (dark red) development over time, and (c) comparison of the experimental results and simulation results of the FL thickness development over immersion time.
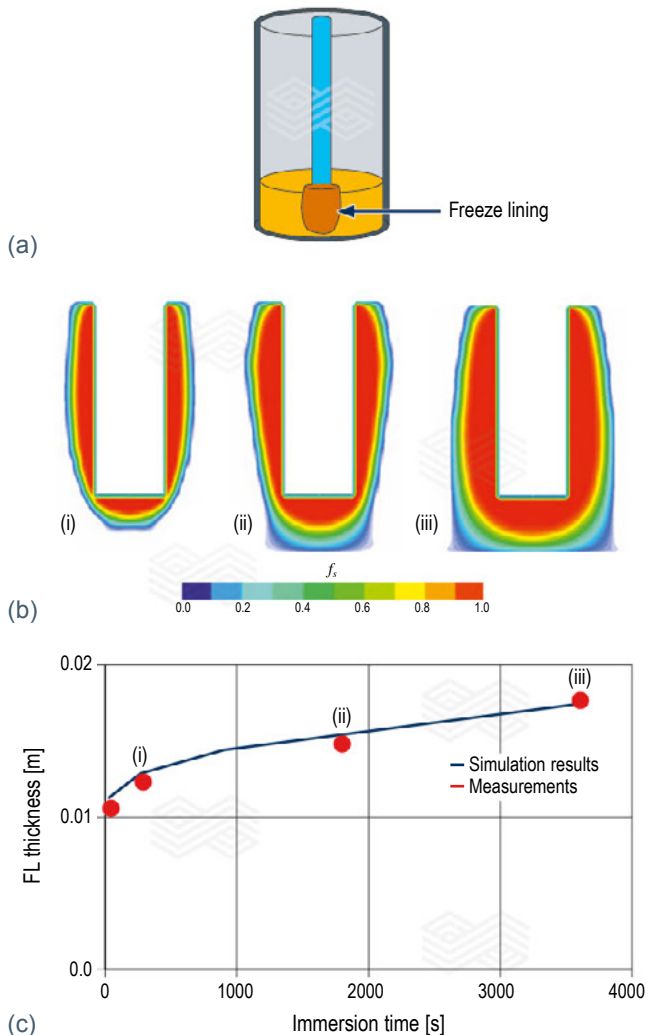
Industrial Application

Electric smelting furnace

This case represents an industrial electric smelting furnace for the smelting of nickel matte. The furnace is equipped with six electrodes. A schematic of the cross-sectional view of the furnace (through one of the electrodes) is shown in Figure 2. During operation, the electrical energy for smelting the feed is generated by joule heating as the electric current passes between the carbon electrodes and the molten slag bath. After the furnace is charged with the feed, the process produces both slag and a denser nickel-rich layer called matte, which settles at the bottom due to its higher density. The furnace walls incorporate a cooling system (e.g., water-cooled panels) that promotes the FL formation on the interior surface of the furnace/refractory.
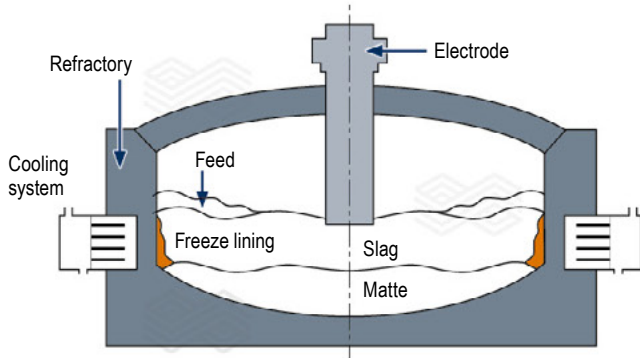
A crucial aspect of modelling the electric smelting furnace involves establishing a valid global energy balance within the furnace. This balance must consider all relevant heat transfer mechanisms occurring during the smelting process. To capture these mechanisms, several energy source terms were incorporated. These terms account for the input power from the electrodes, heat generated from matte production, heat dissipated by the cooling system, heat dissipated by the presence of the feed, and latent heat released during FL formation.

Figure 3 presents the simulation results obtained after reaching a steady state. This means that a thermal balance was achieved in the system. Due to symmetry in the furnace, only one section containing half of one electrode is considered in the model. Figures 3a–3c show the temperature distribution in the section considered, the temperature distribution in a 2D plane intersecting the electrode, and the velocity distribution in a similar 2D plane. The inset in Figure 3a highlights the FL layer formed on the water-cooled wall (black vertical rendering), while the horizontal black rendering corresponds to the solid feed. Figure 3b confirms that the slag temperature is higher closer to the electrode and decreases with distance. This provides the driving force for natural convection in the molten slag. Figure 3c shows an anticlockwise flow pattern in the slag region driven by joule heating. The maximum velocity is approximately 0.05 m/s. These results agree with the plant data reported [9]. The vertical black structure illustrated in the inset of Figure 3a confirms the presence of a FL layer on the water-cooled wall. The results go beyond validating FL formation; they demonstrate the successful integration of key physical phenomena into the model's framework.

Figure 2.

Cross-sectional view of the electric smelting furnace for smelting nickel matte. The freeze lining location is highlighted.

Figure 3.

Steady-state simulation results of (a) temperature distribution in a section of the domain with an inset showing black rendering corresponding to the FL layer on the water-cooled wall predicted by the model and the feed, (b) temperature distribution with isotherms in a 2D plane intersecting the electrode, and (c) velocity distribution with velocity vectors in a 2D plane intersecting the electrode [8].
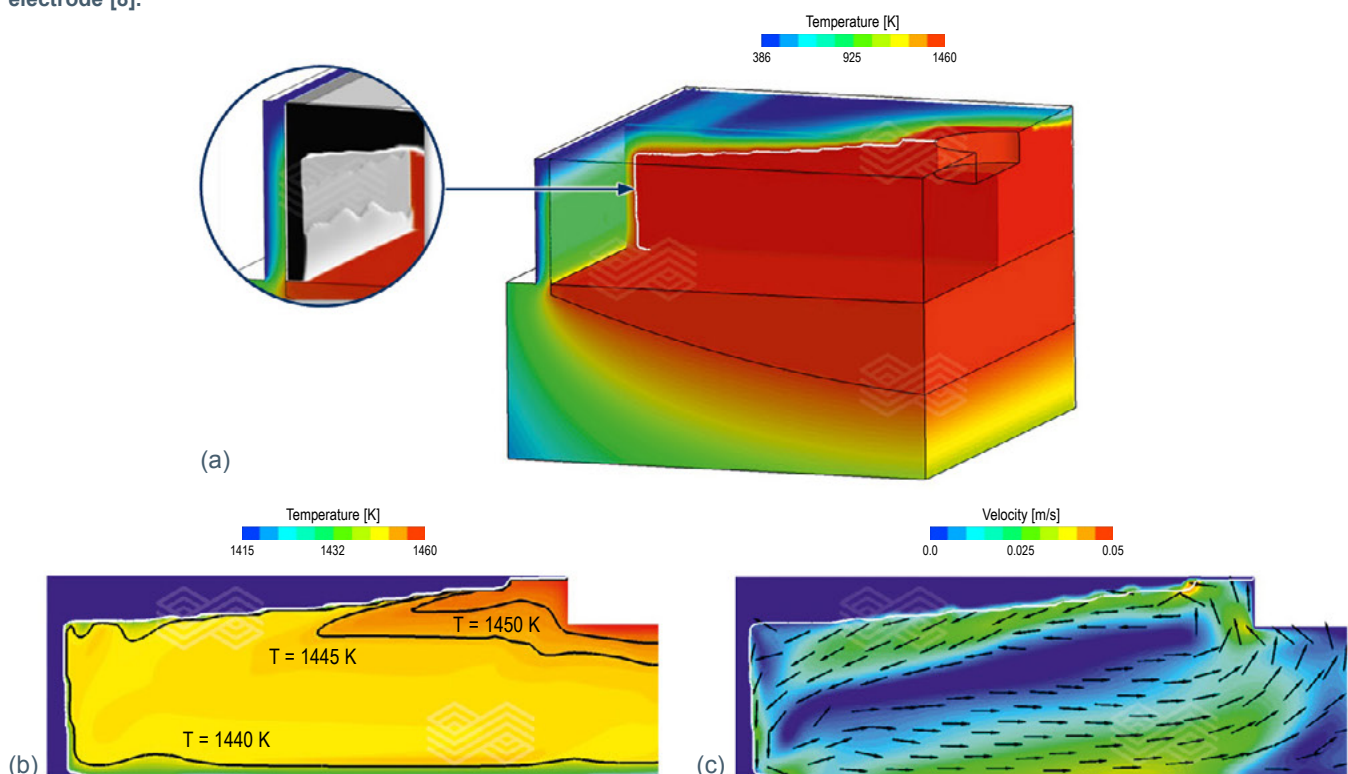
The simulations revealed a critical dependence of the FL layer on heat transfer terms. Notably, variations in feed size were clearly associated with different FL thicknesses. Therefore, an accurate estimation of the thermal effect of the feed is critical and must be considered in the global energy balance calculations of the furnace.

Fuming furnace

Aurubis-Beerse operates a zinc recovery process called slag fuming (Figure 4). This innovative technique recycles zinc from various industrial waste materials by relying on
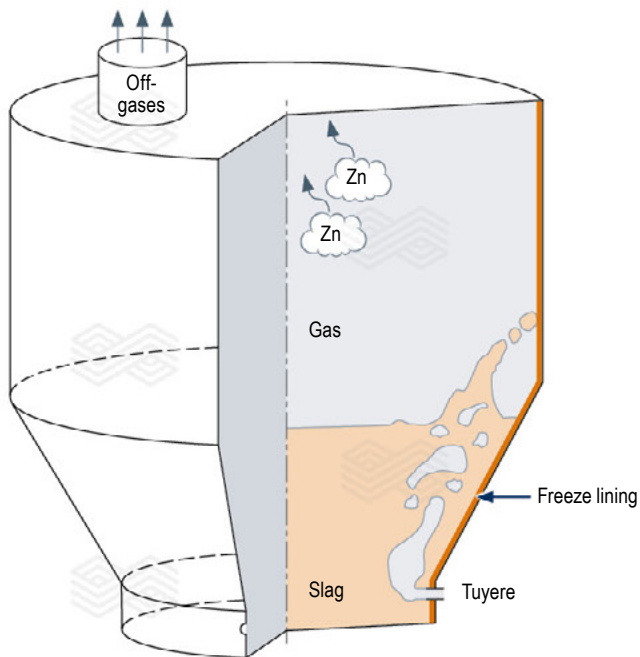
submerged plasma torches for a carbon-free energy source. Three of these torches transform compressed air into high-temperature plasma. This plasma is then injected into the molten slag bath, along with a mixture of natural gas and pulverised coal. This gaseous mixture acts as a heat source, stirring force, and reducing agent in the fuming process. These zinc fumes are then captured in a baghouse after exiting the furnace. To protect the furnace and its refractory linings from the corrosive molten slag, water-cooled jackets are employed around the furnace to promote FL formation. Crucially, industrial data provided by Aurubis-Beerse played a key role in setting up and validating the model. Since the furnace design is symmetrical, only one-third of it needs to be considered in the model.

The flow dynamics observed during the slag fuming process are shown in Figure 5a. The blue iso-surface, representing the slag/gas interface, illustrates the splashing motion of the molten slag across the freeboard. The splashing events are caused by the interaction between the hot gas plumes (created upon injection through the submerged plasma torches) and the molten slag bath. Four coloured streamlines illustrate the complex slag flow pattern, which is driven by the hot gas injection, plume motion, and their interactions with the splashing events. Arrows on each streamline indicate the flow direction. Notably, the streamlines reach most regions of the 3D domain, which confirm the chaotic flow behaviour in the slag bath.

Figure 5b shows the dynamic interplay between splashing and solidification of the FL layer. It captures a moment just after a previously splashed molten slag layer has solidified in the upper right side of the freeboard. This is confirmed by the solid fraction (f_s) colour contour in cyan (which means that it is partially solidified at this moment) and is highlighted in the inset of Figure 5b. This solidification is driven by the heat transfer from the existing, cooler FL layer on the

Figure 4.

Schematic of the batch-type, plasma-driven slag fuming furnace.

Figure 5.

(a) slag splashing and flow dynamics in the slag bath at t = 180.1 seconds. The blue iso-surface depicts the slag/gas interface. The coloured streamlines illustrate the flow patterns. (b) splashing and FL formation in the freeboard at t = 173.9 seconds. The iso-surface colour contour shows the solid fraction (f_s). The inset provides a magnified view of the impact region where splashed slag solidifies.

(a)   (b)
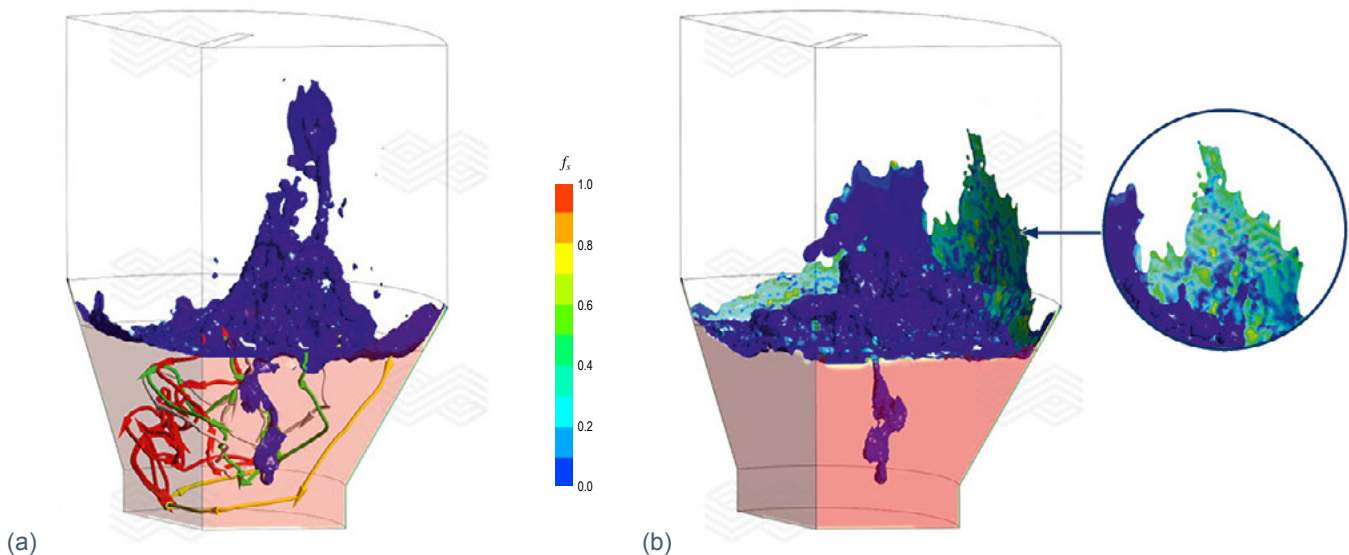
freeboard wall. In contrast, the upper left side of the freeboard shows a fresh splashing event where the slag remains molten (dark blue iso-surface). Figure 6a and 6b show the simulation results of the FL distribution on the reactor wall, and variation of the FL thickness along the reactor height for three angles (φ): 0°, 22°, and 45°.

In the industrial furnace operated by Aurubis-Beerse, the average measured FL thickness was 3 cm. In the slag bath region (height range between 0 and 2 m in Figure 6b), the simulation results show good agreement with industrial data, particularly in regions farther from the submerged plasma torches (φ = 22° and 45°). When φ = 0°, the FL thickness is underestimated because of the simplification made in modelling the submerged plasma torches' inlet (to reduce computational cost). In the freeboard region (height range between 2 and 5.5 m in Figure 6b), the simulation results align reasonably well with the industrial data in the regions where enough splashing events have occurred. However, in regions with fewer splashing events, the model underestimates FL formation. Splashing is more frequent near the centreline of the furnace (φ = 0°) and reduces as the distance from the centre increases (higher φ values), as observed in Figures 6a and 6b. To achieve a complete FL layer across the entire freeboard surface, industrial furnaces typically employ a special operation regime that was not included in the simulation.

Conclusion

Predicting FL formation remains a significant challenge due to the complex interplay of physical and chemical processes. Modelling offers a powerful tool to unravel these mechanisms. This paper explores the results of a collaborative effort between academia and industry, aiming to develop a comprehensive CFD model for simulating FL formation. The positive agreement between simulations and experimental/industrial data validates the model's accuracy and the success of the collaboration: Academia's theoretical expertise combined effectively with industry's real-world knowledge. However, the current model needs further development. Future work should include incorporating new fundamental knowledge of FL formation kinetics, its response to thermal and compositional fluctuations, and modelling the mobile phase (microstructure) observed in some experiments. Additionally, validation in a wider range of industrial applications will enhance the model's robustness.

Acknowledgments

Figure 6.

(a) FL distribution across the reactor wall and (b) FL thickness variation along the reactor height for three azimuthal angles (φ): 45°, 22°, 0°. The 0° azimuthal angle corresponds to the vertical plane intersecting the centre of the submerged plasma torches. The average measured FL thickness in the industrial furnace operated by Aurubis-Beerse was 3 cm.

(a)   (b)
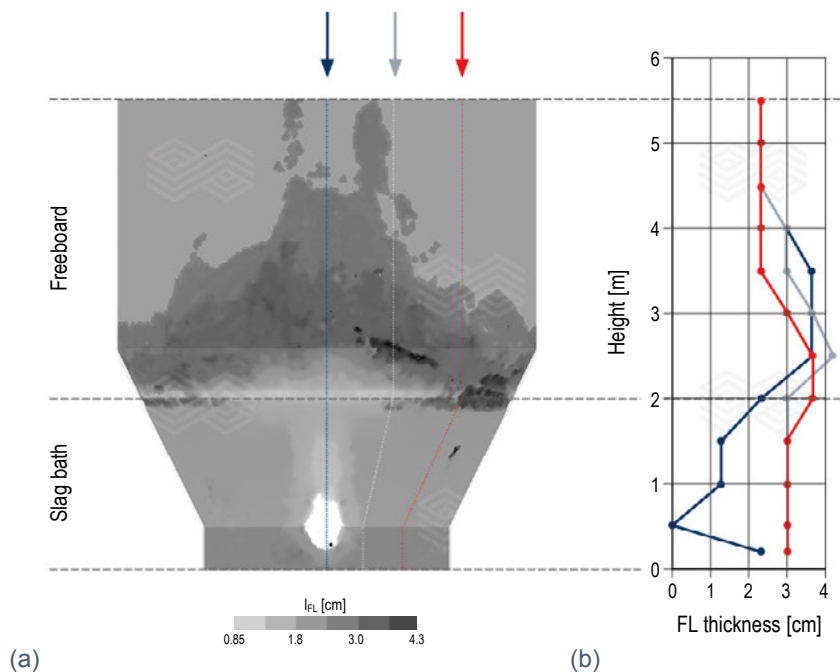
References

[1] Guevara, F. and Irons, G. Simulation of Slag Freeze Layer Formation: Part I. Experimental Study. *Metall. Mater. Trans. B*. 2011, 42, 652–663.

[2] Campforts, M., Verscheure, K., Boydens, E., Van Rompaey, T., Blanpain, B. and Wollants, P. On the Mass Transport and the Crystal Growth in a Freeze Lining of an Industrial Nonferrous Slag. *Metall. Mater. Trans. B*. 2008, 39, 408–417.

[3] Swinbourne, D. The Extractive Metallurgy of Lead. *Miner. Process Extr. Metall.* 2010, 119, 182.

[4] Zietsman, J. and Pistorius, P. Modelling of an Ilmenite-Smelting DC Arc Furnace Process. *Minerals Engineering*. 2006, 19, 262–279.

[5] Verscheure, K., Van Camp, M., Blanpain, B., Wollants, P., Hayes, P. and Jak, E. Continuous Fuming of Zinc-Bearing Residues: Part II. The Submerged-Plasma Zinc-Fuming Process. *Metall. Mater. Trans. B*. 2007, 38, 21–33.

[6] Wong, C., Bao, J., Skyllas-Kazacos, M., Welch, B., Mahmoud, M., Arkhipov, A., and Ahli, N. Studies on Power Modulation of Aluminum Smelting Cells Based on a Discretized Mass and Thermal Dynamic Model. *Metall. Mater. Trans. B*. 2023, 54, 562–577.

[7] Mills, K., Su, Y., Fox, A., Li, Z., Thackray, R. and Tsai, H. A Review of Slag Splashing. *ISIJ Int.* 2005, 45, 619–633.

[8] Rodrigues, C., Menghuai, W., Ishmurzin, A., Hackl, G., Voller, N., Ludwig, A. and Kharicha, A. Modeling Framework for the Simulation of an Electric Smelting Furnace Considering Freeze Lining Formation. *Metall. Mater. Trans. B*. 2023, 54, 880–894.

[9] Sheng, Y., Irons, G. and Tisdale, D. Transport Phenomena in Electric Smelting of Nickel Matte: Part II. Mathematical Modeling. *Metall. Mater. Trans. B*. 1998, 29, 85–94.

Authors

Christian M.G. Rodrigues, Chair of Simulation and Modeling Metallurgical Processes, Metallurgy Department, Montanuniversität of Leoben, Leoben, Austria.

Menghuai Wu, Chair of Simulation and Modeling Metallurgical Processes, Metallurgy Department, Montanuniversität of Leoben, Leoben, Austria.

Abdellah Kharicha, Chair of Simulation and Modeling Metallurgical Processes, Metallurgy Department, Montanuniversität of Leoben, Leoben, Austria.

Anton Ishmurzin, RHI Magnesita, Leoben, Austria.

Gernot Hackl, RHI Magnesita, Leoben, Austria.

Clemens Lind, RHI Magnesita, Vienna, Austria.

Mathias Chintinne, Aurubis-Beerse, R&D, Beerse, Belgium.

Zilong Qiu, Department of Materials Engineering, KU Leuven, Leuven, Belgium.

Annelies Malfliet, Department of Materials Engineering, KU Leuven, Leuven, Belgium.

Muxing Guo, Department of Materials Engineering, KU Leuven, Leuven, Belgium.

Corresponding author: Menghuai Wu, menghuai.wu@unileoben.ac.at

Return to Content

Gregor Arth, Lars Merta, Kateryna Hechu, Bruno Luchini, Florus Beukema and Ed Wortel

Deformation and Wear Analytics in Reheating Furnaces Using 3D Laser Measurement Technology

Reheating furnaces are essential in steel rolling mills to thermally treat blooms, billets, and slabs before subsequent processing. This paper describes the use of portable terrestrial lasers to investigate deformation and refractory wear in these furnaces. Over a period of 2 years, multiple measurements were conducted at Tata Steel in IJmuiden (the Netherlands) to evaluate the time requirement for reality capture of the refractory lining, with respect to scanning resolution and personnel demand. A comparison of the scanned used lining with a theoretical model created from the original furnace dimensions is also described in this article. The potential for time savings using this technology in combination with visualisation tools further substantiate the benefits of RHI Magnesita's digitalisation services for the steel industry.

Introduction

Over the last years, 3D laser scanning technology for wear analytics has been applied at several vessel types within steel plants by RHI Magnesita. The scanning of different lining conditions in the cold state, performed by on site personnel within a few minutes, followed by automated analytics on a web-based cloud architecture has now reached a mature state for ladles and RH degasser vessels. While the developments for electric arc furnaces (EAF) and argon oxygen decarburization (AOD) vessels as well as blast furnace runners and nonferrous vessels are about to reach the step of full implementation, stationary equipment with larger geometric dimensions (e.g., reheating furnaces) requires a slightly different approach.

The operation of reheating furnaces at Tata Steel Netherlands' hot strip mill is crucial for producing high-quality steel products. However, these furnaces are exposed to high temperatures and stresses that can cause deformation and damage to the refractory lining materials over time. This can affect furnace performance and efficiency, as well as have safety and environmental impacts at the plant. Therefore, it is important to regularly monitor and maintain the furnace condition to prevent any potential failures or breakdowns.

One powerful method to evaluate the status of reheating furnaces is using 3D scanning technology. This approach captures the geometry and dimensions of furnace components with high accuracy and resolution. The 3D scan data can then be analysed and compared with design

Figure 1.

(a) RHI Magnesita's Customer Portal for scan analysis and visualisation, (b) ladle fleet management overview, (c) 3D rotatable views, and (d) 2D wall plot.

(a)

(b)

(c)

(d)
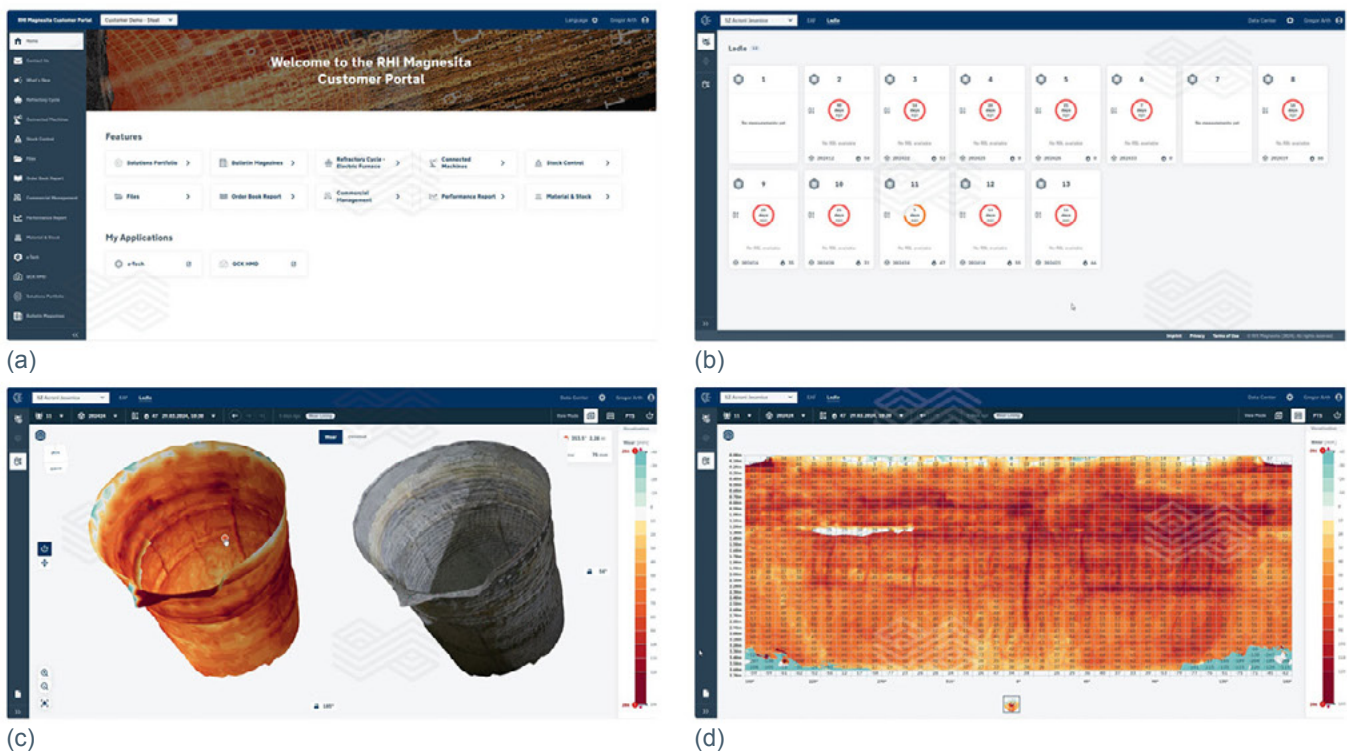
specifications or previous scans to detect any deviations or changes in the furnace structure. This can help create a predictive maintenance plan, optimise operation, and increase the furnace lifespan.

Laser Scanning Procedure and Visualisation

Currently, RHI Magnesita is using portable terrestrial lasers to measure the status of ladle refractory linings under cold conditions [1]. The laser is positioned scan-by-scan around the vessel to capture both the refractory surface as well as the ladle steel shell. The latter is mandatory to ensure reference points for the exact alignment of a created point cloud with previous ones of the same vessel.

By scanning different lining states, such as the permanent (safety) lining and the wear lining before and after operation, the residual brick lengths and amount of wear can be determined within minutes by uploading and analysing the scans using RHI Magnesita's web-based interface. As shown in Figure 1, the scans can be accessed via the RHI Magnesita Customer Portal (Figure 1a), where a fleet management overview (Figure 1b) can be found. Additional visualisation tools include 3D rotatable views (Figure 1c) as well as 2D wall and bottom plots (Figure 1d), with the option to extract data to MS Excel.

Complete vessel scanning can be performed in minutes, depending on the number of scans required to capture the entire lining and reference points, which is related to the vessel or furnace size. For example, approximately 4–5 scanning positions are required per vessel (e.g., ladle) or furnace (e.g., EAF) to encompass every critical area (Figure 2). Depending on the 3D scanning equipment, it can take about 15 minutes in total to complete all the measurements. In addition, it requires about 45 minutes to combine the scans into a single point cloud and visualise the results. While the reality capture of the aforementioned vessels takes place during liquid steel production, the following sections focus on 3D scanning a much larger, stationary furnace used for solid steel treatment in the hot strip mill.
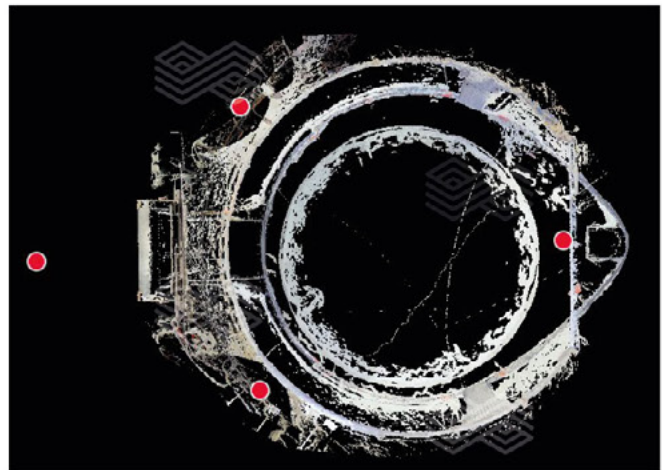
Reheating Furnaces

After the continuous casting process, semi-finished products like slabs are typically taken to separate areas within the steel plant for cooling and storage. Before the hot rolling process, these semis must be reheated to the required temperature, which is typically performed in pusher-type or walking-beam furnaces, known as reheating furnaces. Figure 2 illustrates the major differences in the number of scanning positions (marked as red dots) used to image ladles, EAFs, and reheating furnaces. Notably, it takes only a few scanning positions for a full 3D ladle lining scan (Figure 2a) and even larger vessels such as EAFs (Figure 2b). However, this number can be more than 10 times higher for stationary equipment, such as a walking-beam furnace (Figures 2c and 2d).
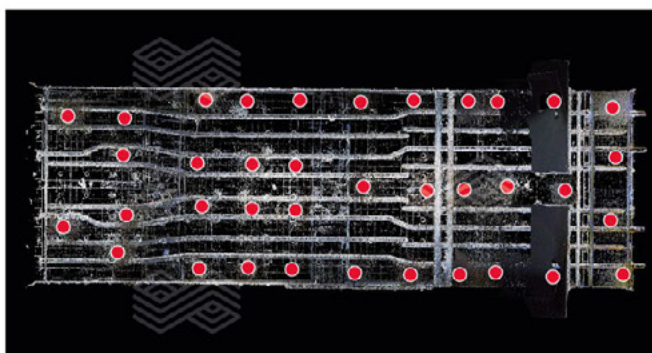
Figure 2.

Overview of scanning positions (red dots) for different vessels and furnaces. (a) ladle, (b) EAF, and (c–d) walking-beam furnace.
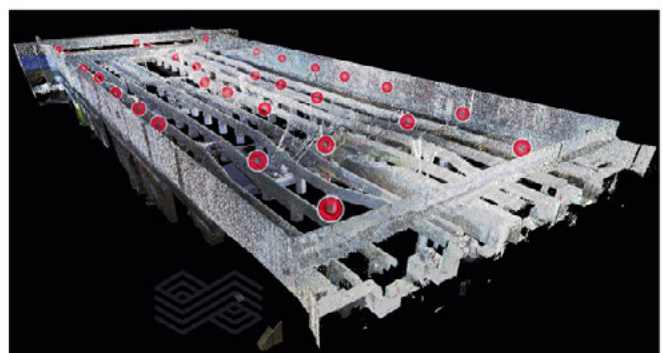

(a)

(b)

(c)

(d)

Tata Steel and RHI Magnesita share a common interest in optimising refractory performance in reheating furnaces, where the reality capture of the lining using 3D scanners is one approach to realise improvements. Following the recent acquisition of Seven Refractories, RHI Magnesita has strengthened its expertise in the area of reheating furnaces and the established laser measuring process perfectly complements Seven Refractories' product portfolio related to reheating furnaces. In addition to their expertise in solutions comprising refractory engineering, project management, energy saving systems, material deliveries, and installations, Seven Refractories can now also support the customer, for example, with wear measurements in the bottom of pusher furnaces. This enables very precise measurements to be obtained for the evaluation of new refractory developments related to material grades.

Over the past years during maintenance stops, multiple 3D scans were performed at Tata Steel's hot strip mill. In one case, a feasibility study was conducted by RHI Magnesita with the aim of reducing scanning duration while maintaining the scan quality at a sufficiently high level because it is necessary to keep the scanning duration inside the furnaces to a minimum, thereby avoiding time losses during production. Although precise details of how the scanning time inside reheating furnaces was minimised will not be covered in this article, another aspect of the feasibility study to assess both the potentials and limitations of this technology, as well as the general applicability to improve refractory and maintenance performance, will be described.

Currently, the most common approach for scan comparison is to create a reference to compare with the scan of interest, for example the permanent lining with the wear lining or an unused versus used lining. However, because of the long duration between maintenance stops for reheating furnaces, and thereby the time between scans, the first results of the joint evaluation presented in the next section are based on using a theoretical model as the reference.

Evaluation and Comparisons

The first 3D scans of the reheating furnace at the hot strip mill were completed in 2022. The scans covered various parts of the furnace, such as the walls, roof, floor, skids, hot riders, and burners. The scan-to-scan registration step during the manual post-processing was performed using commercial software, whereby the combined cloud was cleaned of any moving objects as well as regions of no interest like the furnace bottom/floor. The scan resolution and accuracy affect the file size used for data analyses and there is a large difference between the full scans of reheating furnaces and ladles. For example, when the registration step of a reheating furnace is completed, the resulting file size can range from 5–50 GB, whereas for ladles it is only 100–250 MB. Therefore, the resulting file of the reheating furnace was further processed and evaluated in another locally installed commercial software.

During the first discussions between Tata Steel and RHI Magnesita, the following topics were selected for investigation:

- Alignment of the roof tiles and walls.
- Skid levelness.
- Options for an optical lining status check.

The point cloud data and the associated images were processed in appropriate software to produce functional deliverables. Comparable to the web application described earlier in this article, a colour-coded evaluation is also possible with this software. The applied method enables local deviations to be detected quickly when comparing the actual scan and a theoretical ideal model. One example of the comparative results for roof tile alignment is illustrated in Figure 3, where it can be seen that the roof has a yellow colour over most of its surface, indicating that it is mainly flat. The majority of the measured values were within the range of -10 to +20 mm (91.4%) and the outer sides of the roof had values between 0 and -5 mm (17.5%).

Figure 3.
Deviation of tile positions in the middle roof section compared to an ideal reference model.
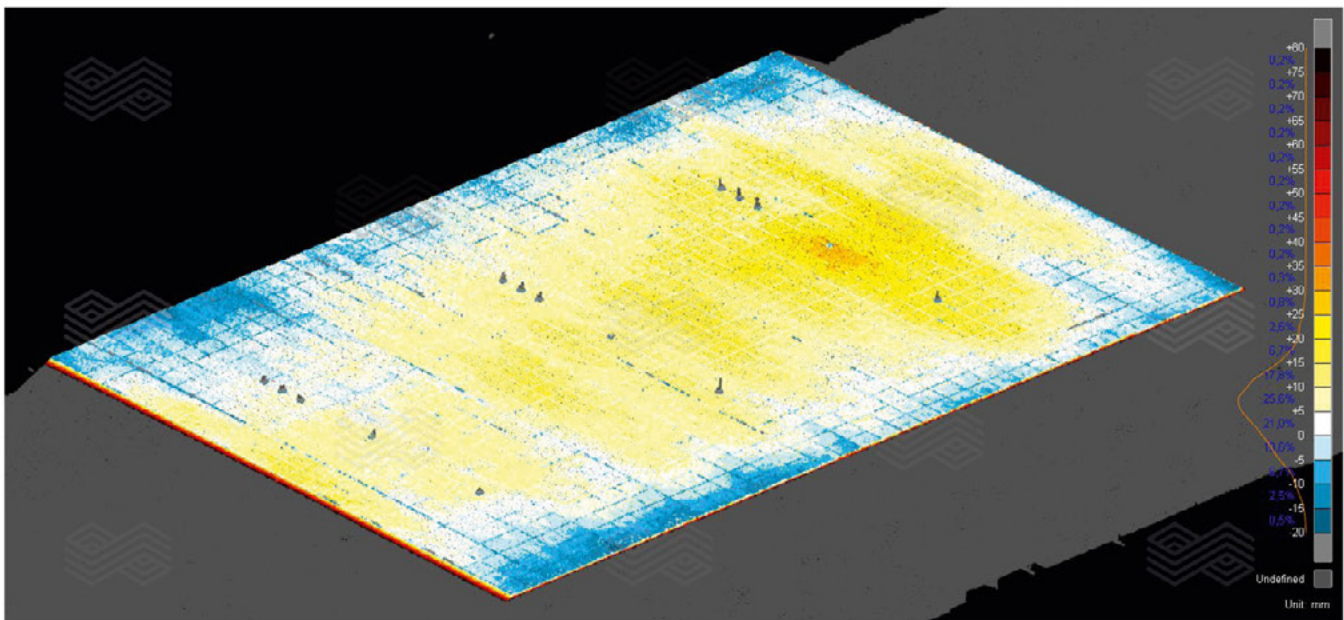
The highest roof tile area was located on the perimeter in the middle zone where it varied between -15 and -20 mm (0.5%), while the lowest roof tiles were located in the central part of the roof in the middle region, closer to the recuperative zone where they varied from +25 to +30 mm (0.8%). The vertical distance between the highest and lowest roof tiles in the middle zone of the roof was approximately 50 mm.

Whereas roof and wall sections are considered stationary objects, half of the skids are moving during operation to transport the semis through the furnace and can thus be in slightly different positions at the maintenance stop. Therefore, the moving and fixed skids were evaluated separately with tailor-made references. Figure 4 provides a magnification of a fixed skid section to underline the necessity for different benchmarks during the investigation. Furthermore, while the local deformation of the roof (see Figure 3) within a centimetre range might have low influence on the semi reheating quality, a deformation or misalignment

of the skids can lead to semi deformation and subsequent issues in the hot rolling mill. As depicted in Figure 4b, the deviation of a small skid section was detected in the millimetre range, confirming the need to check the status of the skids before putting the furnace back in operation.

When scanning the furnace lining, the applied lasers can also capture high density resolution (HDR) panorama images and provide each point of the cloud with a red, green, and blue (RGB) value. Therefore, an additional benefit of this technology is the panoramic image enables optical inspection without any additional manual or drone-based visit, reducing workload in the furnace. Figure 5 provides an example of a panoramic view generated using a freeware viewer. This makes documentation of the lining sustainable and trackable compared to previous, locally captured images that lacked detailed information about image position or depth, namely the differentiation between bearing and wear.

Figure 4.

(a) 3D scan comparison to a reference model of multiple skids and (b) deformation clearly detectable in a skid.

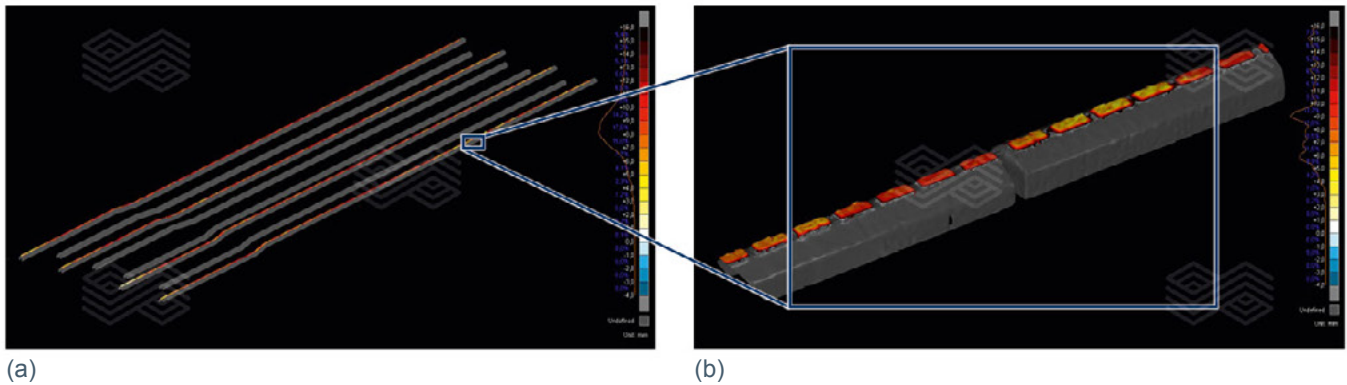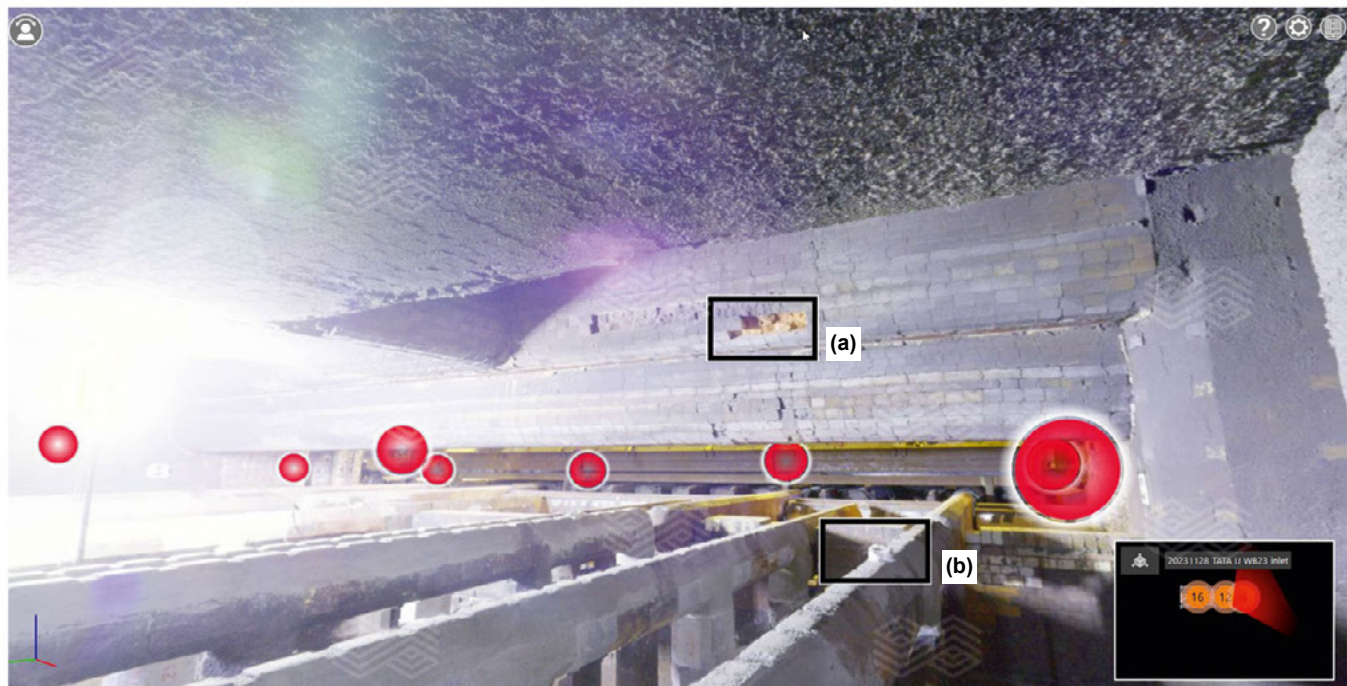(a)   (b)

Figure 5.

HDR panoramic image of the reheating furnace interior showing (a) lining damage and (b) insulation material partially obscuring the view of a skid.

The use of 3D scanning technology is a valuable tool for predictive maintenance, providing a safe and efficient approach for equipment inspection. By creating a digital model of the furnaces, 3D scanning enables personnel to identify and prioritise areas that are most in need of maintenance and plan the actions accordingly. By constantly monitoring and comparing furnace conditions, it becomes possible to identify and predict potential issues, enabling proactive maintenance to be performed. Furthermore, by detecting potential maintenance topics before they occur, predictive maintenance using 3D scanning helps to minimise downtime, as repairs can be scheduled in advance.

Conclusion

Over the last years, open communication between Tata Steel and RHI Magnesita has led to a better understanding of the reality capture potential for reheating furnaces. Currently, data evaluation is performed manually using stand-alone software on local computers. However, all the findings are being used as the basis for developing web-based visualisation to provide a more efficient and automatised report generation. The 3D scan technology can rapidly capture and compare the geometry and dimensions of furnace components with high accuracy and resolution, thereby helping to create a predictive maintenance plan that can optimise the performance and lifespan of a furnace. Follow-up data assessment will focus on evaluating the two real scans performed during maintenance stops of the reheating furnaces after the furnaces were in operation for about a year. This will open up the potential to start determining the refractory performance per region and provide the basis for a tailor-made balanced lining within the furnace.

References

[1] Santos, J.P., Macedo, J., Avila, H., Lima, G., Arruda, E. and Lazaroni, A. Innovative Refractory Wear Measurement Method for Steel Ladles Using 3D Laser Scanning. *Bulletin*. 2023, 57–60.

Authors

Gregor Arth, RHI Magnesita, Leoben, Austria.
Lars Merta, RHI Magnesita, Wiesbaden, Germany.
Kateryna Hechu, Tata Steel, IJmuiden, the Netherlands.
Bruno Luchini, Tata Steel, IJmuiden, the Netherlands.
Florus Beukema, Tata Steel, IJmuiden, the Netherlands.
Ed Wortel, Tata Steel, IJmuiden, the Netherlands.
Corresponding author: Gregor Arth, Gregor.Arth@rhimagnesita.com

bulletin

2024